I. MIXING IN DOORWAY FLOWS
II. ENTRAINMENT IN FIRE PLUMES

Thesis by
Christopher S. Lim

In Partial Fulfillment
of the Requirements for the Degree of
Aeronautical Engineer

California Institute of Technology
Pasadena, California

1984
(Submitted 30 April 1984)

I. MIXING IN DOORWAY FLOWS
II. ENTRAINMENT IN FIRE PLUMES

Christopher S. Lim

1984

ACKNOWLEDGEMENTS

The author takes this opportunity to thank all those who have helped him in this research effort. He is indebted to Professors Edward Zukoski and Toshi Kubota for their many helpful comments and suggestions; to J.P. Huot, Hamid Johari and Brian Kravitz for their invaluable assistance in the experimental work; and to his fellow graduate students for their advice and suggestions. The financial support provided by the National Bureau of Standards and the California Institute of Technology are also very much appreciated.

ABSTRACT

The motion of hot combustion products through a burning structure plays a dominant role in fixing the spread of the fire and the spread of toxic gases. The first part of this report is concerned with the effect of door geometry on the rate of turbulent mixing between the hot and cold layers near a doorway. The second part of the report deals with the entrainment rates in the near field of a buoyant diffusion methane flame.

In the study of the motion of the hot combustion products near a doorway, the gas in the burning room is assumed to be divided into two homogeneous layers--the ceiling layer which contains the hot combustion products and the floor layer which contains the denser fresh air. Temperature and carbon dioxide measurements are taken from a half-scale room which uses a pump and furnace to simulate the entrainment and heating of the fresh air by the fire plume. The mass transfer rates are calculated from these measurements and are found to be a function of a Richardson number that uses the interface height measured from the floor as the characteristic length and the average inflow velocity of fresh air as the characteristic velocity. This form for Ri_o is derived from an analysis based on Taylor's entrainment hypothesis. For a given fire size, i.e., for a given mass flow of fresh air into the room, the effect of reducing the door area is to reduce the value of Ri_o and hence increase the mixing rate in the room. The door height is found to be a much stronger influence on the mixing rate and interface height than the door width.

The entrainment rates of fresh air in the near field of a buoyant diffusion methane flame whose flames extend well above the interface between the hot gas layer and the fresh air layer are measured for several interface heights. In

the experiments, the ceiling layer-fire plume interaction is simulated by placing a large steel hood over an axisymmetric burner. The hood may be raised or lowered to change the interface height. The entrainment measurements are obtained from a chemical analysis of a dried sample of combustion products taken from the ceiling layer. The measured species concentrations are compared with the theoretical equilibrium composition of the ceiling layer gas. For a given interface height, the ceiling layer gas temperature is found to be a linear function of the fuel-air ratio up to the stoichiometric fuel-air ratio. Increasing the fuel-air ratio above the stoichiometric value did not change the gas temperature significantly. This maximum temperature is observed to decrease with interface height. The air entrainment rates are found to be a weak function of the fuel-air ratio at very low elevations of the interface.

TABLE OF CONTENTS

LIST OF FIGURES

LIST OF TABLES

LIST OF SYMBOLS

A. MIXING IN DOORWAY FLOWS

b	Door width.
$E(x)$	Local entrainment coefficient (Eq. 3.5).
F	Froude number defined by Eq. 3.16c
H	Room height (= 48 in.)
K	CO_2 concentration expressed as $\%CO_2$ by volume.
$\dot{m}(x)$	Total mass flowrate of the cold layer jet; $= \dot{m}_d(x) + \dot{m}_{1c}$.
$\dot{m}_{1c}$	Total mass flowrate of inflowing fresh air.
$\dot{m}_{1h}$	Total mass flowrate of outflowing hot gas.
$\dot{m}_2$	Floor suction rate.
$\dot{m}_3$	Mass flowrate of gas leaving the furnace.
$\dot{m}_d(x)$	Mass entrainment rate of hot gas into the cold layer from x = 0 (doorway) to x.
$\dot{m}_d$	Total mass entrainment rate of hot gas into the cold layer; $\equiv \dot{m}_d(x_{cr})$.
$\dot{m}_u$	Mass entrainment rate of fresh air into the hot layer.
$\dot{Q}_f$	Fuel heat release rate. $\equiv 47.5\ MJ/kg \times \dot{m}_f$.
Ri_o	Overall Richardson number (Eq. 3.1).
$Ri_x(x)$	Local Richardson number (Eq. 2.6).
t_{res}	Residence time of the hot gas in the ceiling layer.
T	Gas temperature.
$U^*(x)$	Velocity scale based on jet momentum (Eq. 3.6).
$U_{max}(x)$	Local maximum velocity in the cold layer.
U_{1c}	Average velocity of the inflowing fresh air (Eq. 3.3).

W	Room width (= 48 in.)
x	Axis normal to the plane of the door.
y	Probe height measured from the floor.
Y_i	Interface height measured from the floor.
$\delta(x)$	Mixing layer thickness at station x (Fig. 2.3).
δ_C	Mixing layer thickness measured at the center of the room.
ρ	Density.

Subscripts

c	Property of the floor (or "cold") layer gas.
cr	Critical point where mixing is suppressed.
f	Property of the fuel.
h	Property of the ceiling (or "hot") layer gas.
3	Property of the hot gas leaving the furnace.
∞	Property of the ambient (or "fresh") air.

B. ENTRAINMENT IN FIRE PLUMES

C_f	Mass fraction of fuel in the ceiling layer.
C_o	Mass fraction of oxygen in the ceiling layer.
C_∞	Mass fraction of oxygen in the ambient air (=0.23).
D	Burner diameter (= 0.19 m.).
f_s	Stoichiometric fuel-air ratio (= 0.056 for methane).
$\dot{m}_E$	Mass entrainment rate of air into the plume.
$\dot{m}_f$	Mass flowrate of fuel.
$\dot{m}_{f_{added}}$	Mass flowrate of fuel injected directly into the ceiling layer.
$\dot{m}_{p_{in}}$	Plume mass flux into the small hood.
$\dot{m}_{p_{fl}}$	Plume mass flux at the flame top.
n_i	Number of moles of species i per mole fuel.

N_{hood}	Total number of moles in the hood per mole fuel.
N_{sample}	Total number of moles in the dried sample per mole fuel.
φ	Equivalence ratio.
$\dot{Q}_f$	Fire size; = 47.5 $MJ/kg \times \dot{m}_f$.
t_{res}	Residence time of the hot gas in the hood.
T_h	Average ceiling layer gas temperature.
T_∞	Ambient air temperature.
Y_i	Mole fraction of species i in the dried sample.
$\bar{Y}_i$	Mole fraction of species i in the ceiling layer.
Z_i	Interface height.
α	Fraction of added fuel consumed in the plume.

Chapter 1

INTRODUCTION

The motion of hot combustion products through a burning structure plays a dominant role in fixing the spread of the fire and the spread of toxic gases. The first part of this report is concerned with the effect of door geometry on the rate of turbulent mixing between the hot and cold layers near a doorway. The second part of the report deals with the entrainment rates in the near field of a buoyant diffusion flame.

1.1. Mixing in Doorway Flows

The motion of gases in a burning room is strongly influenced by the fire size, room geometry, and the presence of windows, doorways, and other openings. Fresh air in the floor region is entrained and heated by a buoyant plume produced by the fire. The hot gases then rise to the top of the room to form a distinct ceiling layer of hot combustion products. This ceiling layer of hot gases gradually becomes thicker, then flows out to the adjacent rooms through open doorways. Fresh air enters the room through the lower part of the door to replace the air entrained into the plume. Near the doorway, the motion of the hot gas and fresh air are in opposite directions, and a shear layer is formed between the two layers. The amount of mixing between the hot gas and fresh air in the shear layer is controlled largely by inertial and buoyancy forces. As the temperature in the room increases, the unignited objects in the room begin to pyrolize and contribute fuel to the ceiling layer. Since the room is evenly heated, the unburned fuel and objects in the room ignite at about the same time. This results in the phenomenon known as flashover: a sudden increase in temperature, a rapid increase in gas production, and an explosive and

spectacular fire growth that consumes the entire room.

During the period prior to flashover, the hot gas layer is usually so sharply stratified that the room may be approximated by dividing it into two homogeneous regions: the ceiling layer which contains the hot gases, and the floor layer which contains the cooler gas. Mass and energy conservation equations may then be applied to each layer to calculate the amount of mixing between the ceiling and floor layers, and the entrainment of outside air into the room.

The two-layer model for smoke movement was first used by Kawagoe (1958) who studied the movement of gases through an opening connecting two regions (i.e., the ambient air region and the room region which was considered to be a well-mixed, homogeneous region). A few years later, P. H. Thomas, et al (1963) studied flows in rooms with well-defined stratified hot and cold layers. Other works which use the model are discussed in papers by Zukoski, et al (1975, 1978, 1979, 1980).

The present investigation is concerned with the measurement of the amount of hot gas entrained by the fresh air entering through the door. In particular, the purpose of the experiments is to determine the effect of door geometry and fire size on the mixing rate. In the experiments, we used a pump and a furnace to simulate the entrainment and heating of the fresh air by the fire plume. Chapter 2 describes the model and the techniques used in calculating the mass flowrates. Chapter 3 discusses the results obtained for four different door geometries. The equations used in the calculations are derived in Appendix A and the data gathered from the experiments are tabulated in Appendix C.

1.2. Entrainment in Fire Plumes

While the turbulent mixing between the hot and cold layers generated by presence of doorways accounts for some of the entrainment of lower region air into the upper layer, the fire plume transports a much larger mass flowrate of gas into the ceiling layer. The entrainment rate of air into the plume is strongly dependent on the fire size, fire geometry, and the interface height. Experiments indicate that the fire plume may be divided into three regions: a region close to the burner surface where plume entrainment rates are independent of fire size; a far field region well above the top of the flames where a simple point source model may be used; and a not so well-defined intermediate region where turbulent flame approximations apply.

In the initial region near the base of the fire, Cetegen (1982) observed that the entrainment rates are independent of the fuel flowrate and scale with height above the burner raised to a power of approximately 3/4.

In this report, we describe the plume mass flux measurements in the near field of axisymmetric diffusion flames. The measurements were made by chemical analysis of the species in the ceiling layer. Chapter 4 describes in detail the technique and the apparatus used in the experiments. Chapter 5 discusses the experimental results and compares the results with the theoretical values obtained from a chemical equilibrium analysis. The equations used in the experiments are derived in Appendix B, and the experimental data are tabulated in Appendix D.

Chapter 2

ROOM EXPERIMENTAL SETUP

2.1. Experimental Technique and Apparatus

The motion of gases in a burning room is strongly influenced by the fire size, room geometry, and the presence of windows, doorways, and other openings. We have investigated the effects of fire size and door geometry on the turbulent mixing between the hot and cold layers in a half-scale model room, and the entrainment of outside air into the room. The room model used in our experiments is shown schematically in Figure 2.1. To simulate the fire entrainment rate, $\dot{m}_2$, a pump was used to draw room air through the floor and into a furnace where the air was heated to about 160 degrees Celsius. The furnace used city gas (methane) as fuel. Screens were placed in the furnace to ensure that the gas was heated uniformly. The walls of the room were well insulated to minimize heat loss to the surrounding air.

Gas samples from the room were obtained from six probes on an arm that extended across the width of the room. The probe arm could be swung 180 degrees in the horizontal plane, as well as moved in the vertical direction to reach most parts of the room. Additional probes were also placed in the furnace and in the ambient air.

A Beckman Model 864 Nondispersive Infrared Analyzer was used to measure the volume concentration of carbon dioxide. The analyzer was calibrated three times during each run with the use of certified calibration gases obtained from the Matheson Company. Iron-Constantan thermocouples were used to measure the gas temperatures.

In the experiments, the interface height was varied by increasing or decreasing the flowrate through the pump ($\dot{m}_2$), and appropriately adjusting the fuel flowrate to achieve the desired furnace temperature.

2.2. Mass Transfer Model

To model the mass transfer process, we assume that the room can be separated into four distinct regions with uniform thermodynamic properties: the hot layer, the cold layer, the furnace, and the ambient or outside air regions (Figures 2.2a,b). Then by applying mass balance equations to each region, the following mass flow relations can be obtained (see Appendix A):

$$\dot{m}_{1h} = \frac{(K_\infty - K_c)\dot{m}_2 + (K_3 - K_\infty)\dot{m}_3}{K_h - K_\infty} \tag{2.1}$$

$$\dot{m}_{1c} = \dot{m}_2 - \dot{m}_3 + \dot{m}_{1h} \tag{2.2}$$

$$\dot{m}_u = \frac{\dot{m}_3(K_h - K_3)}{K_c - K_h} \tag{2.3}$$

$$\dot{m}_d = \dot{m}_u + \dot{m}_2 - \dot{m}_{1c} \tag{2.4}$$

where $\dot{m}_{1h}$ is the mass flow of hot layer gas leaving the room through the door; $\dot{m}_{1c}$ the mass flow of ambient outside air entering the room through the door; $\dot{m}_u$ the mass flow of cold layer gas entrained into the hot layer; and $\dot{m}_d$ the mass flow of hot layer gas entrained into the cold layer. Here $\dot{m}_2$ is the floor suction rate, and $\dot{m}_3$ is the mass flowrate of gas leaving the furnace. K_h is the mole fraction of CO_2 in the hot layer; K_c the mole fraction in the cold layer; K_3 the mole fraction of the hot gas leaving the furnace; and K_∞ is the mole fraction of CO_2 in the ambient air.

The following quantities were measured in the experiments: $\dot{m}_2$, $\dot{m}_f$, K_h, K_c, K_3, and K_∞. These data and the above equations were then used to estimate the values of $\dot{m}_{1h}$, $\dot{m}_{1c}$, $\dot{m}_u$, and $\dot{m}_d$. The derivations of the above equations are presented in Appendix A.

2.3. Determination of Interface Height

Since the shear layer that separates the ceiling and floor layers has a finite thickness, the interface height is not clearly defined. In the experiments, we chose to base the interface height on both the temperature and carbon dioxide concentration profiles in the room. The interface height, Y_i, is defined to be the height where

$$\frac{T(y) - T_\infty}{T_3 - T_\infty} \text{ and } \frac{K(y) - K_\infty}{K_3 - K_\infty} \textit{ equals } \frac{1}{2}.$$

$T(y)$ and $K(y)$ are the temperature and mole fraction of CO_2 measured y inches from the floor; T_∞ the temperature of the ambient air outside the room; and T_3 the furnace temperature. For cases where the two heights did not coincide, the average value was used. This arbitrarily defined interface height, Y_i, was used to calculate the average velocity, U_{1c}, of the ambient air entering through the door. Both terms appear in the definition of the overall Richardson number.

2.4. The Richardson Number

The Richardson number is a measure of the stability of flows with density variations. It is a dimensionless number and is equal to the ratio of the buoyancy force and the momentum flux, i.e.,

$$Ri_o = \frac{\Delta\rho g L}{\rho U^2} \tag{2.5}$$

where L is a characteristic length; ρ the density; g the gravitational constant; and U a characteristic velocity. The mixing process is suppressed by the gravitational forces when the momentum of the gases is small enough, i.e, at large Ri_o values. On the other hand, at low values of Ri_o, considerable mixing between the two layers occurs. Since Eq. 2.5 describes the entire flow, Ri_o is called the "overall" Richardson number.

A "local" Richardson number, which represents the stability of the layers at a given cross section in the room, is defined by

$$Ri_x(x) = \left[\frac{-\frac{1}{\rho}\frac{\partial \rho}{\partial y} g}{\left[\frac{\partial u}{\partial y}\right]^2} \right]_{y = Y_i} \tag{2.6}$$

where $\partial\rho/\partial y$ and $\partial u/\partial y$ are the local density and velocity gradients respectively.

From the experimental results, we have found that the mass transfer rates in the room correlate very well when plotted against an overall Richardson number that uses the interface height as the characteristic length and the average inflow velocity of fresh air into the room as the characteristic velocity. This form for Ri_o was derived from an assumption that the fresh air entered the room like a wall jet with a mixing layer separating the hot and cold layers (Figure 2.3). The mixing layer will grow with x and reach a stable thickness at a critical local Richardson number, $(Ri_x)_{cr}$. Beyond this point there is no mixing between the hot and cold layers (see Section 3.2).

2.5. Room Flow Patterns

The flow field within the room is sketched in Figure 2.3 where the flow is shown in two views. In the first, the viewing plane is the vertical plane perpendicular to the floor and including the centerline of the room and the door. The mixing (or shear) layer, which forms between the cool incoming flow and the hot ceiling gas, grows due to turbulent mixing up to a critical point, x_{cr}. Beyond this point, the effects of buoyancy are strong enough to suppress the mixing and entrainment processes, and the mass flux into the mixing layer stops. However, the layer does continue to move toward the back wall of the room and will eventually reach that wall and form a stagnation point flow in that impingement region. Thus, more mixing can occur there. Finally, the velocity profile in the cold jet will be affected by friction at the floor.

The second view in Figure 2.3 describes the flow in a plane parallel to the floor and slightly elevated above it. Mixing layers form between the cool jet of fresh air entering the through the door and the recirculating flows in the corners. Clearly, there will be a strong exchange between the cool gas in the door jet and the gas in the recirculation region. This exchange occurs as a result of entrainment along the shear layer, shown in this second view, and from the recirculation of shear layer gas required to supply material lost from the recirculation zone due to the entrainment process. In addition, hot gas from the ceiling layer will be entrained into this region across a horizontal surface which lies between the recirculation zone and the ceiling layer.

In the above picture, we assumed that the fluid velocities in the hot upper layer were negligible. In flow visualization experiments conducted in a salt water room model, Tangren, et. al. (1978) observed the existence of several counterflowing sublayers present in the ceiling layer. The flow in the upper layer is therefore very complicated and not well understood at the present time.

Because of the complex nature of the ceiling layer, we are forced to ignore the influence of currents present in that layer.

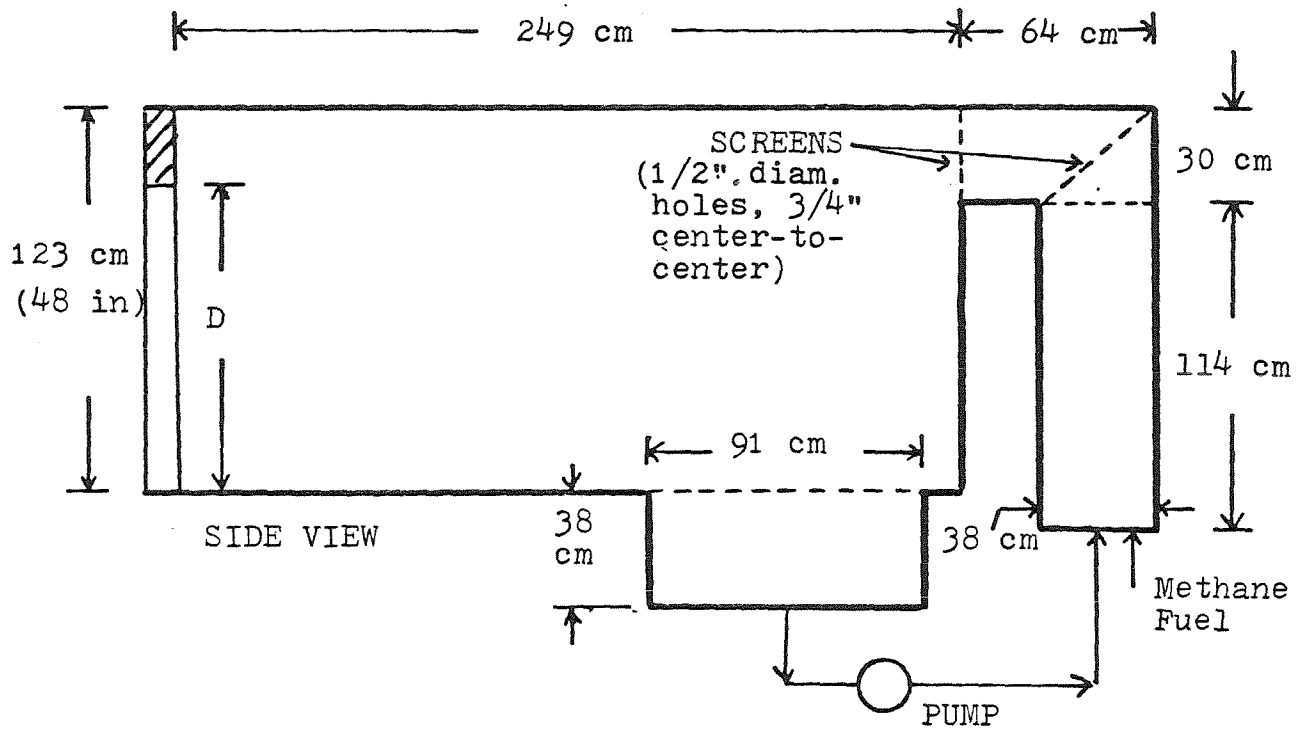
249 cm
64 cm
SCREENS
(1/2" diam.
holes, 3/4"
center-to-
center)
30 cm
123 cm
(48 in)
D
114 cm
91 cm
SIDE VIEW
38
cm
38 cm
Methane
Fuel
PUMP

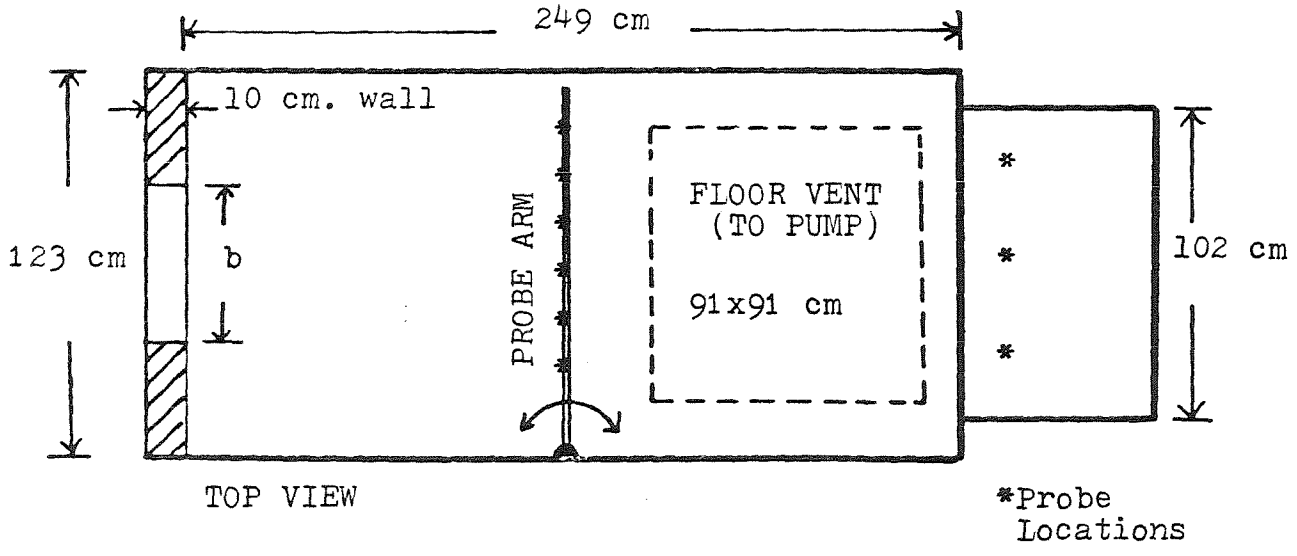
249 cm
10 cm. wall
123 cm
b
PROBE ARM
FLOOR VENT
(TO PUMP)
91x91 cm
102 cm
TOP VIEW
*Probe
Locations

Figure 2.1

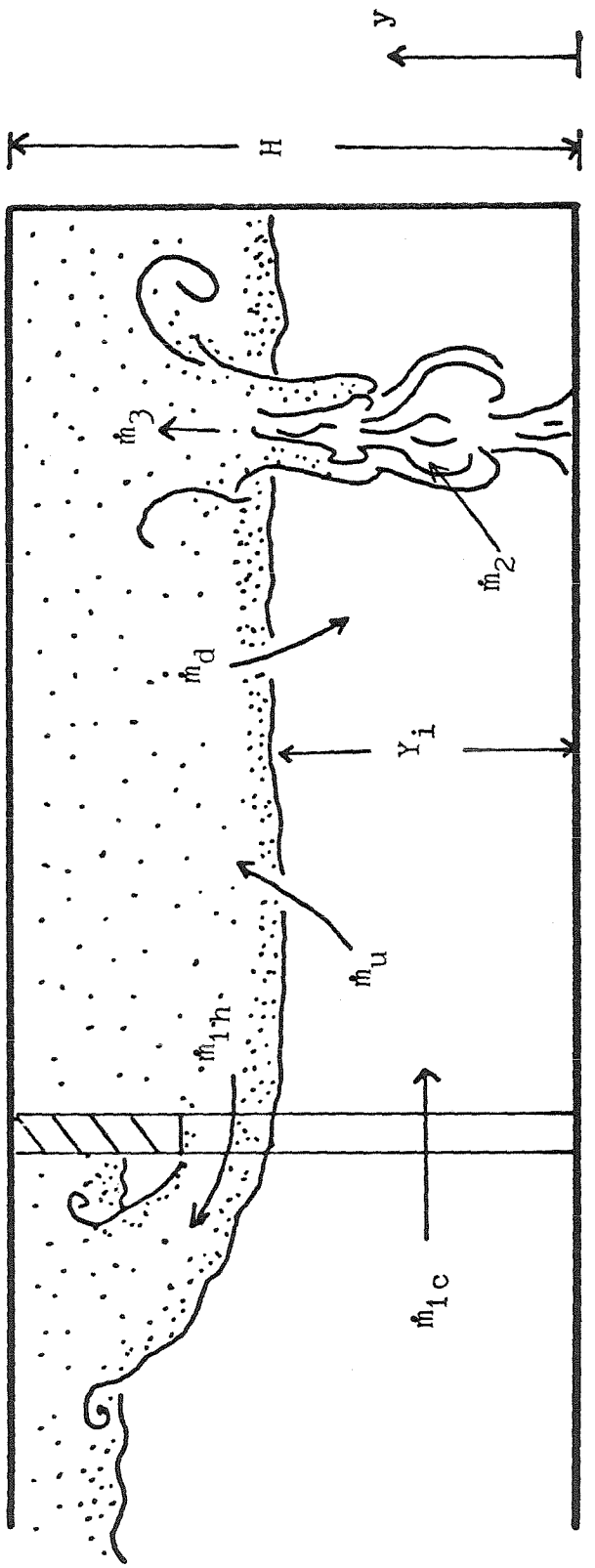

Figure 2.2 (a)

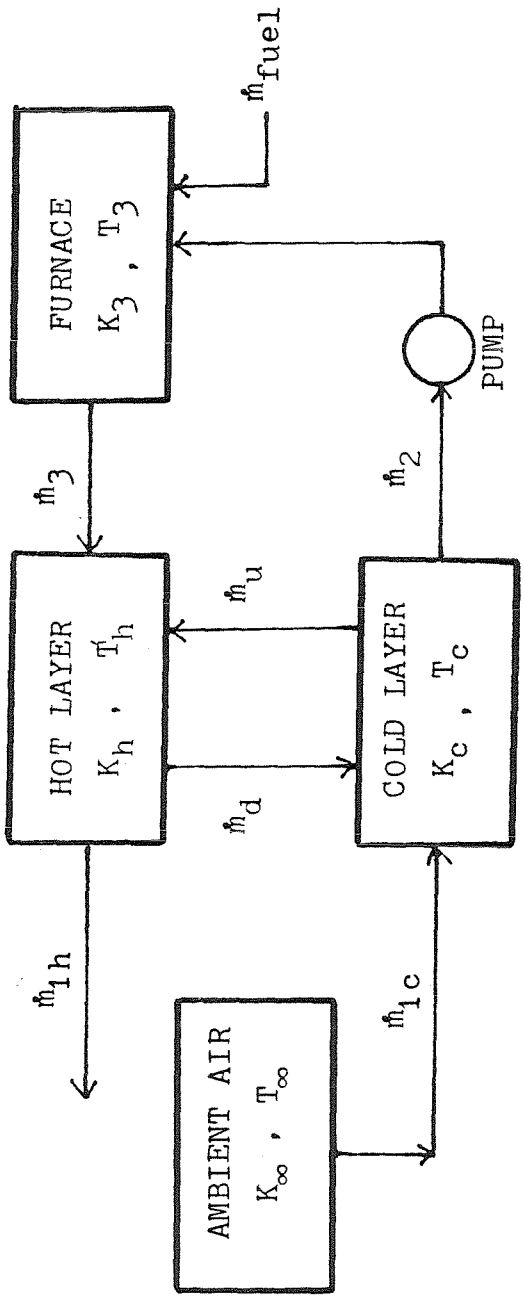
FURNACE
K_3 , T_3
$\dot{m}_{fuel}$
PUMP
$\dot{m}_3$
$\dot{m}_2$
HOT LAYER
K_h , T_h
$\dot{m}_u$
COLD LAYER
K_c , T_c
$\dot{m}_d$
$\dot{m}_{1h}$
$\dot{m}_{1c}$
AMBIENT AIR
K_∞ , T_∞

Figure 2.2(b)

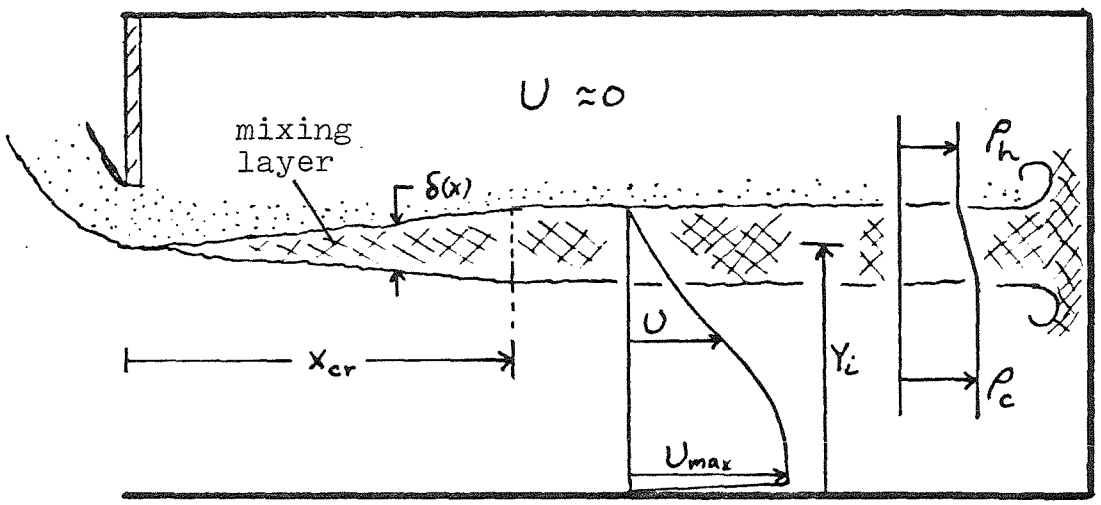
U ≈0
mixing
layer
δ(x)
x_{cr}
U
U_{max}
Y_i
ρ_h
ρ_c

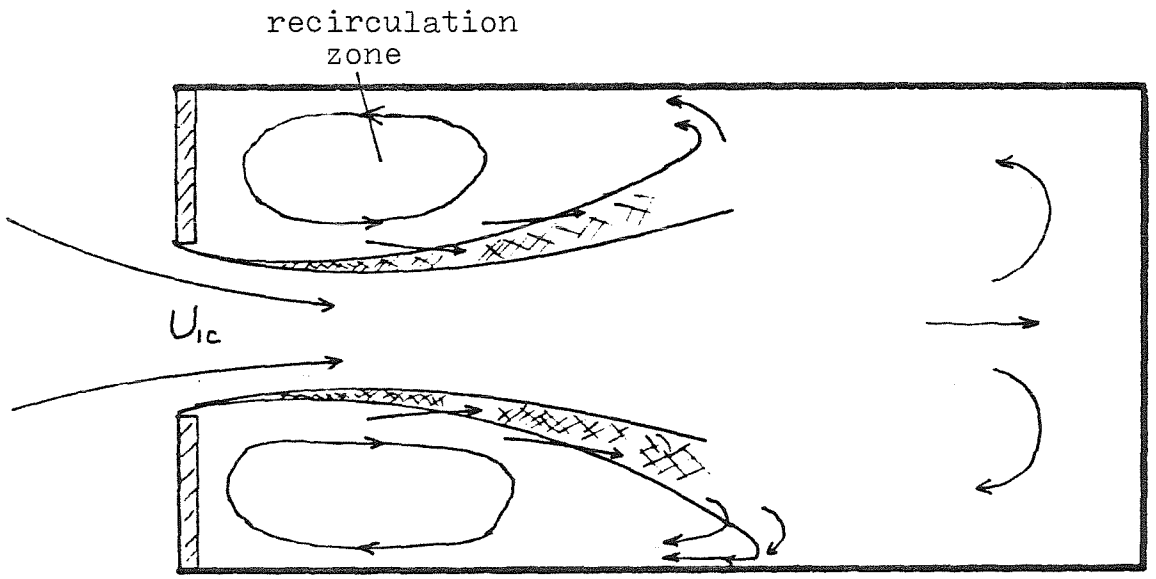
recirculation
zone
U_{ic}

Figure 2.3

Chapter 3

ROOM EXPERIMENTAL RESULTS

To determine the accuracy of the two-layer approximation, temperature measurements were made at various locations in the room (Figure 3.1). The measurements show that the vertical temperature profiles do not vary significantly in the room. Comparing the temperature profiles at corners A and E, it is observed that the temperature at the corner near the door (A) is about 10 to 20 degrees higher than in the corner near the furnace exit (E). Along the centerline (locations C,D,E), the temperature variation is less than 10 degrees Celsius. It may then be concluded that the room may be accurately approximated by the two-layer model. In the following experiments, we placed the probe in the center of the room and assumed that the vertical temperature and carbon dioxide profiles measured in the center of the room represent the average properties of the room gas.

Temperature and carbon dioxide concentration profiles in the center of the room were obtained for the following door geometries: 12"x39", 18"x39", 18"x24", and 12"x26" (width x height) doors. The temperature profile was used to estimate the density gradients, and the CO_2 profile was used to calculate the mass transfer rates.

3.1. Effect of Floor Suction Rate

We have studied the case where the furnace temperature was set at approximately 160 $^{\circ}C$ while the floor suction rate was varied from 0.03 kg/s to 0.20 kg/s. Typical temperature and carbon dioxide concentration profiles for low and high values of $\dot{m}_2$ are shown in Figure 3.2. For low values of $\dot{m}_2$, the interface is well above the floor and the carbon dioxide concentrations in the hot and

cold layers are sharply separated by a thin shear layer. For large values of $\dot{m}_2$, the interface is drawn very close to the floor and the boundary between shear layer and the cold layer becomes indistinguishable. It is also observed that for high interface heights, the temperature and the carbon dioxide profiles differ in shape in the hot layer but have a similar shape in the cold layer. On the other hand, when the interface is very close to the floor, both profiles have very similar shapes. Figure 3.3 is a dimensionless plot of Figure 3.2(a) where the ambient and furnace properties are used to normalize the temperature and carbon dioxide concentrations in the room. Figure 3.3 also demonstrates how we defined the interface height, Y_i.

3.1.1. *Temperature Profiles.* A comparison of Figures 3.2(a) and 3.2(b) shows that the slopes of the temperature profiles in the the shear layer do not change with interface height. Figure 3.4(a) shows the result when the dimensionless temperature profiles for the 12"x39" door are plotted as a function of distance from the interface for various values of $\dot{m}_2$. As expected, the dimensionless temperature profiles agree very well within the shear layer, but it is surprising that the profiles are also similar outside the shear layer. Figure 3.5(a) shows the temperature profiles when the door is widened. Again the profiles agree very well within and outside the shear layer.

Figure 3.6(a) shows the temperature profiles for the 12"x26" door which has the same aspect ratio as the 18"x39" door. Again the profile shapes are similar but the shape is substantially different from the profiles in Figures 3.4(a) and 3.5(a).

Figure 3.7(a) shows the profiles for the 18"x24" door. For low values of $\dot{m}_2$, the profiles are similar to those of the 12"x26" door. But when the floor suction rate is increased, the profiles become more similar to that of the 18"x39" and 12"x39" doors; i.e., the temperature distribution in the hot layer becomes more

uniform as $\dot{m}_2$ is increased.

3.1.2. *Carbon Dioxide Concentration Profiles.* Although the temperature profiles show good correlation when plotted against distance from the interface, the carbon dioxide concentration profiles are not similar to each other as is shown in Figure 3.4(b). This is because the slopes of the profiles are an indication of the amount of mixing between the hot and cold layers and, hence, we do not expect the slopes to be independent of $\dot{m}_2$. Figure 3.4(c) gives a clearer view of the effect of changing $\dot{m}_2$. As $\dot{m}_2$ is increased, the interface is drawn closer to the floor and the shear layer becomes thicker. Figures 3.5(b), 3.6(b), and 3.7(b) show the profiles for the other door geometries. Unlike the temperature profiles, the carbon dioxide concentration in the hot layer is constant regardless of door geometry. The difference between the shapes of the temperature and CO_2 profiles may be attributed to the fact that the mass transfer and heat transfer processes are not similar; the heat transfer from the hot gas occurs along the walls of the room as well as through the shear layer, while the mass transfer process between the hot gas and fresh air is essentially confined to the thin shear layer.

3.1.3. *Mixing between the Hot and Cold Layers.* For a given floor suction rate, the effect of decreasing the door area (lowering and/or narrowing the door) is to lower the interface and increase the velocity of the inflowing fresh air. This translates into a higher mixing rate in the room (see Table 3.1 on the following page). It is observed from Table 3.1 that the door height has a much stronger influence on the mixing rate and interface height than the door width.

The mixing process is dependent upon the Richardson number which was discussed in section 2.4. (In our experiments, the Reynolds number of the inflowing fresh air ranged from 5000 to 20,000; the flow is therefore turbulent and Reynolds number effects may be neglected.) From the experimental results,

Table 3.1. Effect of Door Geometry on the Mixing Rate

$\dot{m}_2$	Door Geometry	Y_i	$\dot{m}_d/\dot{m}_2$
0.146 kg/s	18"x 39"	19.7 in.	0.113
	12"x 39"	13.7 in.	0.180
	18"x 24"	6.5 in.	0.373
0.067 kg/s	18"x 39"	27.0 in.	0.015
	12"x 39"	25.4 in.	0.017
	18"x 24"	13.2 in.	0.104

we have found that the mixing rates correlated well when plotted against an overall Richardson number that has the interface height as the characteristic length and the inflow velocity of fresh air as the characteristic velocity. We propose that the appropriate form for the Richardson number is

$$Ri_o = \frac{\Delta\rho g Y_i}{\rho_\infty U_{1c}^2} \tag{3.1}$$

where Y_i is the interface height (see section 2.3), $\Delta\rho$ is $\rho_c - \rho_h$, the difference in density of the cold and hot layers, and U_{1c} is the average inflow velocity of fresh air through the door. If the pressure and molecular weight of the gas in the room are assumed to be nearly equal to the ambient pressure and molecular weight, the densities ρ_c, and ρ_h can be calculated by measuring the appropriate temperatures, i.e.,

$$\frac{\Delta\rho}{\rho_\infty} \equiv \frac{\rho_c - \rho_h}{\rho_\infty} \approx \frac{T_\infty}{T_c} - \frac{T_\infty}{T_h}. \tag{3.2}$$

The inflow velocity U_{1c} is estimated with the use of the the inflow mass flowrate, $\dot{m}_{1c}$; the interface height, Y_i; and the door width, b.

$$U_{1c} = \frac{\dot{m}_{1c}}{\rho_\infty b Y_i} \tag{3.3}$$

Experimental values of the ratio of the cold layer entrainment rate, $\dot{m}_d$, to the floor suction rate, $\dot{m}_2$, are shown in Figure 3.8 as a function of $Ri_o^{-1/2}$ for the four different door geometries used in the experiments. The experimental curve from a salt water model used by Tangren, et. al. (1978) is also shown in Figure 3.8 as a comparison with our gas model. The salt water technique is based on the use of water to model the unheated fluid medium and a flow of salt brine to represent the heat source. The salt water experiments were conducted in a 38 cm. x 38 cm. x 38 cm. room with a 4.6 cm. wide x 10 cm. high door. The fresh water to salt water density ratio was about 0.9. From Figure 3.8, we see that the mixing between the two layers is five times greater in the gas model than in the salt water model for a given value of Ri_o. It must be noted that the salt water technique ignores the effects of heat transfer and is accurate only for extremely weak fires. The salt water model simulates the mass transfer rates in an isothermal room, while in our experiments the mass transfer process is inherently connected with the temperature distribution in the room. For example, when the hot gas cools along the walls, the resulting denser gas flows down the wall into the mixing layer; this form of mass transfer is not present in the isothermal salt water experiment.

Two questions may arise concerning Figure 3.8: First, in the definition of the Richardson number, why did we use the interface height and the inflow velocity as the characteristic properties of the entire flow? Several different forms for the Richardson number were tried, and it was found (by trial and error) that Eq. 3.1 gave the best correlation for the data; we really have not presented any evidence that Eq. 3.1 is indeed the appropriate form for Ri_o. Second, because the door and room geometries are certainly important parameters, we question how do these parameters affect the mixing rates? In Figure 3.8, we note that that the spread of the data points may be reduced by multiplying $1/\sqrt{Ri_o}$ by b/W, where b is the door width and W is the room width (= 48 in. for our experiments). In fact, since (b/W) is about 0.3 for our gas experiments and about 0.12 for the salt water experiments, multiplying $1/\sqrt{Ri_o}$ by the parameter b/W would reduce significantly the large difference between the salt water and gas experimental data in Figure 3.8. In the next section, we will present a simple entrainment model in which we will make an attempt to find the exact relationship between the mixing rates and the parameters Ri_o, b, and W.

3.2. Entrainment Model

As was pointed out in Sec. 2.5, the flow under study is clearly a very complex one, even when we ignore the currents which are present in the ceiling layer. The analysis which follows is more in the nature of a complex dimensional analysis than an attempt to derive flow properties from first principles. Our aim is to develop the scaling parameters in a rational manner. The analysis ignores the influence of the counterflowing jets at the door and the mixing in the impingement region near the back wall opposite the door.

The relationship between the mixing rates and Ri_o may be derived from an assumption that the fresh air enters the room like a turbulent wall jet with a mixing layer separating the hot and cold layers (Figure 2.3). This mixing layer

will grow with x (the distance normal to the door) and reach a stable thickness at a critical local Richardson number, $(Ri_x)_{cr} \approx 0.25$ (Scotti & Corcos 1972). (The term "local Richardson number" refers to the gradient Richardson number at the interface; see section 2.4.) Beyond this point there is no mixing between the hot and cold layers.

The jet may then be divided into two distinct regions: the "supercritical" region where the flow is independent of the downstream conditions and has entrainment characteristics similar to a neutral wall jet; and the "subcritical" region where gravitational forces suppress the mixing between the hot and cold layers. The supercritical and subcritical regions are separated by a not well-defined "hydraulic (or density) jump" region which is characterized by the breaking of internal waves and reverse flow (Chu & Vanvari 1976).

Behind the door, there is a recirculation region which actively exchanges material with both the hot layer and the door jet (Fig. 2.3). Since the flow is steady, the amount of hot layer gas entrained into the recirculation region is equal to the amount of material lost to the door jet. In other words, the door jet is entraining hot layer gas indirectly through the recirculation region. As far as the entrainment process is concerned, it follows then that we may approximate the actual three-dimensional jet whose width varies with x by an "equivalent" two-dimensional jet with a width equal to that of the room. Instead of an initial jet velocity of U_{1c}, the equivalent two-dimensional jet will have an initial velocity of $U_{1c}b/W$. This is equivalent to saying that the jet expands suddenly and instantaneously from an initial width of b (the door width) to a final width of W (the room width). It must be noted that this assumption is a rather drastic simplification of the actual flow.

The basic assumption of the following analysis is that the entrainment characteristics of the inflowing fresh air is similar to that of a two-dimensional

wall jet flowing under a semi-infinite layer of lighter gas; i.e., wall effects and the velocity of the hot layer gas are taken to be negligible. Taylor's entrainment hypothesis (Morton, et. al. 1956) states that the local entrainment rate into a jet is proportional to the local maximum velocity and the local entrainment coefficient, i.e.,

$$\frac{d\dot{m}_d(x)}{dx} = \rho_h E(Ri_x) U_{max}(x) W \tag{3.4}$$

where $\dot{m}_d(x)$ is the mass flowrate of hot layer gas entrained into the mixing layer from the door (x = 0) to station x (the x-axis is the axis normal to the plane of the door); $E(Ri_x)$ is the local entrainment coefficient; and $U_{max}(x)$ is the local maximum velocity of the two-dimensional wall jet.

The entrainment coefficient, E, is a function of the local Richardson number and a function of x since $Ri_x = Ri_x(x)$ (Ellison & Turner 1959). As a first approximation, we will use a simple power law relation between E and x:

$$E(x) = E_0\left[1 - \frac{x}{x_{cr}}\right]^n \tag{3.5}$$

where x_{cr} is defined by $Ri_x(x_{cr}) \equiv (Ri_x)_{cr}$, and E_0 and n are constants to be determined experimentally. For neutral (constant density) wall jets, $E(x) = E_0$ = constant. From the experimental data of Chu & Vanvari (1976), we found that

$$E(Ri_x) \approx 0.036\left[1 - \frac{Ri_x}{(Ri_x)_{cr}}\right]^2 .$$

If we assume that $Ri_x(x) \propto x$ (Scotti & Corcos 1972), the constants E_0 and n in

Eq. 3.5 are 0.036 and 2 respectively.

Since we have not made any measurements of the velocity profiles in the room, we do not know the exact relation between U_{max} and x. To complicate the problem, the jet may be divided into three regions with a different relationship between U_{max} and x for each region (Abramovich 1963): (1) the near field (potential core) region where U_{max} = constant; (2) the far field (self-preserving) region where $U_{max} \propto x^{-n}$, $n > 0$; and (3) a transition region between the near field and far field, usually between 5 and 15 diameters downstream of the jet exit. With few exceptions, most of our entrainment data fall within the transition region. However, we are able to avoid the problems involved in using U_{max} by introducing an alternate velocity scale based on the momentum of the jet (see Appendix A.2):

$$\dot{m}(x)\, U^*(x) = \dot{m}_{1c}\, U_{1c}\, \frac{b}{W} \tag{3.6}$$

where $U^*(x)$ is the new velocity scale; $\dot{m}_{1c}\, U_{1c}$ is the initial jet momentum; $\dot{m}(x) = \dot{m}_{1c} + \dot{m}_d(x)$, the total mass flow at station x; b is the door width; and W is the room width. The term $(\dot{m}_{1c}\, U_{1c})(b/W)$ is the momentum of the jet after the loss due to the sudden expansion of the jet width (from b to W) has been taken into account. The basic assumption of Eq. 3.6 is that the total momentum of the jet does not vary significantly in the supercritical (momentum-dominated) region where the entrainment process takes place, i.e., we have assumed that the losses due to the presence of pressure gradients and wall friction are negligible compared to $(\dot{m}_{1c}\, U_{1c})(b/W)$. In the far field region, U_{max} may be shown to be related to U^* by (see Appendix A.3)

$$U_{max}(x) = A_1 U^*(x) = A_1 \frac{\dot{m}_{1c} U_{1c}}{\dot{m}_{1c} + \dot{m}_d(x)} \frac{b}{W} \tag{3.7}$$

where A_1 is a constant which must be determined experimentally. After substituting Eqs. 3.3, 3.5, 3.6 and 3.7 into Eq. 3.4, we have

$$\left[\frac{\dot{m}_d(x)}{\dot{m}_{1c}} + 1\right] \frac{d(\dot{m}_d(x)/\dot{m}_{1c})}{d(x/Y_i)} = A_1 E_0 \frac{\rho_h}{\rho_\infty} \left[1 - \frac{x}{x_{cr}}\right]^n . \tag{3.8}$$

This equation is valid for the self-preserving region of a turbulent, two-dimensional, constant momentum jet. Note that, since $U^* \rightarrow (b/W)U_{1c}$ as $x \rightarrow 0$, the solution to Eq. 3.8 may extend as far upstream as the near field (potential core) region. If we assume that buoyancy effects prevent mixing for $x > x_{cr}$, the total entrainment rate, $\dot{m}_d \equiv \dot{m}_d(x_{cr})$, can be found by integrating Eq. 3.8 from $x = 0$ to $x = x_{cr}$:

$$\frac{1}{2}\left[\frac{\dot{m}_d}{\dot{m}_{1c}}\right]^2 + \frac{\dot{m}_d}{\dot{m}_{1c}} = A_1 \frac{E_0}{n+1} \frac{\rho_h}{\rho_\infty} \left[\frac{x_{cr}}{Y_i}\right] . \tag{3.9}$$

The critical length, x_{cr}, may be calculated from the definition of the critical local Richardson number, $(Ri_x)_{cr}$:

$$(Ri_x)_{cr} = Ri_x(x_{cr}) = \left[\frac{-\frac{1}{\rho}\frac{\partial \rho}{\partial y} g}{\left(\frac{\partial U}{\partial y}\right)^2}\right]_{x = x_{cr},\, y = Y_i} . \tag{3.10}$$

To evaluate the right hand side of Eq. 3.10, we will make the following approximations for the density gradient:

$$\left[-\frac{1}{\rho}\frac{\partial \rho}{\partial y}\right]_{y=Y_i} \approx \frac{1}{\delta(x)}\frac{\rho_c - \rho_h}{\rho_h} = \frac{1}{\delta(x)}\frac{\Delta\rho}{\rho_h} \tag{3.11}$$

where $\delta(x)$ is the thickness of the mixing layer at station x. For the velocity gradient, we assume that (cf. Chu & Vanvari 1976)

$$\left[\frac{\partial U}{\partial y}\right]_{y=Y_i} \approx \frac{U_{max}(x)}{\delta(x)}. \tag{3.12}$$

For the growth rate of the mixing layer, we will assume that (Abramovich 1963):

$$\delta(x) = A_2 x\ , \qquad (x < x_{cr}) \tag{3.13}$$

where A_2 is approximately 0.23 for two-layer stratified flows with a density ratio of about 1.4 (Abramovich 1963). After substituting Eqs. 3.11 to 3.13 into 3.10 and using Eq. 3.7 to evaluate U_{max}, we have

$$\begin{aligned}(Ri_x)_{cr} &= \frac{\Delta\rho\, g\, \delta(x_{cr})}{\rho_h\, U_{max}^2(x_{cr})} \\ &= \frac{\Delta\rho\, g\, A_2 x_{cr}}{\rho_h A_1^2 \left[\dfrac{\dot{m}_{1c} U_{1c}}{\dot{m}_{1c} + \dot{m}_d(x_{cr})}\dfrac{b}{W}\right]^2}.\end{aligned} \tag{3.14}$$

Eq. (3.14) may then be rearranged to find $\frac{x_{cr}}{Y_i}$:

$$\frac{x_{cr}}{Y_i} = \left[\frac{A_1^2}{A_2}(Ri_x)_{cr}\frac{\rho_h}{\rho_\infty}\left[\frac{b}{W}\right]^2\frac{1}{Ri_0}\right]\left[\frac{\dot{m}_{1c}}{\dot{m}_{1c} + \dot{m}_d(x_{cr})}\right]^2 \tag{3.15}$$

where Ri_o is the overall Richardson number defined in Eq. 3.1. The equation for the entrainment rate into the cold layer is finally obtained by substituting Eq. 3.15 into Eq. 3.9:

$$\left[\frac{1}{2}\left(\frac{\dot{m}_d}{\dot{m}_{1c}}\right)^2 + \frac{\dot{m}_d}{\dot{m}_{1c}}\right]\left[1 + \frac{\dot{m}_d}{\dot{m}_{1c}}\right]^2 = A\,F^2 \tag{3.16a}$$

where

$$A \equiv \frac{A_1^3}{A_2}\frac{E_0}{n+1}(Ri_z)_{cr} \tag{3.16b}$$

$$F \equiv \frac{\rho_h}{\rho_\infty}\frac{b}{W}\frac{1}{\sqrt{Ri_o}}. \tag{3.16c}$$

Using the relationship suggested by Eq. 3.16, the experimental data are replotted in Figure 3.9. From our data, we found the mean value of the empirical constant A to be 11.7 ± 5.3. When we use the mean value of A, Eq. 3.16a becomes

$$\left[\frac{1}{2}\left(\frac{\dot{m}_d}{\dot{m}_{1c}}\right)^2 + \frac{\dot{m}_d}{\dot{m}_{1c}}\right]\left[1 + \frac{\dot{m}_d}{\dot{m}_{1c}}\right]^2 = 11.7\,F^2 \tag{3.17}$$

This is the equation of solid line shown in Figure 3.9. Despite the large deviation of the empirical constant, A, which is attributable to the numerous simplifying assumptions we had made, our simple analysis accurately predicts the shape of the curve. Our analysis did not take into account the following: (1) three-dimensional effects (see, for example, Sforza & Herbst 1970); this would mean that the maximum velocity decay, U_{max}, the entrainment coefficient, E, and the rate of growth of the mixing layer layer may be functions of the door geometry; (2) the presence of the wall normal to the flow has not been taken into account,

i.e., we have not considered the effect of the jet impinging on the wall; (3) the losses due to the presence of wall friction and pressure gradients in the room may be large in certain portions of the room; this is certainly true far downstream of the door where the influence of the wall boundary layer and wall heat transfer are no longer negligible; (4) effect of a counterflowing hot layer.

We can estimate the value of A_1 from our data with the aid of the following relationships obtained from the literature: (1) for the critical Richardson number: $(Ri_x)_{cr} \approx 0.25$ (Scotti & Corcos 1972); (2) for the entrainment coefficient: $E_0 \approx 0.036$ and $n \approx 2$ (Chu & Vanvari 1976); (3) for the growth rate of the mixing layer: $A_2 \approx 0.23$ (Abramovich 1963). With these relationships, we found the mean value of the empirical constant A_1 to be 9.46 ± 1.37 for our range of experiments. The value of A_1 is dependent on the shape of the velocity profile; as a comparison, A_1 is approximately 1.4 for a Gaussian velocity profile (see Appendix A.3).

3.3. Effect of Furnace Temperature

To determine the effect of the magnitude of the furnace temperature, we ran a series of experiments in which the floor suction rate, $\dot{m}_2$, was held constant while the furnace temperature was varied.

The temperature and carbon dioxide concentration profiles for the 12"x26" door are presented in Figure 3.10. As the furnace temperature is decreased the temperature gradient in the hot layer is reduced, and the temperature and carbon dioxide concentration profile shapes become more and more similar. It is interesting to note that, even though the maximum temperature in the hot layer was lowered from 150 °C to 65 °C, the temperatures in the cold layer did not change significantly. The carbon dioxide profiles show a similar behavior. This phenomenon can be explained by the fact that reducing the temperature of the hot gas will reduce the buoyant energy of the hot layer and hence increase

the rate of mixing between the hot and cold layers. Apparently, the increase in mixing rates is just enough to keep the temperature and carbon dioxide concentrations in the cold layer constant. The mixing rates versus Richardson number are plotted in Figures 3.8 and 3.9 as a comparison with the previous results where the furnace temperature was held constant. The data agree very well, and it is observed that the mixing rate increased by a factor of 2.3 when the furnace temperature was reduced by a factor of 1.3. Note that the correlation between the 12'x26" door data points in Figure 3.9 is much better than in Figure 3.8. This suggests that the density ratio, ρ_h/ρ_∞, is an important factor in Eq. 3.16. To summarize: the mixing rate between the hot and cold layers is strongly influenced by the ratios b/W and ρ_h/ρ_∞ in addition to the overall Richardson number defined by Eq. 3.1.

Figure 3.10(c) shows the dimensionless temperature as a function of distance from the interface. As in the case where we held the furnace temperature constant (Figure 3.6(a)), the profiles are similar in shape for furnace temperatures above 67 °C.

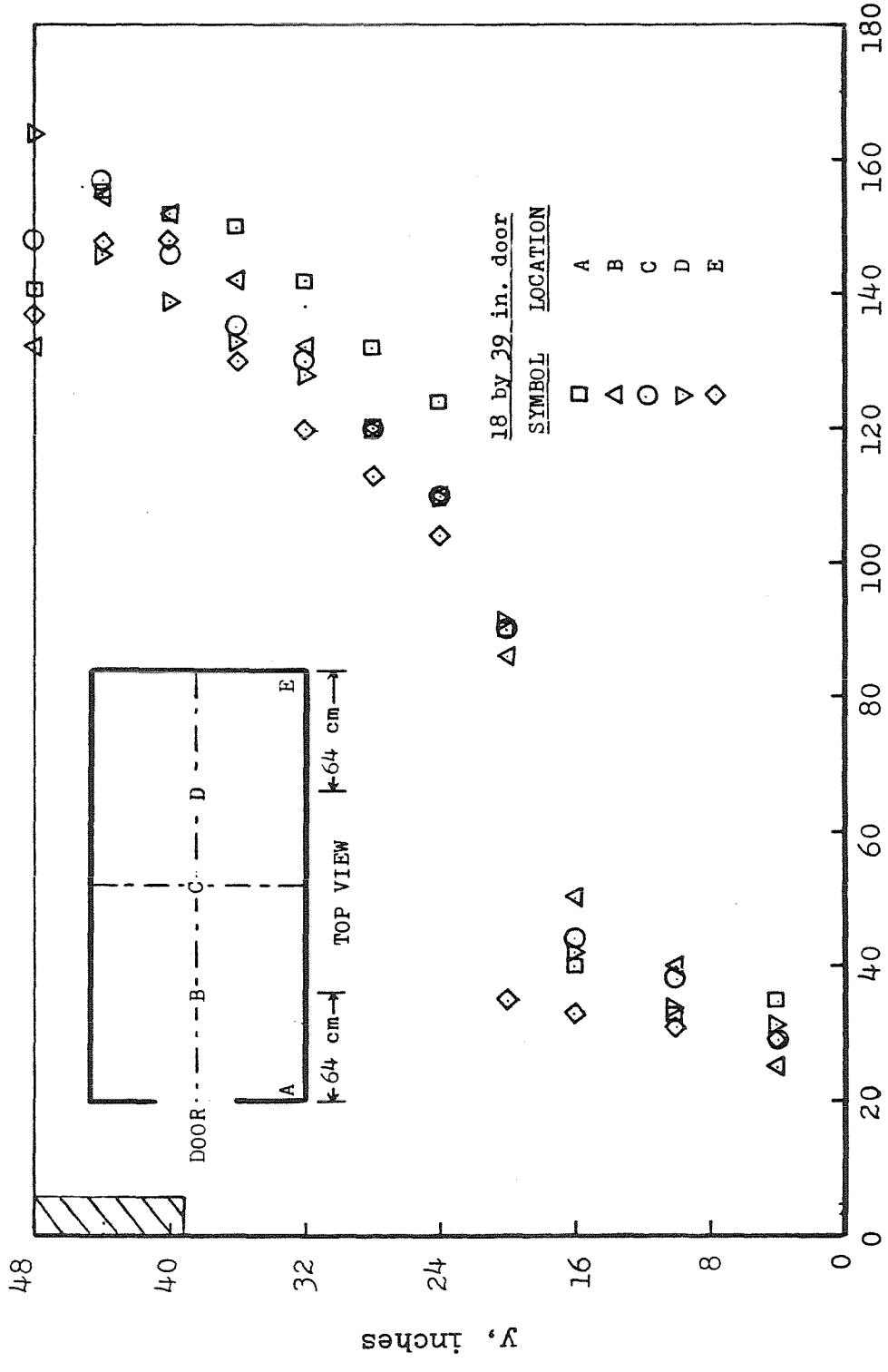
y, inches
TEMPERATURE, °C
18 by 39 in. door
SYMBOL LOCATION
A
B
C
D
E
DOOR
TOP VIEW
64 cm
64 cm

Figure 3.1

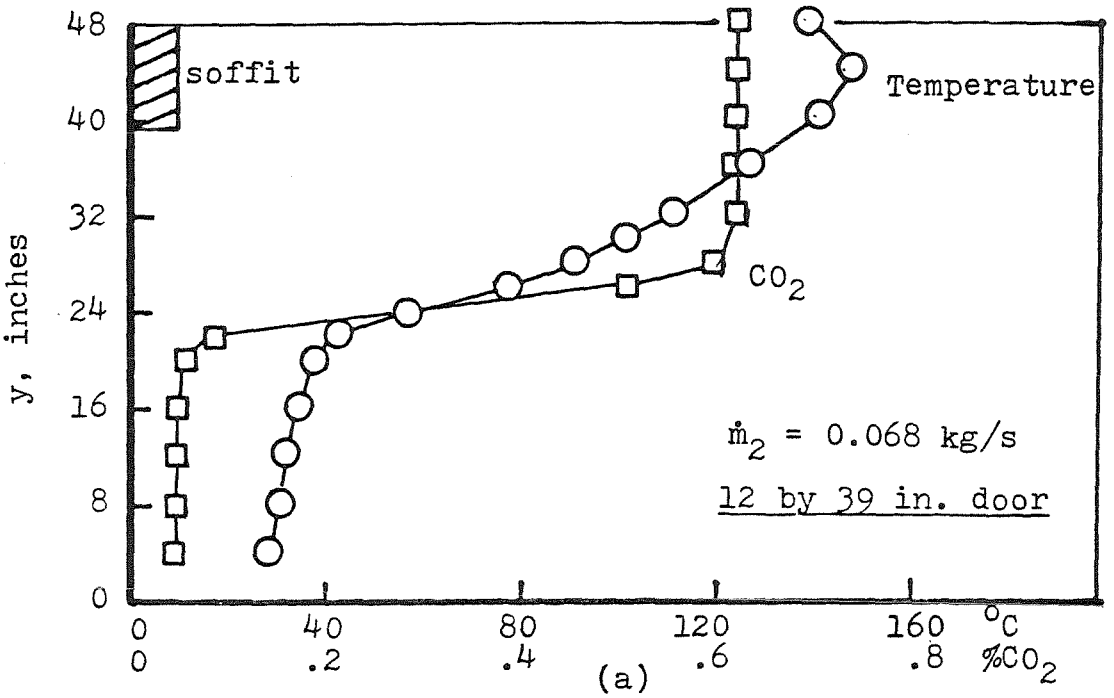
48
40
32
24
16
8
0
y, inches
soffit
Temperature
CO_2
$\dot{m}_2$ = 0.068 kg/s
12 by 39 in. door
0
40
80
120
160
°C
0
.2
.4
.6
.8
$\%CO_2$
(a)

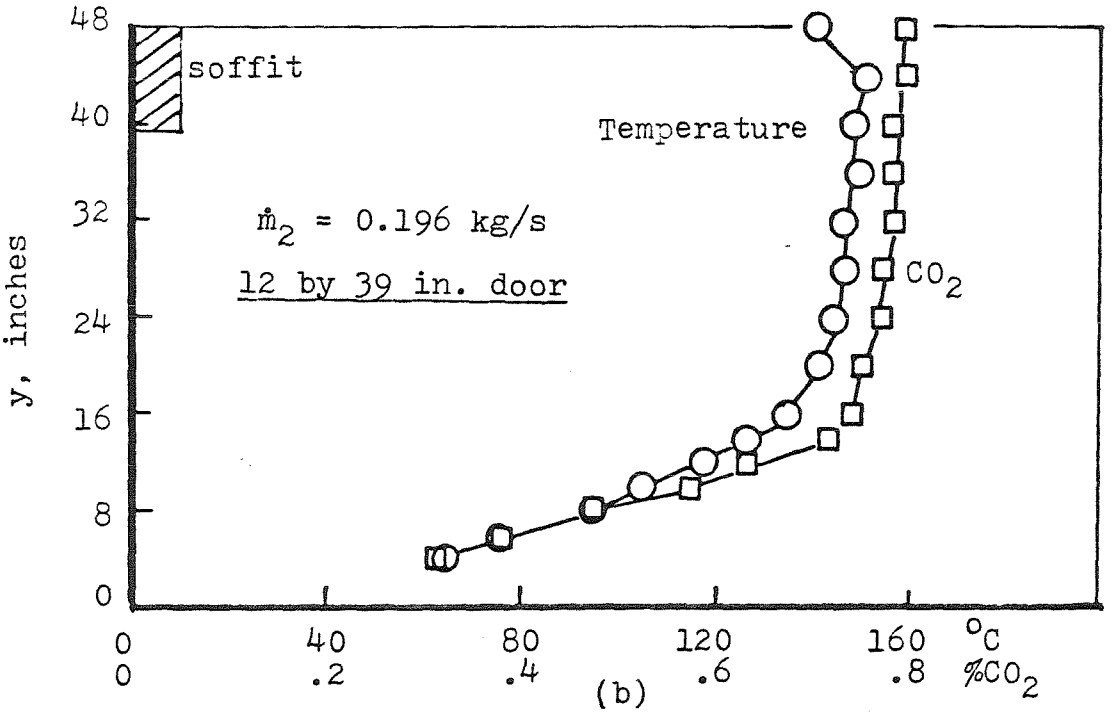
48
40
32
24
16
8
0
y, inches
soffit
Temperature
$\dot{m}_2$ = 0.196 kg/s
12 by 39 in. door
CO_2
0
40
80
120
160
°C
0
.2
.4
.6
.8
$\%CO_2$
(b)

Figure 3.2

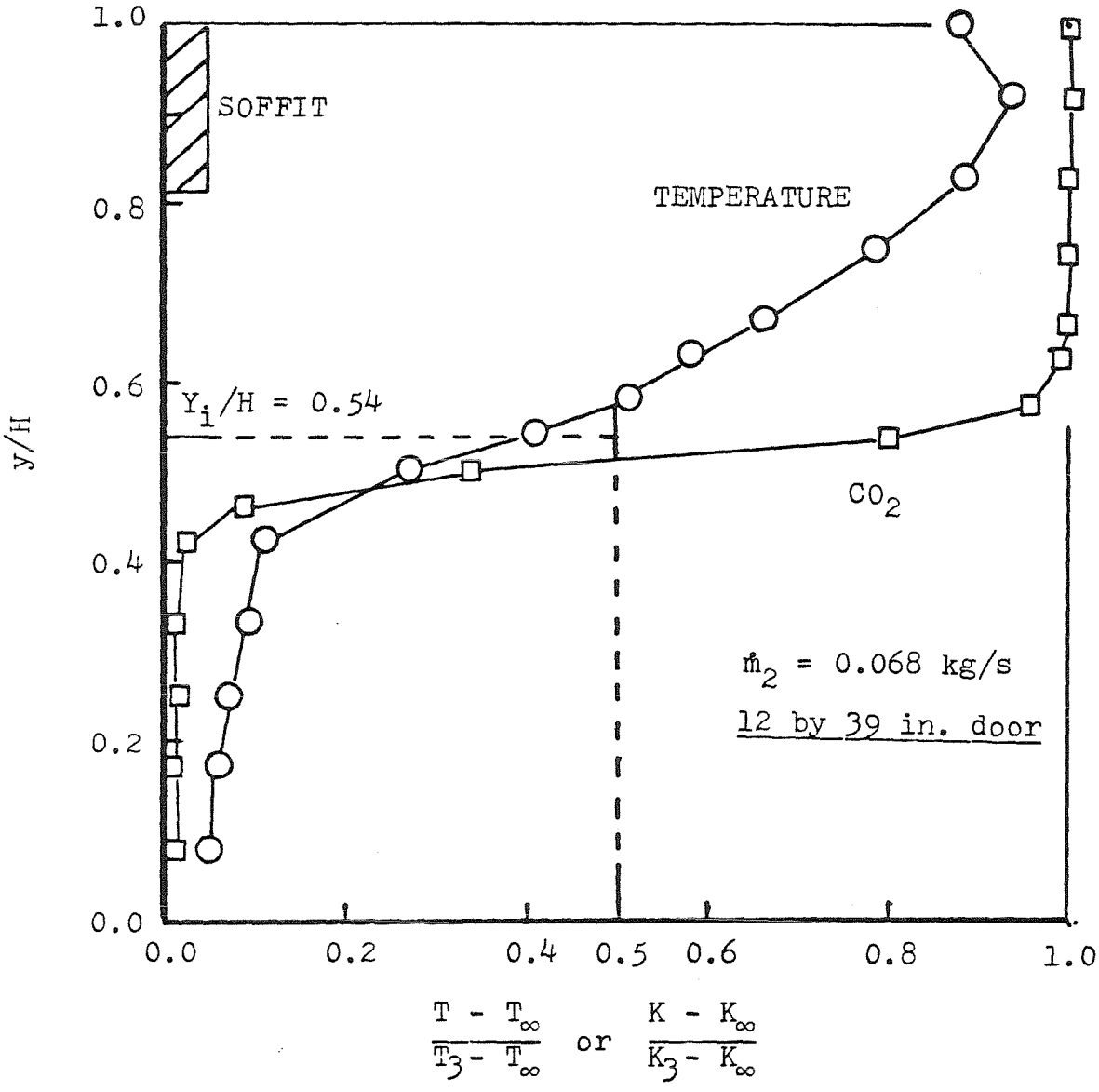
1.0
0.8
0.6
0.4
0.2
0.0
y/H
SOFFIT
TEMPERATURE
$Y_i/H = 0.54$
CO_2
$\dot{m}_2$ = 0.068 kg/s
12 by 39 in. door
0.0
0.2
0.4
0.5
0.6
0.8
1.0
$\frac{T - T_\infty}{T_3 - T_\infty}$ or $\frac{K - K_\infty}{K_3 - K_\infty}$

Figure 3.3

Legend for Figures 3.4 (a,b,c)

Symbol	$\dot{m}_2$, kg/s	Y_i, in.	Run
◇	0.196	7.0	41
△	0.147	13.7	39
+	0.112	17.8	42
▽	0.100	21.1	43
○	0.068	25.4	38
□	0.044	31.2	40

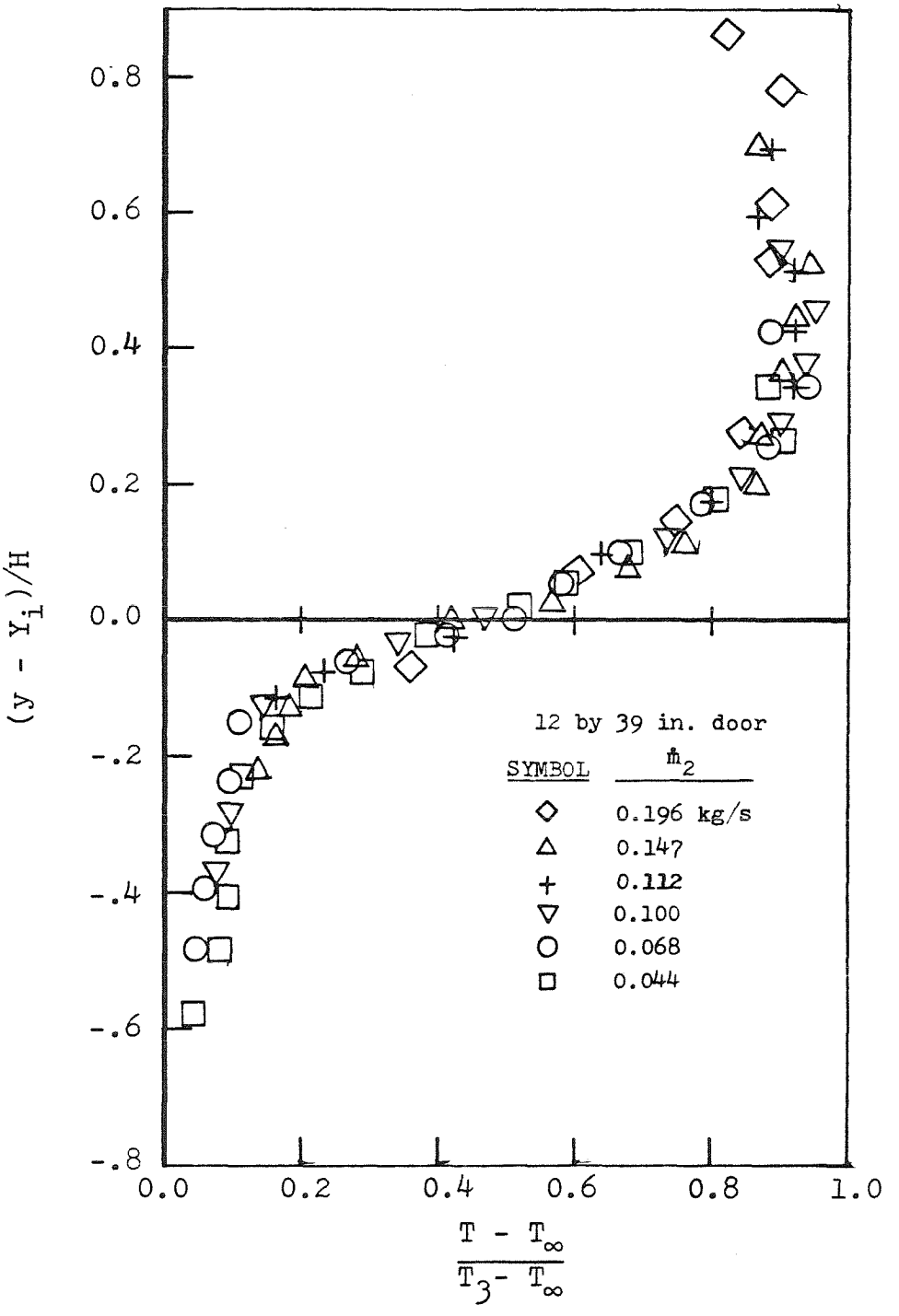
0.8
0.6
0.4
0.2
0.0
-.2
-.4
-.6
-.8
0.0
0.2
0.4
0.6
0.8
1.0
(y - Yi)/H
T - T∞
T3 - T∞
12 by 39 in. door
SYMBOL
ṁ2
0.196 kg/s
0.147
0.112
0.100
0.068
0.044

Figure 3.4(a)

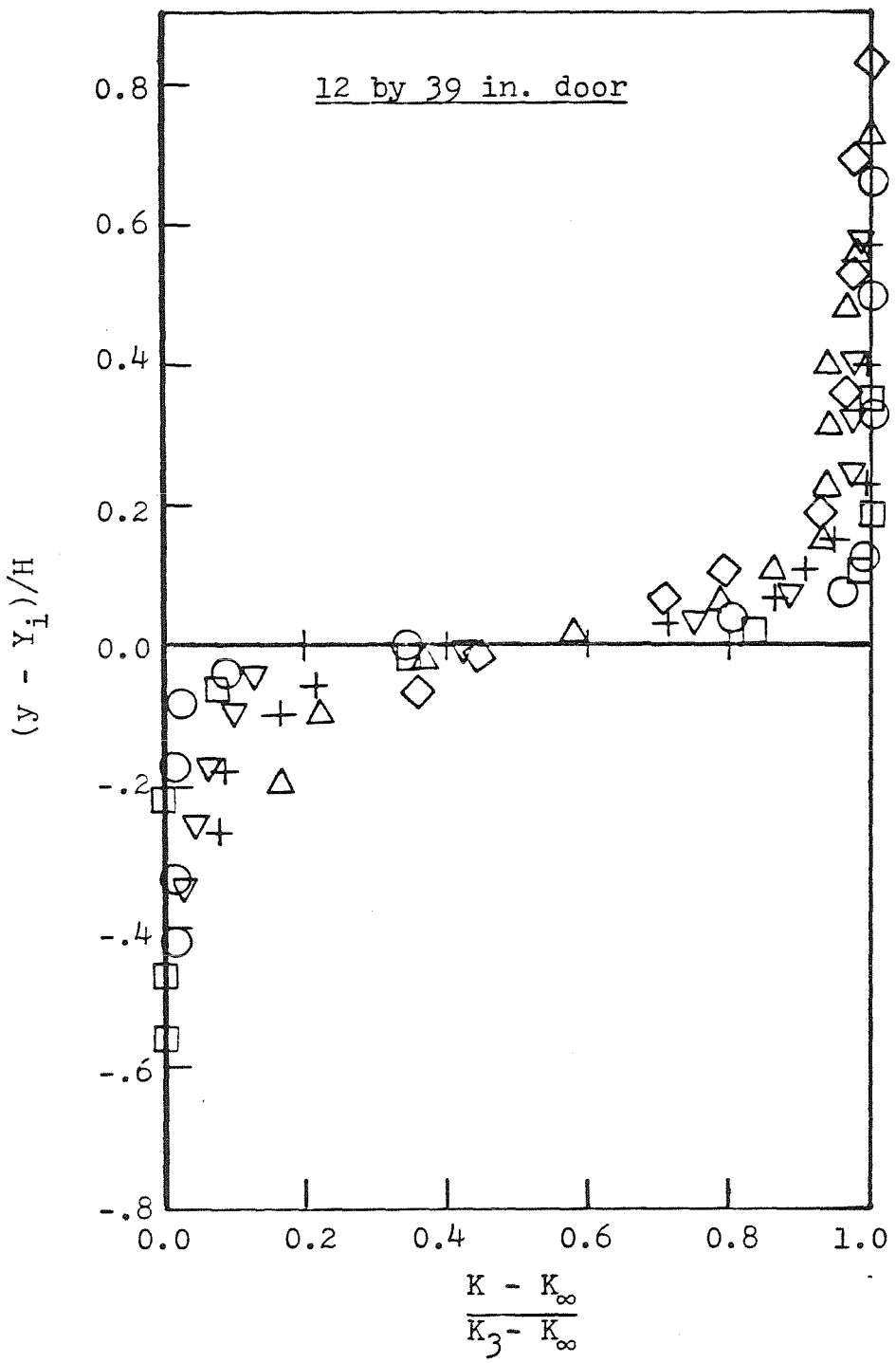

Figure 3.4(b)

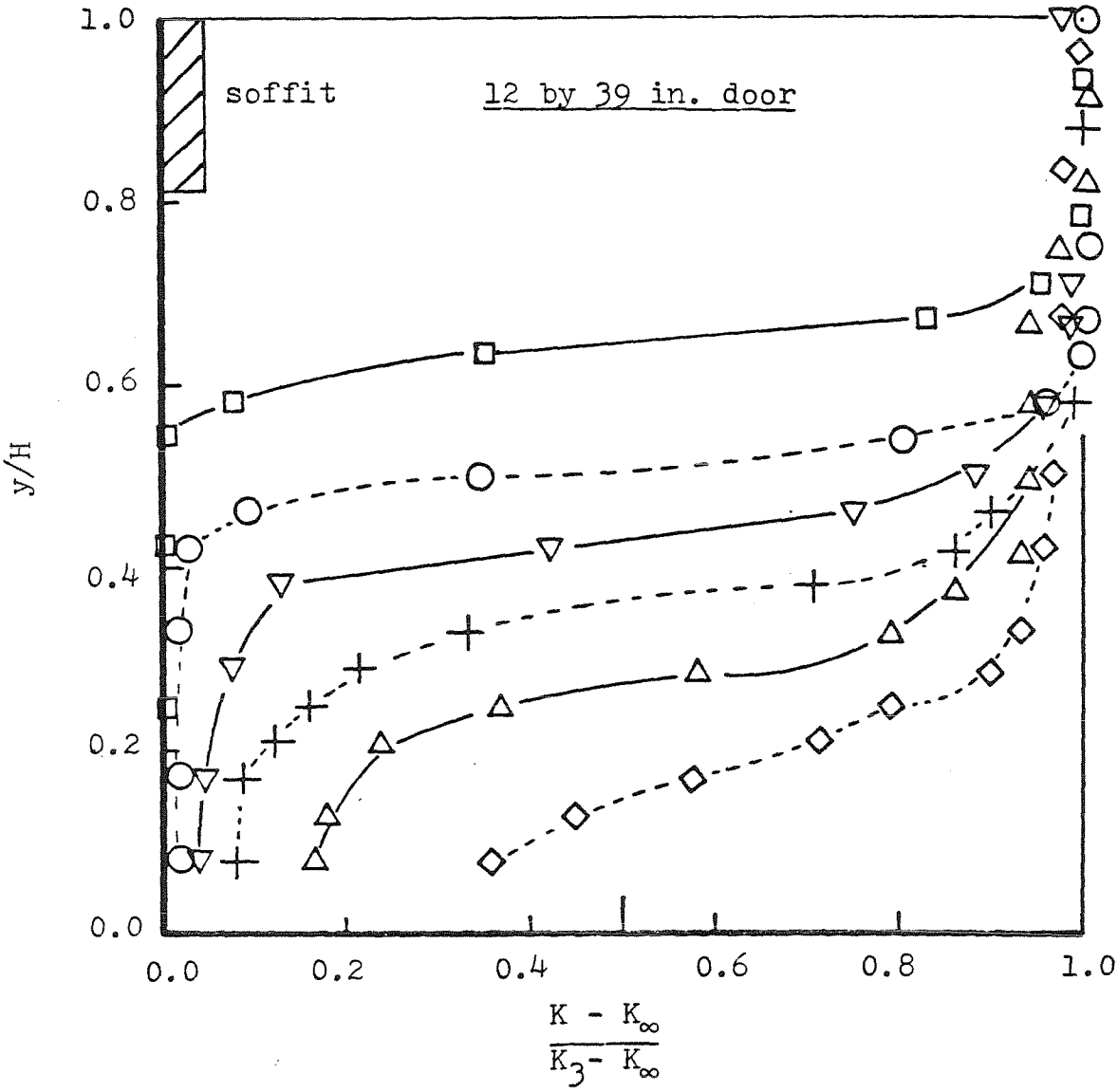

Figure 3.4(c)

Legend for Figures 3.5 (a,b)

Symbol	$\dot{m}_2$, *kg/s*	Y_i, *in.*	Run
⬡	0.200	11.5	31
◇	0.186	14.0	28
△	0.176	14.9	26
▽	0.165	17.3	30
□	0.146	19.7	25
○	0.076	27.6	24
+	0.037	34.3	29

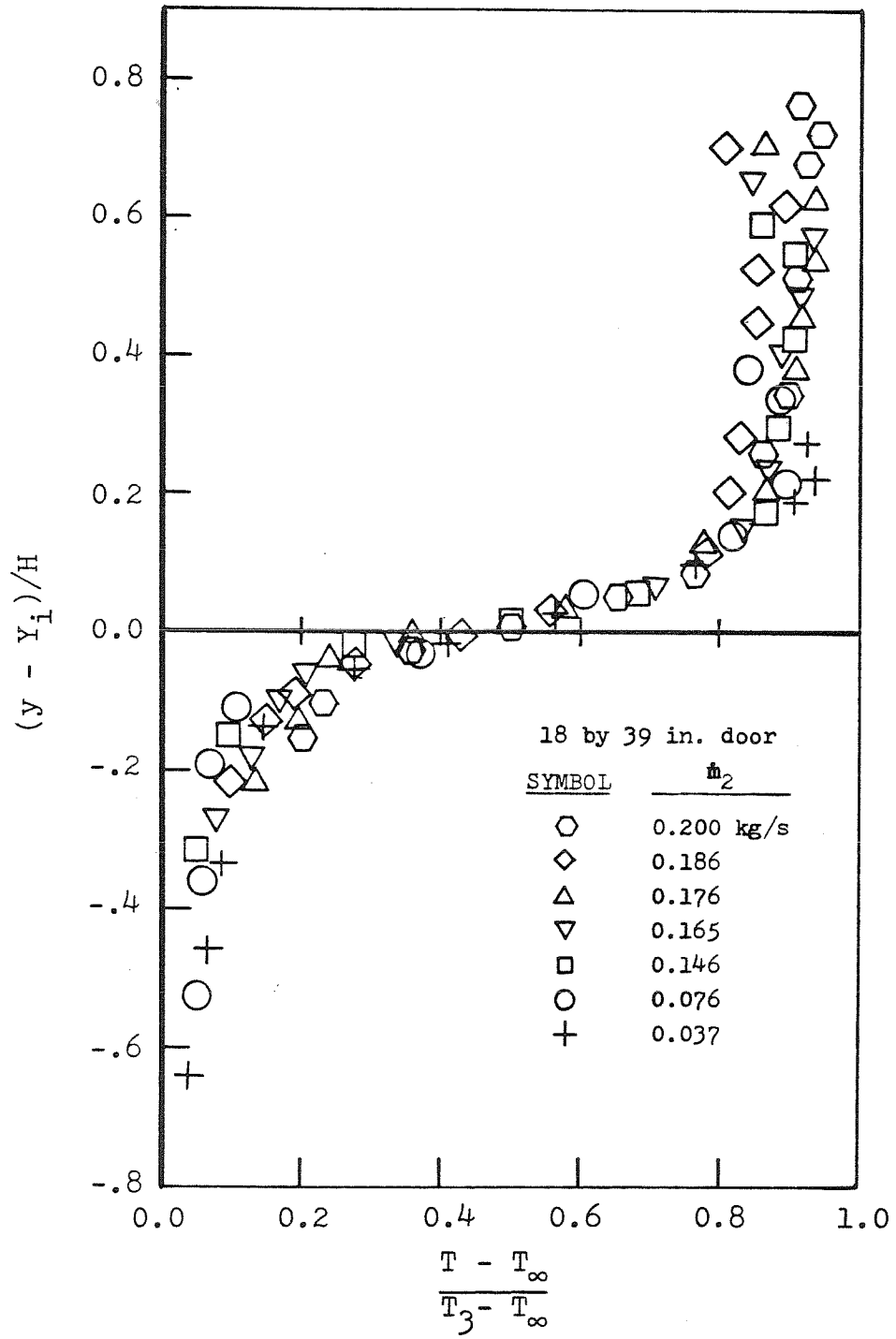
0.8
0.6
0.4
0.2
0.0
-.2
-.4
-.6
-.8
0.0
0.2
0.4
0.6
0.8
1.0
(y - Yi)/H
T - T∞ / T3 - T∞
18 by 39 in. door
SYMBOL
ṁ2
0.200 kg/s
0.186
0.176
0.165
0.146
0.076
0.037

Figure 3.5(a)

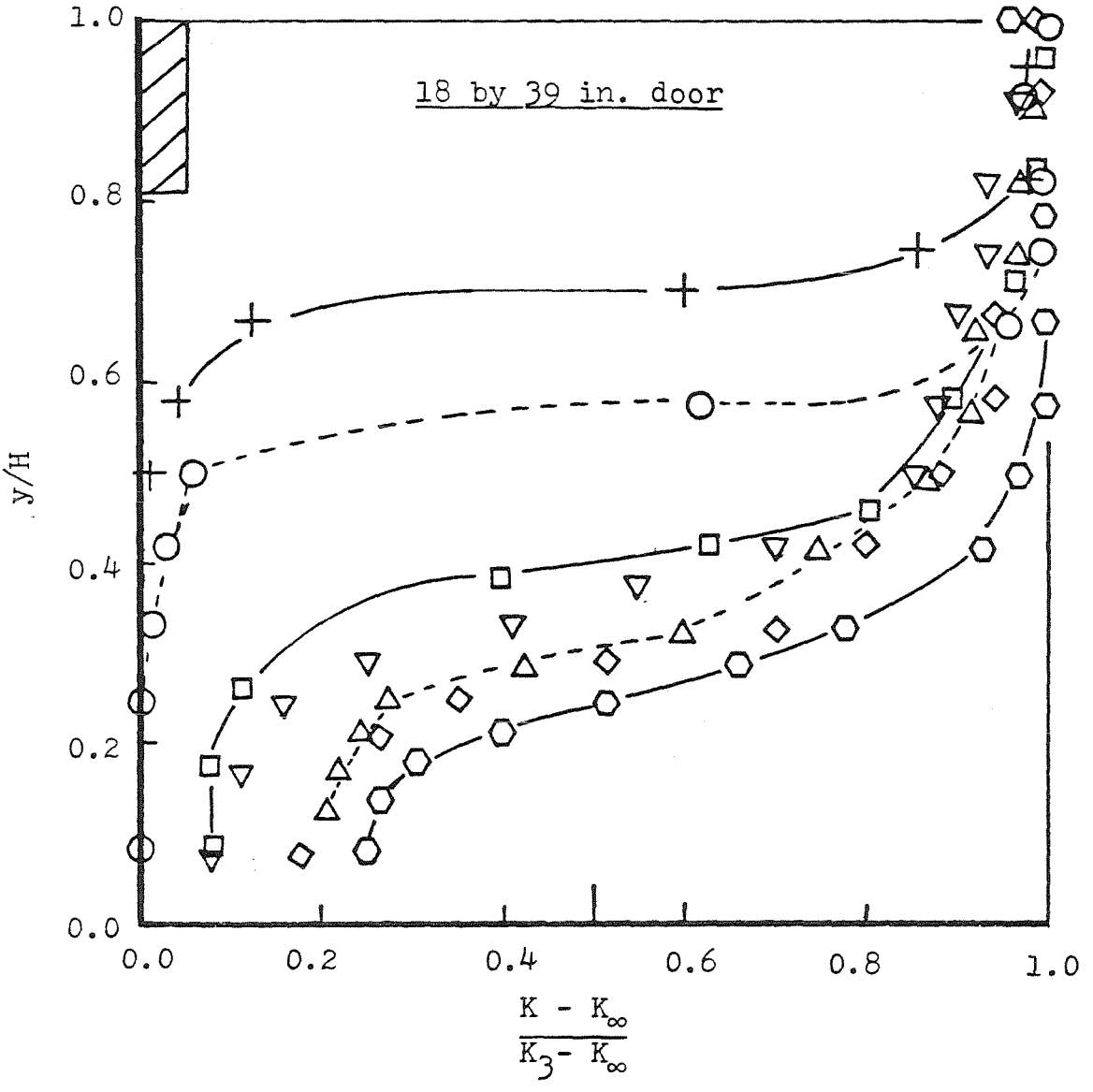

Figure 3.5(b)

Legend for Figures 3.6 (a,b)

Symbol	$\dot{m}_2$, kg/s	Y_i, in.	Run
⬡	0.094	7.2	49
◇	0.078	9.1	47
○	0.067	11.0	44
▽	0.057	13.4	48
□	0.044	15.4	45
△	0.033	18.7	46

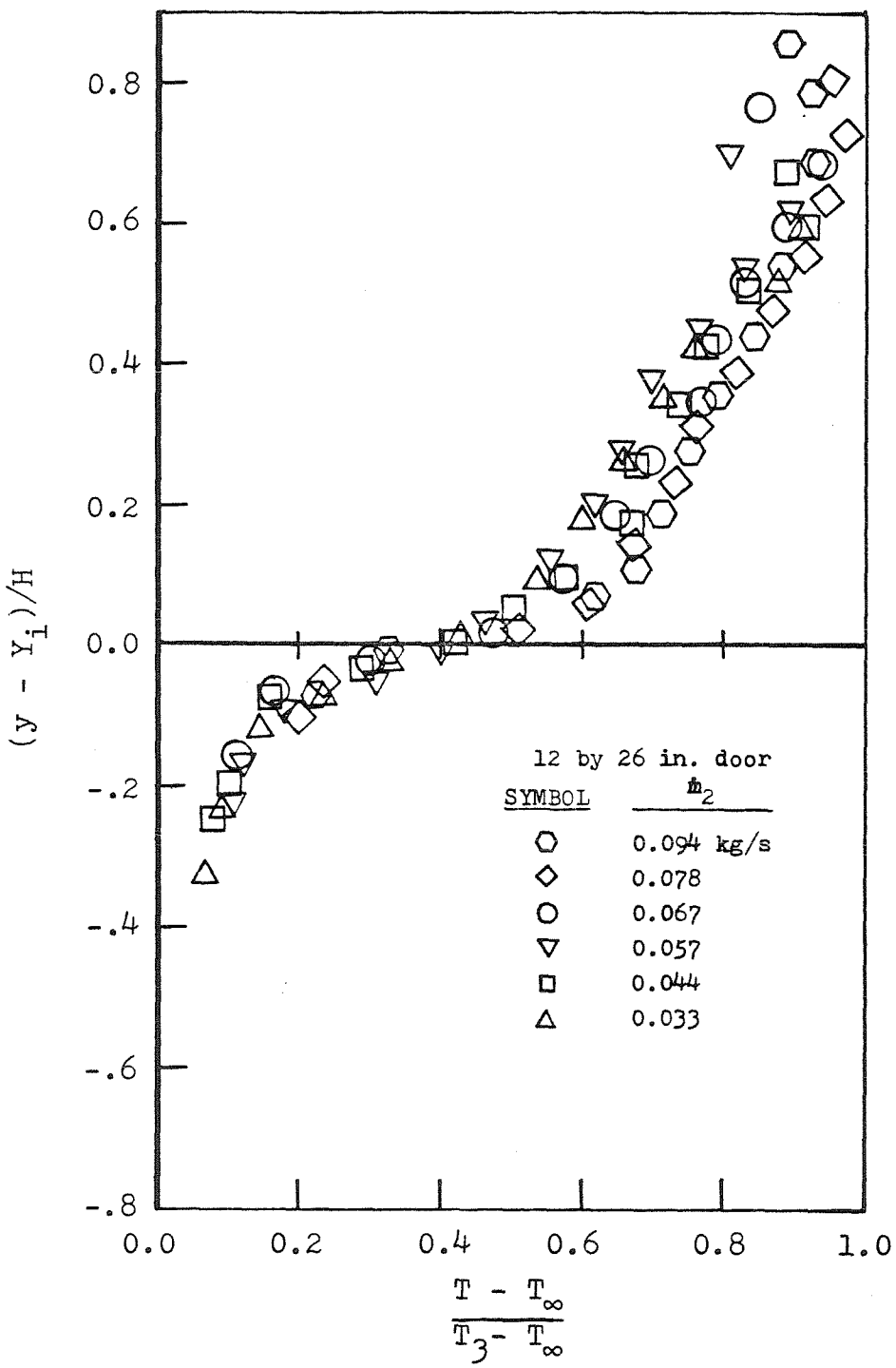
0.8
0.6
0.4
0.2
0.0
-.2
-.4
-.6
-.8
0.0
0.2
0.4
0.6
0.8
1.0
(y - Y_i)/H
(T - T∞)/(T3 - T∞)
12 by 26 in. door
SYMBOL
ṁ2
0.094 kg/s
0.078
0.067
0.057
0.044
0.033

Figure 3.6(a)

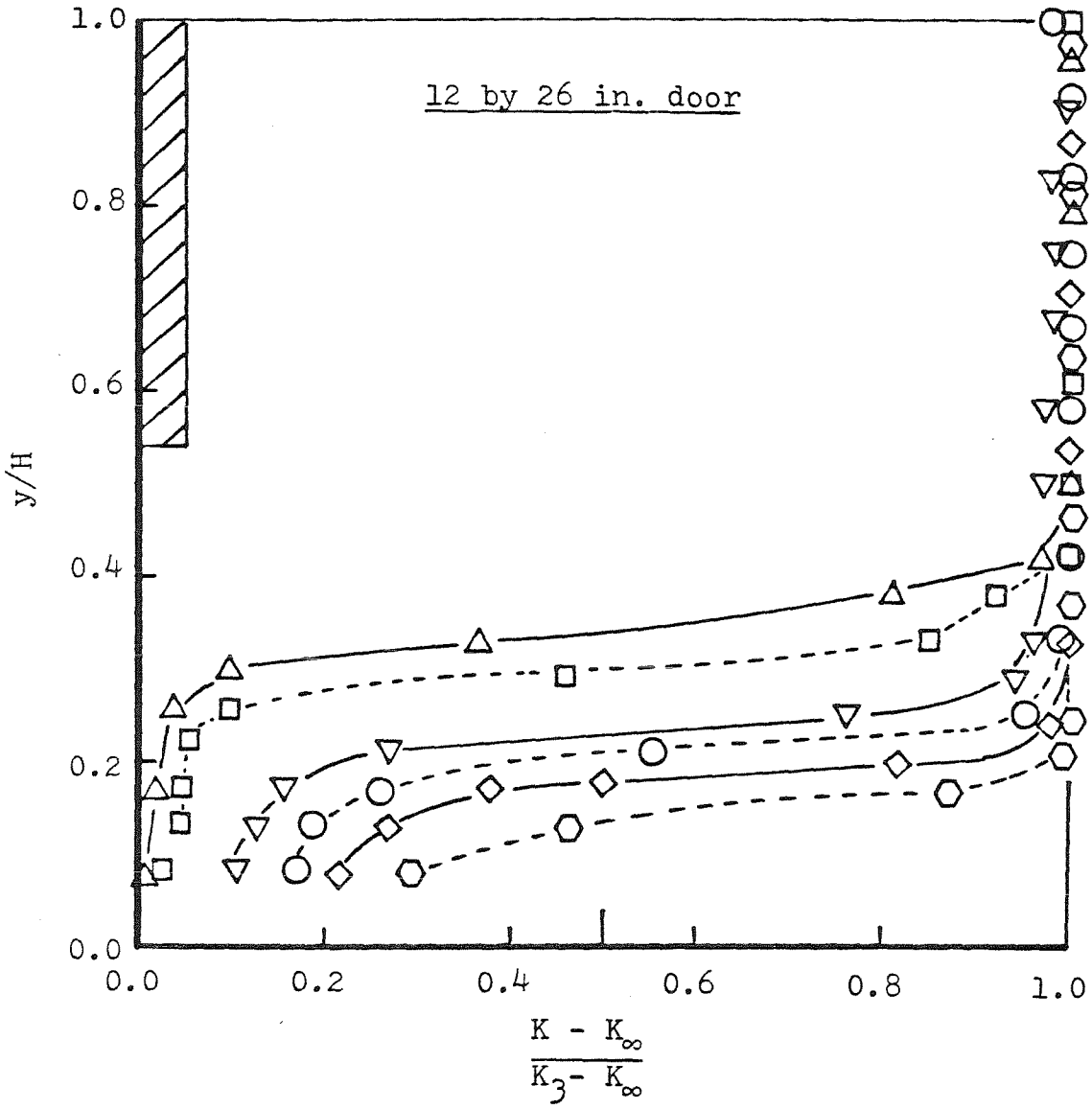

Figure 3.6(b)

Legend for Figures 3.7 (a,b)

Symbol	$\dot{m}_2$, kg/s	Y_i, in.	Run
△	0.208	4.3	34
▽	0.146	6.5	36
○	0.067	11.0	32
◇	0.067	13.2	35
⬡	0.050	15.8	37
□	0.030	18.2	33

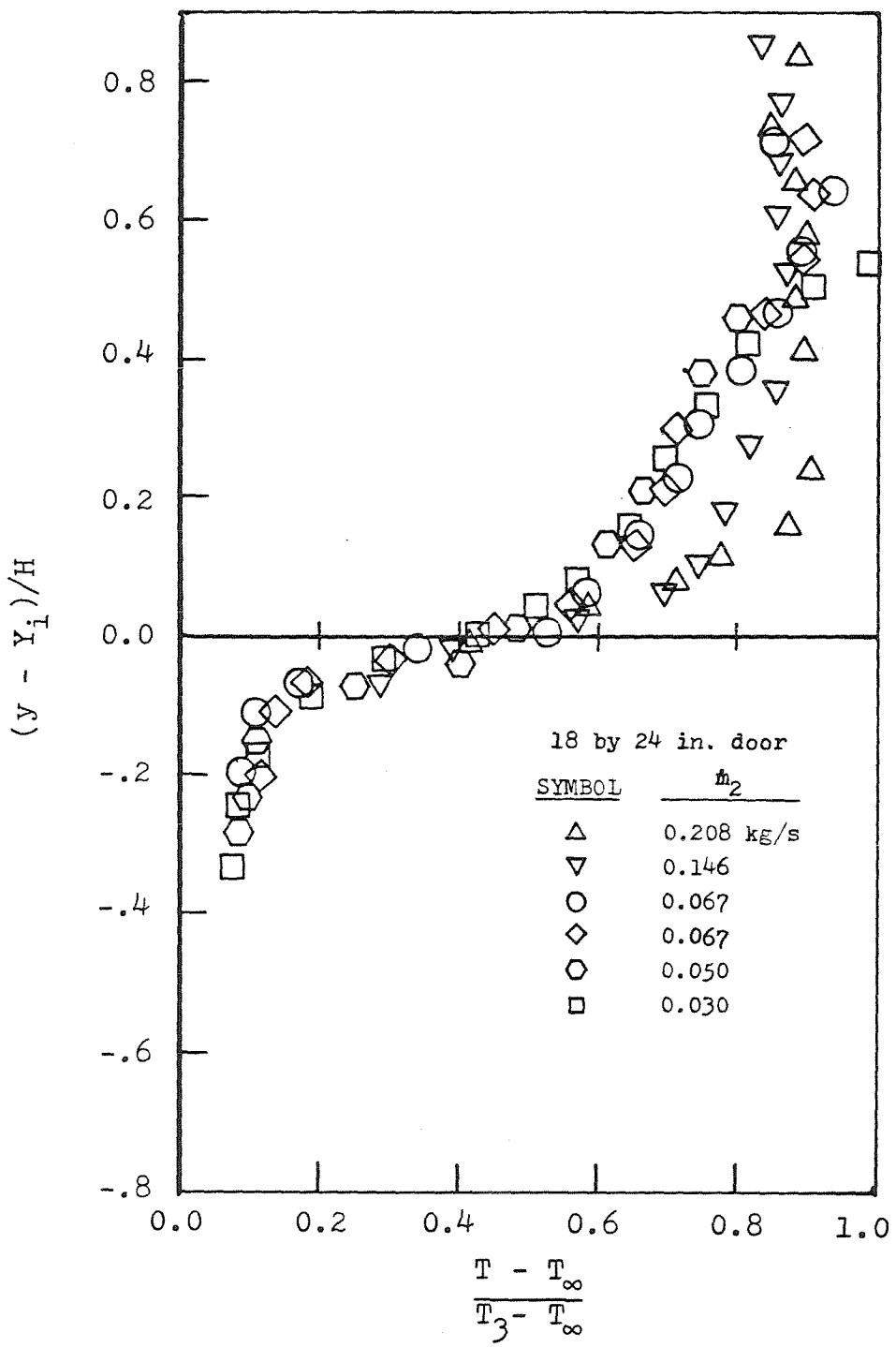
0.8
0.6
0.4
0.2
0.0
-.2
-.4
-.6
-.8
0.0
0.2
0.4
0.6
0.8
1.0
(y - Y_i)/H
(T - T∞)/(T3 - T∞)
18 by 24 in. door
SYMBOL
ṁ2
0.208 kg/s
0.146
0.067
0.067
0.050
0.030

Figure 3.7(a)

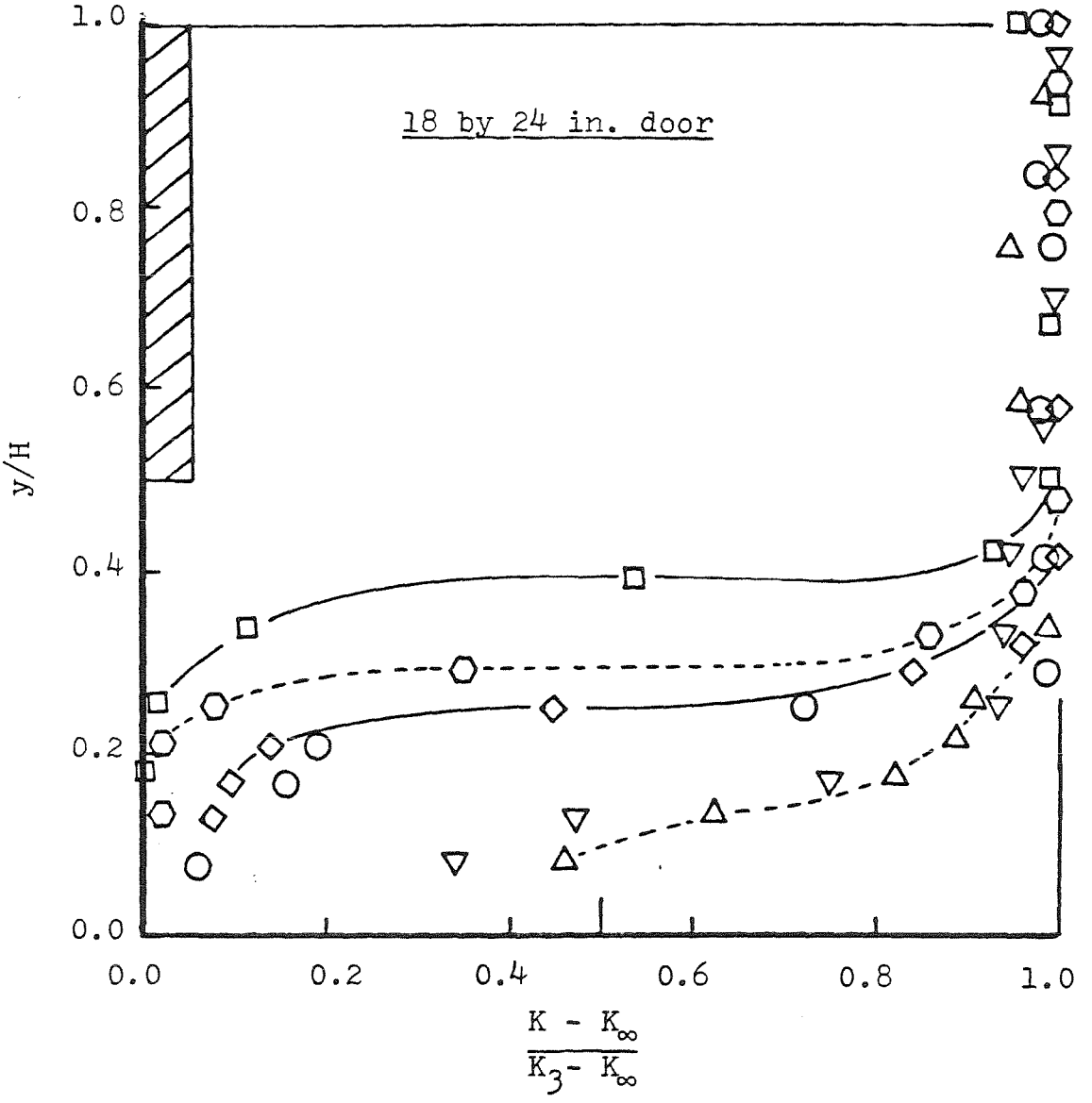

Figure 3.7(b)

Legend for Figures 3.8 and 3.9

Symbol	Door Geometry	
⊙	18"x39"	
◇	18"x24"	
⊡	12"x39"	
△	12"x26"	
◺	12"x26"	variable T_s

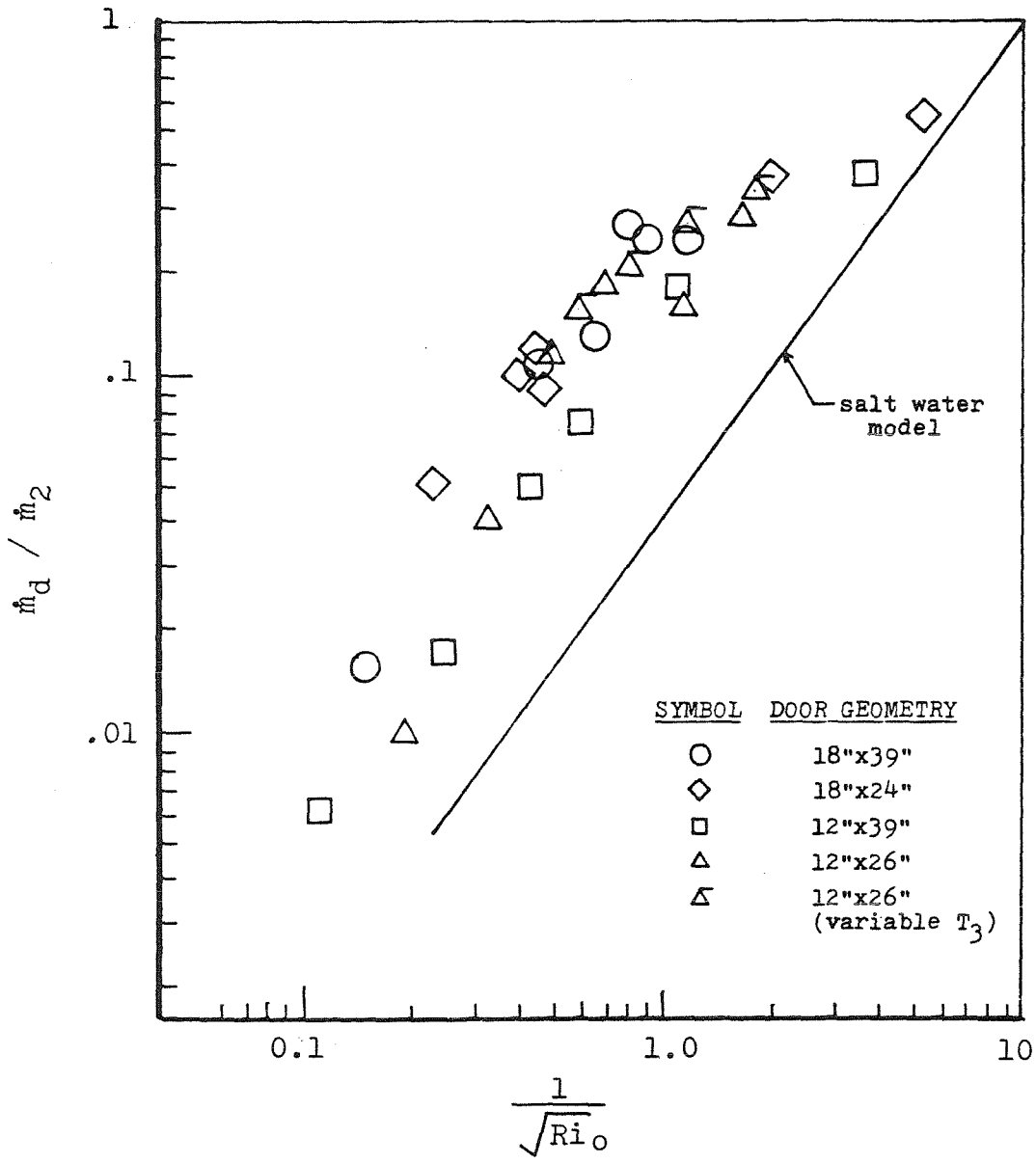
1
.1
.01
$\dot{m}_d / \dot{m}_2$
0.1
1.0
10
$\frac{1}{\sqrt{Ri_o}}$
salt water model
SYMBOL
DOOR GEOMETRY
18"x39"
18"x24"
12"x39"
12"x26"
12"x26" (variable T_3)

Figure 3.8

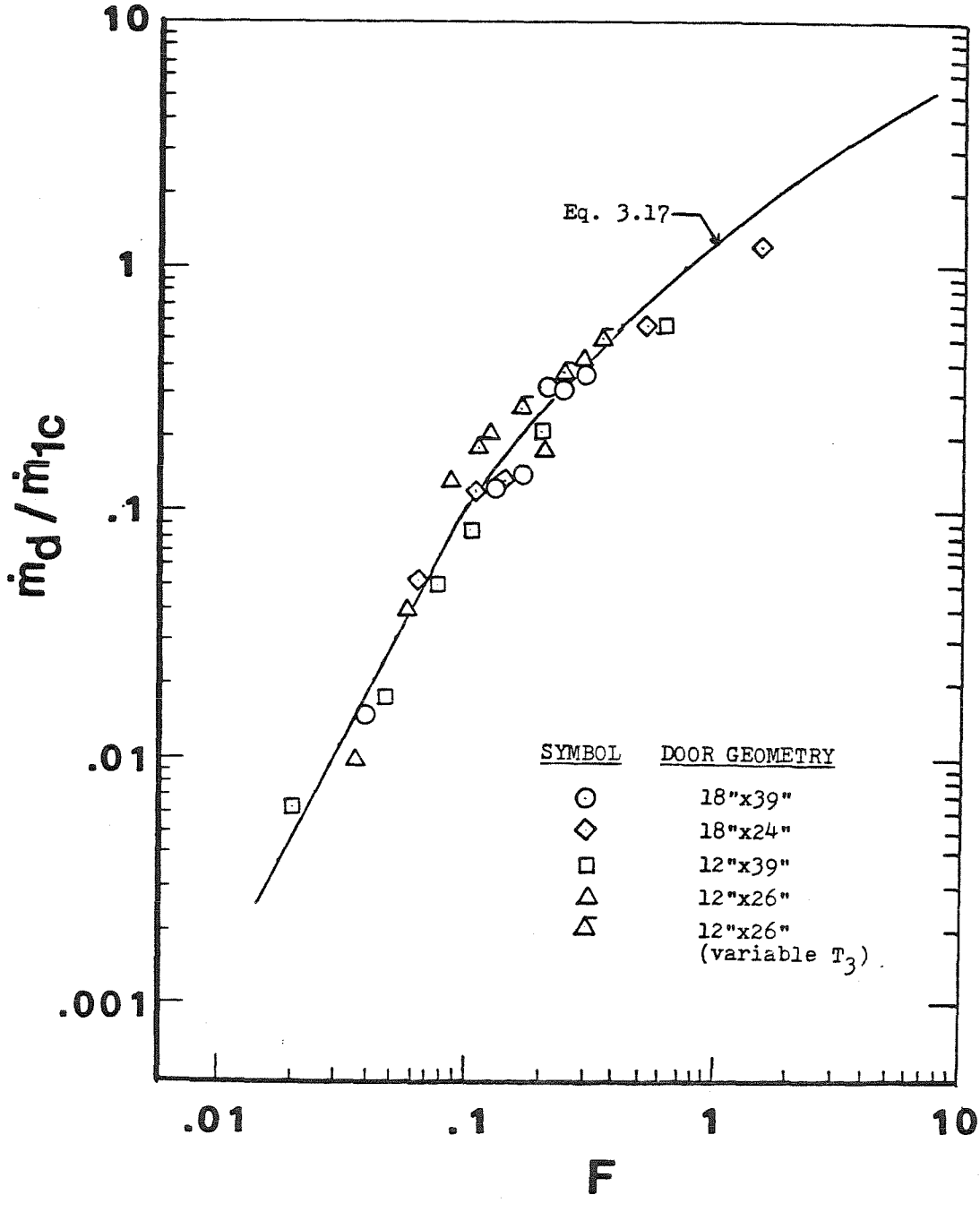
10
1
.1
.01
.001
$\dot{m}_d / \dot{m}_{1c}$
Eq. 3.17
SYMBOL
DOOR GEOMETRY
18"x39"
18"x24"
12"x39"
12"x26"
12"x26"
(variable T_3)
.01
.1
1
10
F

Figure 3.9

Legend for Figures 3.10 (a,b,c)

Symbol	T_3, °C	Y_i, in.	Run
○	166	13.4	48
⊡	131	12.0	50
△	98	10.3	52
⬡	67	9.0	53

$\dot{m}_2 = 0.057$ kg/s

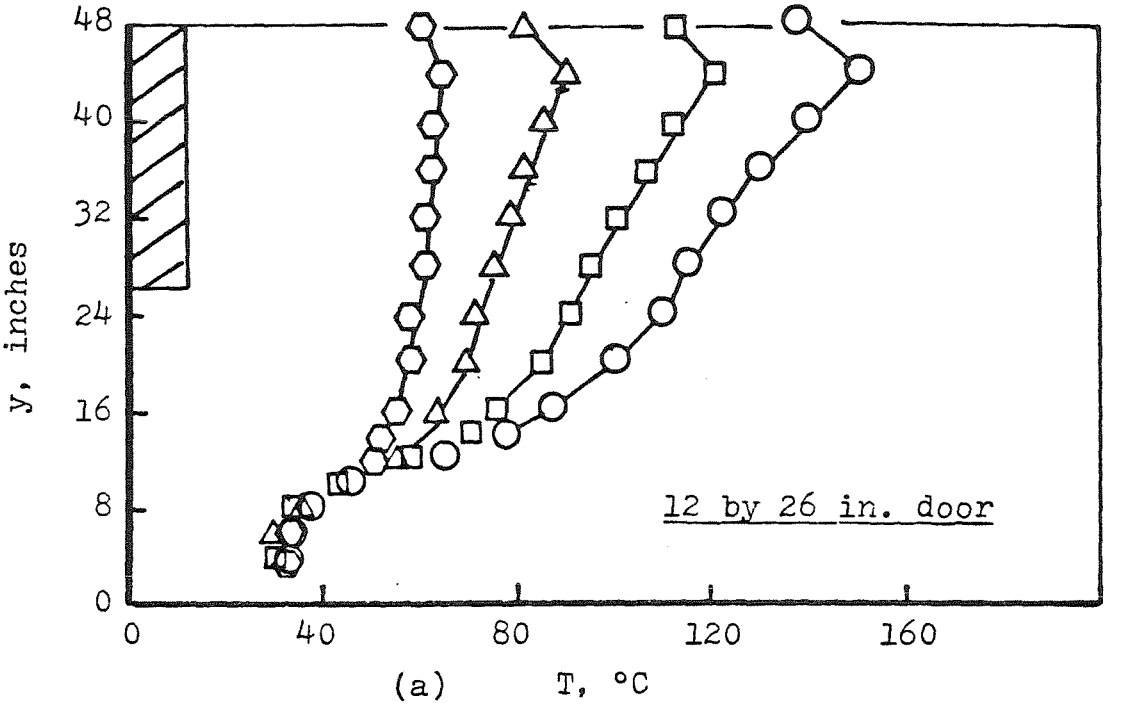
48
40
32
24
16
8
0
y, inches
0
40
80
120
160
12 by 26 in. door
(a) T, °C

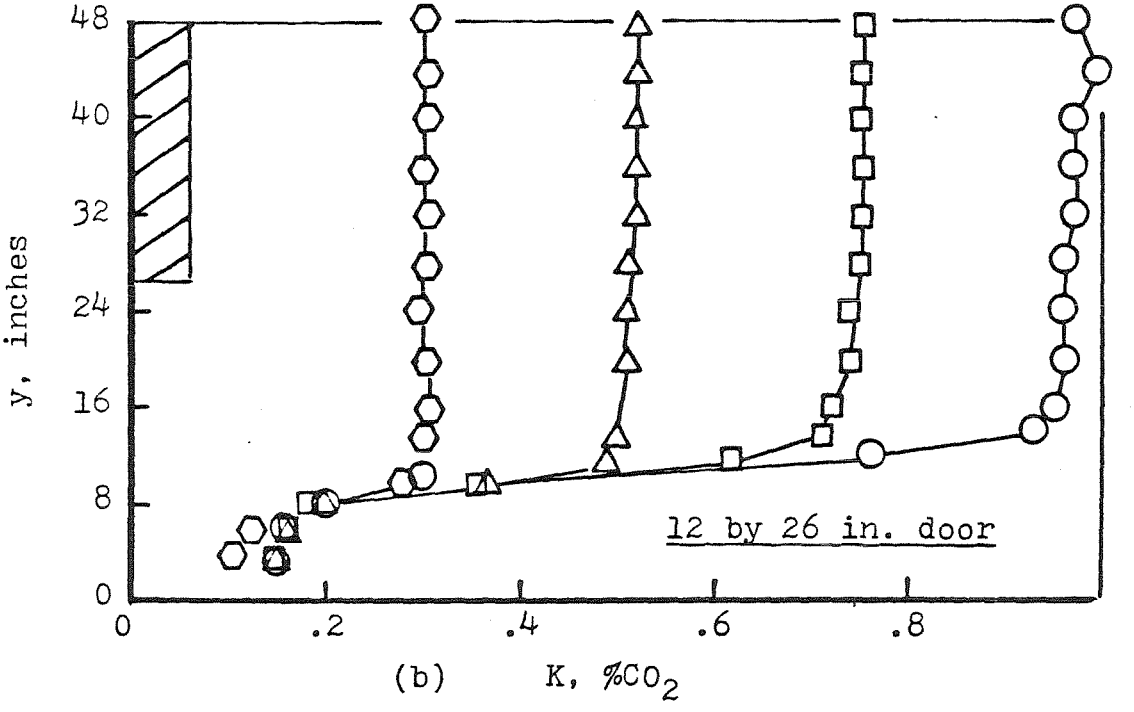
48
40
32
24
16
8
0
y, inches
0
.2
.4
.6
.8
12 by 26 in. door
(b) K, %CO2

Figure 3.10

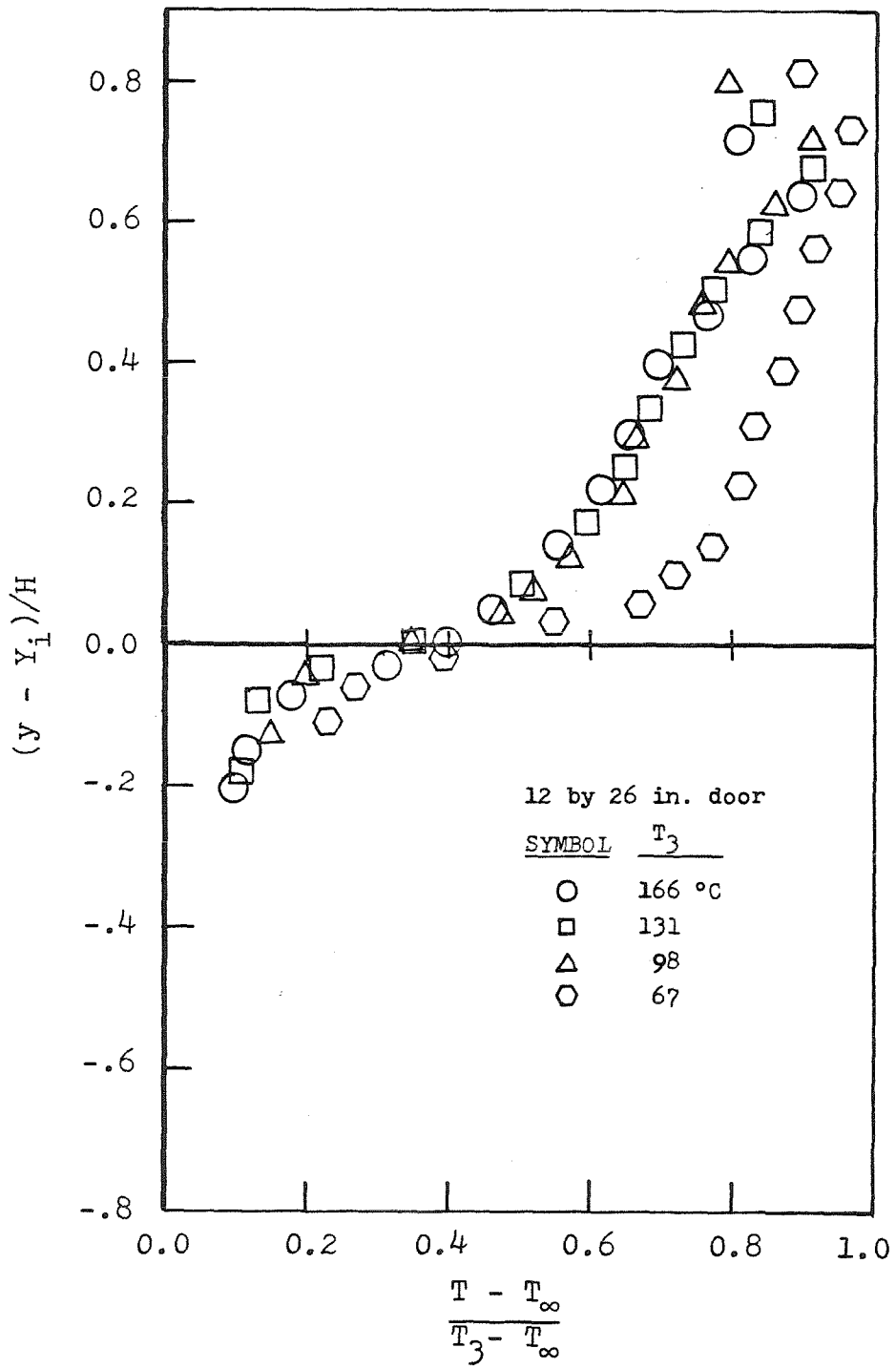
0.8
0.6
0.4
0.2
0.0
-.2
-.4
-.6
-.8
0.0
0.2
0.4
0.6
0.8
1.0
(y - Y_i)/H
(T - T∞)/(T3 - T∞)
12 by 26 in. door
SYMBOL T3
166 °C
131
98
67

Figure 3.10(c)

Chapter 4

ENTRAINMENT IN FIRE PLUMES

4.1. Experimental Technique and Apparatus

The primary purposes of the experiment are to measure the air entrainment rates, $\dot{m}_E$, in the near field of a buoyant diffusion flame where the interface height is below the top of the flames and to determine the chemical composition of the product gas in the hot layer above the interface. The entrainment rates and the gas composition are expressed as functions of the interface height, Z_i; heat release rate, $\dot{Q}_f$; and the initial fire geometry, D. A 0.19 m. diameter stainless steel burner was used in all the experiments. This experiment is an extension of the work done by Cetegen (1982).

The method used to measure the mass flow rates in the near field of the fire plume was based upon measuring the fuel flow rate and the mole fractions of combustion products taken from a small hood. The apparatus used in the experiments is shown in Figure 4.1. The burner is under a 1.2 meter cubical hood which is inside a much larger hood. The small hood is made out of steel and is lowered upon the fire by a pulley mechanism. The large hood dimensions are 2.4x2.4x1.56 m. deep; it is made out of steel and insulated with 10 cm. thick glasswool.

The hot gas was allowed to spill out under the edges of the bottom side of the small hood and up into the large hood where an exhaust fan was used to remove the gas from the laboratory. Two layers of 16x18 mesh screens made of 0.05 cm diameter wire were placed around the large hood so as to reduce the disturbances present in the laboratory air as this gas was sucked into the plume by

the entrainment process. The location of the hot-cold gas interface was determined by a shadowgraph system.

A sample of combustion products was withdrawn from inside the small hood at a rate of about 1.25 liters/minute through a 6.4 mm. diameter stainless-steel tube. An aspirated chromel-alumel thermocouple with a radiation shield was placed at the entrance of the probe to measure the incoming gas temperature. The sample was first sent through two cold (ice) baths to remove the moisture, then filtered to remove the particulates in the gas stream. The sample was then sent through a Beckman Model 864 Nondispersive Infrared CO_2 analyzer, a Beckman Model 400 Flame Ionization Hydrocarbon (CH_4) analyzer, a Beckman Model 755 O_2 analyzer, and an Anarad Model AR-600 Infrared CO analyzer. The analyzers would then give the mole fractions of CO_2, CO, O_2, and CH_4 in the dried sample.

By assuming that the sample was completely free of water vapor and solid carbon (soot), the measured mole fractions of CO_2, CO, O_2, and CH_4 were used (by mass balance) to calculate the actual mole fractions of CO_2, CO, O_2, CH_4, N_2, H_2, and H_2O. The equivalence ratio, φ, was then computed along with the entrainment rate, $\dot{m}_E$.

The fuel used in the experiments was city gas (methane) taken without processing from the Southern California Gas Company mains. The lower heating value of the methane fuel is about 47.5 MJ/kg and the density is about 0.72 kg/m^3 at 20 degrees Celsius and one atmosphere. A Meriam laminar flowmeter was used to measure the volume flow rate of the fuel.

The fuel was fed into the flame after passing through a porous bed of spherical glass beads, whose surface was made flat and flush with the metal edge of the burner. The burner used in the experiments had a diameter of 0.19 m. and

had a 5 cm. thick layer of 6.3 mm. diameter glass beads. The burner-hood set-up described above is identical to the one used by Cetegen (1982) in his experiments.

4.2. Calculation of Species Concentrations

The combustion of methane in the presence of x moles of excess air can be written as

$$\left[CH_4 + (2+x)(O_2 + 3.76N_2)\right] \rightarrow \left[n_{CO_2}CO_2 + n_{CO}CO + \right.$$
$$\left. + n_{CH_4}CH_4 + n_{O_2}O_2 + n_{H_2O}H_2O + n_{H_2}H_2 + n_{N_2}N_2 + n_C C\right] \qquad (4.1)$$

where n_i represents the number of moles of species i per mole of CH_4 fuel input. The air entrainment rate can then be calculated if the composition of the products is known.

In our experiments, the concentrations of CH_4, CO_2, CO, and O_2 in a dried sample were measured, and the concentration of solid carbon (soot) was assumed to be negligible. To calculate the mole fractions of the other species, mass balance equations were written for each of the elements O, C, H, and N. Then by manipulating the equations, we were able to obtain the following equations for the concentrations of the other species in the dried sample (see Appendix B):

$$Y_{N_2} = \frac{1}{0.4681}\left[Y_{CH_4} - 3Y_{CO_2} - 2Y_{CO} - 3Y_{O_2} - \frac{2}{N_{sample}} + 1\right] \qquad (4.2)$$

$$Y_{H_2O} = 2\left[\frac{1}{3.76}Y_{N_2} - Y_{CO_2} - Y_{O_2}\right] - Y_{CO} \qquad (4.3)$$

$$Y_{H_2} = \frac{2}{N_{sample}} - 2Y_{CH_4} - Y_{H_2O} \tag{4.4}$$

where Y_i is the mole fraction of species i in the dried sample, and N_{sample} is the total number of moles in the dried sample per mole of CH_4 fuel input, i.e.,

$$N_{sample} = n_{CO_2} + n_{CO} + n_{CH_4} + n_{O_2} + n_{N_2} + n_{H_2}$$

and it may be shown that

$$N_{sample} = \frac{1}{Y_{CO_2} + Y_{CO} + Y_{CH_4}}. \tag{4.5}$$

It must be noted that since water vapor was not present in the analyzed sample, the term Y_{H_2O} does not represent the mole fraction of water vapor in the sample. The term Y_{H_2O} is simply defined to be the ratio of the number of moles of water in the initial sample, n_{H_2O}, to the total number of moles in the *dried* sample.

To obtain the actual mole fractions of the species in the ceiling layer, the sample mole fractions, Y_i, must be multiplied by the factor $\frac{1}{1 + Y_{H_2O}}$. Thus,

$$\bar{Y}_i = \frac{Y_i}{1 + Y_{H_2O}} \tag{4.6}$$

where $\bar{Y}_i$ is the actual mole fraction of species i in the ceiling layer.

Finally, the equivalence ratio, φ, of the reactants is given by

$$\varphi = \frac{2}{2 + x} = \frac{7.52}{Y_{N_2} N_{sample}}. \tag{4.7}$$

The equivalence ratio is defined to be the fuel-air ratio divided by the stoichiometric fuel-air ratio (= 0.056 for methane fuel).

The derivations of the above equations are presented in Appendix B.

4.3. Calculation of Air Entrainment Rates

The air entrainment rate into the plume is given by

$$\dot{m}_E = \left[\frac{17.16}{\varphi}\right] \dot{m}_f \tag{4.8}$$

and the plume mass flowrate into the hood is

$$\dot{m}_{p_{in}} = \dot{m}_E + \dot{m}_f \tag{4.9}$$

where $\dot{m}_f$ is the mass flowrate of fuel.

4.4. The CEC72 Program

The theoretical composition of products was obtained through the use of the "CEC72 (Chemical Equilibrium Calculation)" computer program developed at the NASA Lewis Research Center by S. Gordon and B.J. McBride (1976). Briefly, the program can be used to calculate equilibrium composition of a mixture for assigned thermodynamic states. The thermodynamic states were assigned by specifying two thermodynamic state functions: temperature and pressure.

The program uses the ideal gas law as the equation of state for the mixture. The analysis assumes that interactions between phases are negligible. In the

event that condensed species are present, it is assumed that the condensed species occupies a negligible volume and exerts a negligible pressure compared to the gaseous species.

A free-energy minimization technique is used by the program to determine the equilibrium composition. The program considers gaseous species, condensed species, and ions. With a few exceptions, the thermodynamic data (e.g., heats of formation) are taken from the JANAF Thermochemical Tables.

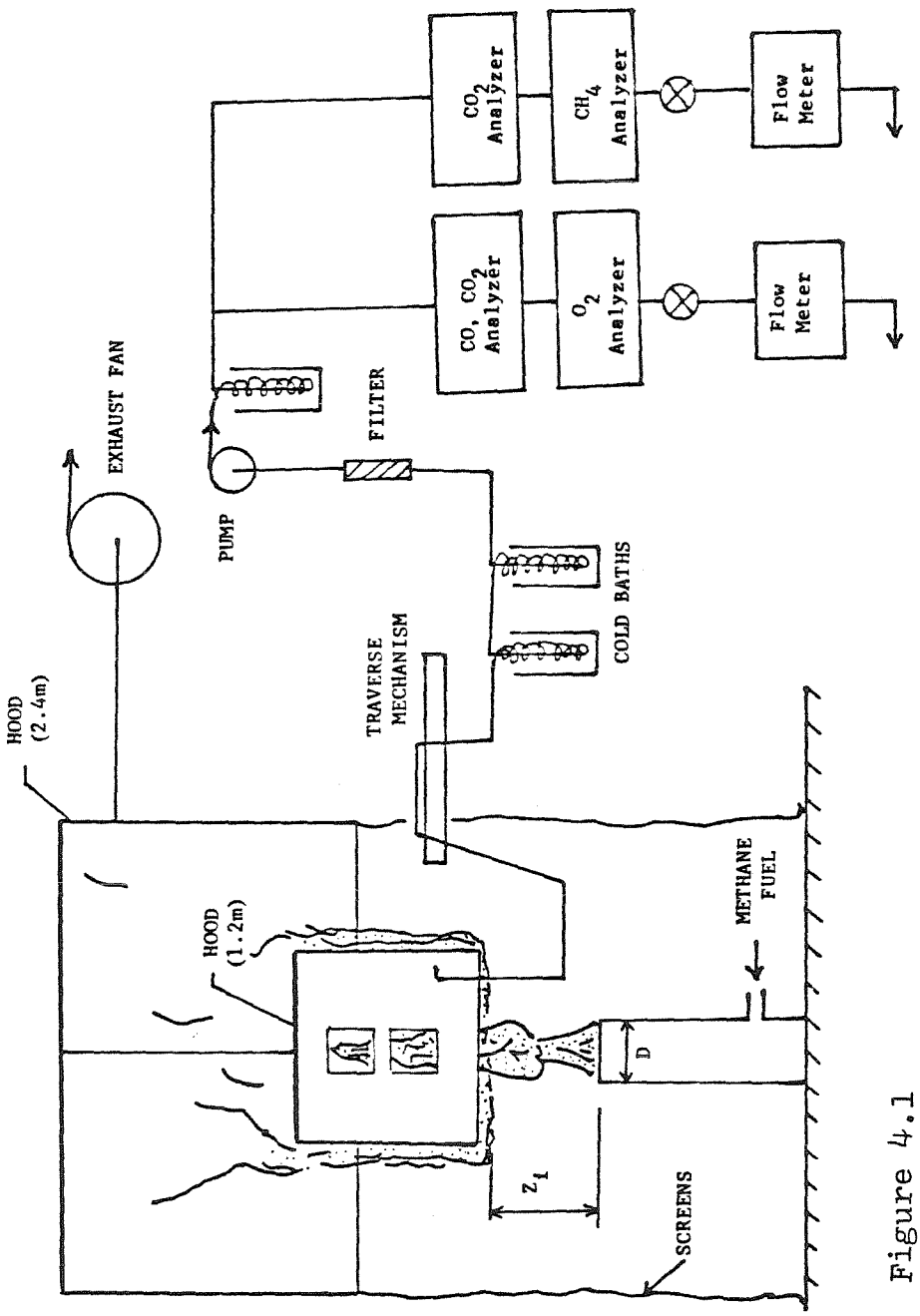
HOOD (2.4m)
EXHAUST FAN
PUMP
FILTER
TRAVERSE MECHANISM
COLD BATHS
HOOD (1.2m)
METHANE FUEL
D
z_1
SCREENS
CO, CO_2 Analyzer
O_2 Analyzer
CO_2 Analyzer
CH_4 Analyzer
Flow Meter
Flow Meter

Figure 4.1

Chapter 5

FIRE PLUME EXPERIMENTAL RESULTS

Measurements of the plume entrainment rates in the near field of a buoyant methane diffusion flame were made for interface heights of 0.01 m., 0.07 m., 0.10 m., and 0.23 m. above a 0.19 m. diameter burner. The entrainment measurements were made by analyzing the composition of the combustion products in the ceiling layer. In calculating the species concentrations, it was assumed that the solid carbon concentration was negligible in our experiments.

A problem that arose in the initial experiments was that the water vapor in the sample was not completely removed — water was observed to be condensing downstream of the pump. The problem was that the mole fraction of water vapor in the sample must be known in order to solve our system of equations. A non-zero value for the mole fraction of water vapor in the sample would make our estimates of the actual water vapor concentrations too high. The problem was eliminated in subsequent experiments by the addition of another cold bath downstream of the pump. Tests for leaks in the system were made by sending pure nitrogen into the sampling system and using the analyzers to detect any leak in the system by measuring the oxygen concentration of the gas at the detection station.

It was found that the temperature and species concentrations in the hood did not vary significantly with the vertical probe location as long as the probe was well away from the flame plume (see Table 5.1). Using this fact, the probe was placed in a corner half way between the top and lower edges of the hood. The temperature and species concentrations measured at this position were assumed to be representative of the properties of the combustion products.

Figure 5.1 shows the equivalence ratio, φ, as a function of the heat release rates, $\dot{Q}_f$, for four interface heights. For a given fuel flow rate, lowering the interface results in a higher equivalence ratio. This is because the air entrainment rate into the plume is proportional to the interface height, and lowering the interface will decrease the amount of oxygen available for combustion. The measured values of this air entrainment rate will be discussed in the section 5.3.

Figure 5.2 shows the average temperature of the ceiling layer gas, T_h, as a function of the equivalence ratio of the reactants. For $\varphi < 1$, the gas temperature increases linearly with equivalence ratio for a fixed interface height. But as the fuel-air ratio is increased above the stoichiometric value ($\varphi > 1$), the temperature reaches a maximum value. This implies that the air entrainment rate in the near field of a fire plume is independent of the fire size since the heat release is limited by the amount of oxygen available for combustion. Lowering the interface decreases the amount of oxygen available for combustion and therefore reduces the maximum temperature in the hood.

To summarize: For a fixed fuel flow rate, reducing the interface height results in a lower gas temperature and a higher equivalence ratio. This result can be explained by the fact that the amount of fuel consumed (and hence the heat released) is strongly dependent upon the mass flowrate of oxygen entrained into the plume. This fact is important since, theoretically, the equilibrium composition of a mixture is a strong function of the equilibrium temperature of the mixture. In the next section, we will compare the species concentrations measured in our experiments with the theoretical values obtained from the CEC72 computer program written by Gordon and McBride (1976).

5.1. Species Concentrations

Figures 5.3 to 5.9 show the estimated species concentrations in the hood as a function of the equivalence ratio. The plots also compare the experimental data with the theoretical equilibrium composition obtained from the CEC72 computer program. The results show that the measured CO_2, CO, O_2, and CH_4 concentrations are almost independent of the gas temperatures while the H_2O and H_2 data points show a great deal of scatter. When φ is less than 0.7, the estimated concentrations of the incomplete combustion products, CO and CH_4, are negligible but the concentration of H_2 is quite high. The differences between the experimental and theoretical values may be due to: (1) the accuracy of the instruments; (2) our assumption of negligible soot formation; (3) equilibrium not being established in the hood.

5.1.1. *Sensitivity of Calculations.* The accuracies of the instruments are: $Y_{CO_2} \pm 0.005$, $Y_{O_2} \pm 0.005$, $Y_{CH_4} \pm 0.001$, and $Y_{CO} \pm 0.0005$. To test the sensitivity of the calculations, the measured mole fractions of CO_2, O_2, and CH_4 were varied by ± 0.005. The error bars in Figures 5.3 to 5.9 show the range of values when this was done. The results show that the equivalence ratio and the mole fractions of CO_2, O_2, CO, and CH_4 are moderately sensitive to changes in the measured data. On the other hand, the calculated mole fractions of H_2 and H_2O have a very large range of values. The fact that the $\overline{Y}_{H_2}$ and $\overline{Y}_{H_2O}$ are very sensitive to the accuracy of the measurements could explain the large scatter in Figures 5.7 and 5.8

5.1.2. *The Concentration of Solid Carbon.* In making the calculations, we had assumed that the concentration of soot was negligible to the other species concentrations. Figure 5.10 is a plot of the theoretical solid carbon concentration obtained from the CEC72 computer program as a function of the equilibrium temperature. The plot shows that the equilibrium concentration of solid carbon

is a strong function of the equilibrium temperature and becomes negligible at very high temperatures. In our experiments, the temperature range was approximately from 500 to 900 degrees Kelvin, and the maximum equivalence ratio was approximately 2.5. From Figure 5.10, the highest solid carbon concentration in our experiments would be about 0.06. So the *maximum* error resulting from the assumption of negligible solid carbon is approximately 6% for our experiments. Since the calculated mole fractions of H_2 and H_2O are very sensitive to small changes in the measured data, this error is enough to create a considerable amount of scatter in the data.

5.1.3. *Effect of Equilibrium Temperature.* For $\varphi > 1$ the theoretical equilibrium species concentrations are strong functions of the equilibrium temperature. Figures 5.11 to 5.15 show the theoretical species concentrations as a function of equilibrium temperature. It is observed that a species may have the same concentration at two different temperatures. Care should therefore be used in comparing the experimental data with the theoretical curves in Figures 5.3 to 5.10 because the theoretical curves may cross or even overlap each other. Figure 5.13 shows that the theoretical concentration of methane vanishes at 300 degrees Kelvin even in fuel-rich mixtures. This error results from the assumption in the equilibrium analysis that the condensed species (water) occupies a negligible volume and exerts a negligible pressure compared to the gaseous species. This assumption greatly simplifies the theoretical analysis and allows the use of the ideal gas law as the equation of state. At 300 degrees Kelvin, the condensed water is no longer negligible and the calculations break down. Therefore the theoretical equibrium calculations are accurate for equilibrium temperatures which are well above the boiling point of water.

It was found that while the temperature of the gas differed by as much as 40 degrees Kelvin between the top and bottom of the hood, the measured species

concentrations hardly changed (see Table 5.1). The residence times of the hot gas in the hood (mass of gas in the hood divided by the plume mass flowrate) ranged from a low of 30 seconds for $Z_i = 0.23m$ to as long as 190 seconds for $Z_i = 0.01m$. It would seem then that the gas in the hood is well mixed and that chemical equilibrium would be established.

5.2. Mass Entrainment Rates

The mass entrainment of air into the fire plume is calculated by the chemical analysis of combustion products in the hood as was described in Chapter 4. The plume mass fluxes have been measured for interface heights of 0.23, 0.10, 0.07, and 0.01 m. above a 0.19 diameter burner. The heat input rates ranged from 10 to 120 kW. Figure 5.16 shows the mass entrainment rate of air into the plume as a function of the equivalence ratio for four interface heights. Our data correlated well with the results of Cetegen (1982). As was observed by Cetegen (1982), the entrainment rate is a weak function of the equivalence ratio and heat release rate of the fire at very low elevations of the interface, with the entrainment rate approximately proportional to the interface height above the burner raised to a power of about 3/4.

5.3. Fuel Rich Ceiling Layer

It was observed that there is a critical fire size for a given interface height in which flamelets start to form in the interface and spread until the entire interface is set on fire. Table 5.2 gives the critical fire size, gas temperatures, and equivalence ratios for four interface heights. At this point the interface gas is much hotter than the gas above it and this instability causes an inversion of the hot and cooler gases. This sudden turnover results in the generation of vortices and strong air currents that blow the fire plume to one side of the hood (see Figure 5.17(a)). After a while (a few seconds) the flamelets in the interface burned out and the fire plume returned to its normally upright position. It was

observed that the entire process described above occurred in regular cycles with the period being inversely proportional to the fire size. In fact, after a certain fire size was reached, the interface was observed to be continuously on fire.

Measurements of the period of the inversion cycle were made with the use of a thermocouple placed 4 in. above the lower edge of the hood, and 8 in. away from a corner. The thermocouple was well within the zone where the flamelets in the interface were observed. Table 5.3 shows the periods of the inversion cycle for $Z_i = 0.07\ m$ for several fire sizes.

The thermocouple was then connected to a strip chart recorder to obtain a continuous temperature reading. Figure 5.17(b,II) shows interface temperature as a function of time during the inversion cycle for $Z_i = 0.07\ m$ and $\dot{Q}_f = 91\ kW$. As a comparison, Figure 5.17(b,I) shows the temperature history in the top of the hood, and Figure 5.17(b,III) shows the carbon monoxide concentration in the interface as a function of time.

Between times A and B in Figure 5.17(b), the temperature in the interface is constant while the *CO* concentration rises until it reaches a maximum at time B. At time B, the unburnt fuel (methane, hydrogen, and carbon monoxide) in the interface begin to burn, and the temperatures increase sharply. At time C, the gas temperature reaches a maximum, and the gas starts to cool down. Finally, at time D, the flames in the interface die out and the cycle starts all over again.

5.4. Oxygen Rich Ceiling Layer

In situations where the interface is well below the top of the flames, the gas in the ceiling layer is entrained and heated to very high temperatures by the fire plume several times before it finally leaves the hood. If fuel is supplied directly into an oxygen rich ceiling layer, the resulting mixture may or may not react as it passes through the flames.

We have carried out some preliminary experiments in which methane fuel is injected directly into the ceiling layer to determine if the oxygen inside the hood reacts with the fuel. In the following paragraphs, we will describe the apparatus and techniques used to measure the fraction of the added fuel that reacts in an oxygen rich ceiling layer. Briefly, mass conservation equations for the fuel and oxygen are used to estimate: (1) the mass fraction of methane in the ceiling layer in which the fuel entrained into the flames is *entirely* consumed; (2) the mass fraction of methane in the ceiling layer in which the fuel entrained into the flames *does not react at all* with the oxygen; and (3) the mass fraction of oxygen in the ceiling layer, *given* the fraction of fuel that reacts in the flames. The *measured* mass fraction of methane is then compared with the values obtained from (1) and (2) to determine the fraction of added fuel that actually reacts in the flames. To check the accuracy of the models, the oxygen concentration in the hood is measured and then compared with the value obtained from (3).

5.4.1. *Apparatus.* The apparatus used in these experiments was essentially the same as the one used in the near field measurements. A 0.25 in. diameter copper pipe was used to inject methane fuel into the hood. The heat release rates of the added fuel ranged from 4.0 to 22.8 kW. The pipe and the probe were placed in opposite corners, 0.6 m. from the bottom lip of the hood. To obtain a ceiling layer with a high oxygen content (low φ) and a high gas temperature, we chose to use a fire size of 31.6 kW and an interface height of 0.23 m. (cf. Figure 5.2). The average flame height was about 0.78 m. from the top of the 0.19 m. diameter burner.

5.4.2. *Fuel Mass Model.* For steady state conditions, a mass balance of the fuel entering and leaving the hood may be written as

$$\dot{m}_{f_{added}} - \alpha C_f (\dot{m}_{p_{fl}} - \dot{m}_{p_{in}}) - C_f \dot{m}_{p_{in}} = 0 \qquad (5.1)$$

where $\dot{m}_{f_{added}}$ is the added amount of fuel; C_f the mass fraction of fuel in the ceiling layer; $\dot{m}_{p_{fl}}$ the total plume flux at the flame height; and $\dot{m}_{p_{in}}$ is the total mass flux entering the hood as was defined in section 4.3. The term $\dot{m}_{p_{fl}} - \dot{m}_{p_{in}}$ is the rate of entrainment of the ceiling layer gas into the fire plume. The parameter α represents the fraction of fuel that is consumed by the plume, i.e., if $\alpha = 1$ all the fuel that is entrained into the fire plume is consumed, and if $\alpha = 0$ all the fuel that is entrained into the flames leaves the fire plume unburned. The term $C_f \dot{m}_{p_{in}}$ is the mass flowrate of fuel leaving the hood. Equation (5.1) may be used predict the mass fraction of methane, C_f, if α is known:

$$C_f = \frac{\dot{m}_{f_{added}}}{\alpha (\dot{m}_{p_{fl}} - \dot{m}_{p_{in}}) + \dot{m}_{p_{in}}}. \qquad (5.2)$$

We were able to measure $\dot{m}_{f_{added}}$, C_f, and $\dot{m}_{p_{in}}$ by the same techniques described in Chapter 4. The value for $\dot{m}_{p_{fl}}$ was obtained from the entrainment recipe given by Cetegen (1982). The measured species concentrations and the calculated mass flowrates for the ceiling layer with no fuel added are listed in Table 5.4. Table 5.5 lists the data obtained for four flowrates of added fuel.

In Table 5.6, the measured mass fraction of methane is compared with the values obtained from Eq. 5.2 for the cases where: (1) the entrained fuel is not burned by the flames ($\alpha = 0$); and (2) the entrained fuel is completely consumed ($\alpha = 1$). The results show that a fraction of the fuel entrained into the fire

plume is burned, with the mass consumed being:

$$\frac{(\dot{m}_{f_{added}})_{burned}}{\dot{m}_{f_{added}}} = 1 - C_f \frac{\dot{m}_{p_{in}}}{\dot{m}_{f_{added}}} = 1 - \frac{C_f}{\left[C_f\right]_{\alpha=0}}. \qquad (5.3)$$

5.4.3. *Oxygen Mass Model.* The steady state mass balance of oxygen in the hood may be written as

$$C_\infty (\dot{m}_{p_{in}} - \dot{m}_f) - \dot{m}_{p_{in}} C_o - C_\infty \frac{\dot{m}_f}{f_s} - C_o \frac{(\dot{m}_{f_{added}})_{burned}}{f_s} = 0 \qquad (5.4)$$

where C_∞ is the oxygen mass fraction in the ambient air (= 0.23); $\dot{m}_{p_{in}} - \dot{m}_f$ is the entrainment rate of ambient air into the plume; C_o is the mass fraction of oxygen in the ceiling layer; f_s is the stoichiometric fuel-air ratio (= 0.058 for methane fuel); and $(\dot{m}_{f_{added}})_{burned}$ is the amount of added fuel that was burned in the fire (as was defined in Eq. 5.3). The first term in Eq. 5.4 represents the amount of oxygen entering the hood; the second term is the amount leaving the hood; the third term is the amount of entrained O_2 that reacts with $\dot{m}_f$; and the last term is the amount of O_2 that reacts with $(\dot{m}_{f_{added}})_{burned}$. By neglecting $\dot{m}_f$ compared to $\dot{m}_{p_{in}}$ in the first term and using the relation $\varphi \approx (\dot{m}_f/\dot{m}_{p_{in}})\times(1/f_s)$, Eq. 5.4 may be reduced to

$$C_o = \frac{C_\infty(1-\varphi)}{1 + \dfrac{(\dot{m}_{f_{added}})_{burned}}{f_s \dot{m}_{p_{in}}}}. \qquad (5.5)$$

Using the data in Tables 5.4 to 5.6, Eq. 5.5 may be used to predict the mass fraction of oxygen in the ceiling layer. This predicted value may then be compared

with the measured mass fraction of oxygen to determine the accuracy of the fuel and oxygen mass models (Table 5.7). The term $(\dot{Q}_f)_{added\,Burned}$ in the second column of Table 5.7 was calculated using Eq. 5.3.

The results show that the difference between the predicted and measured concentration of oxygen in the ceiling layer increases as more fuel is injected. This is because we had assumed that $\dot{m}_{p_{in}}$ and $\dot{m}_{p_{fl}}$ were independent of the amount of fuel added into the ceiling layer. In reality, the fire size and plume entrainment rates increase as more of the added fuel is consumed. It must be noted that these are preliminary experiments, and more refined methods must be used to determine accurately the effect of adding fuel into an oxygen rich ceiling layer.

5.4.4. *Critical Oxygen Concentration.* In another experiment to determine if the fuel and oxygen will react in the ceiling layer, the pipe used to inject the fuel was lighted and then placed inside the hood. The heat release rate of the added fuel was set at 1 kW. The fire size of the plume was then varied to change the oxygen concentration in the ceiling layer. It was found that the critical oxygen concentration is about 13% by volume for the injected fuel to keep burning. This value is in close agreement with the critical oxygen index of 12% given by Lewis and Elbe (1951, p. 754). Just above the critical value, the flame on the pipe was observed to have a transparent blue color. The more familiar yellow flames (which are associated with soot formation) became more evident as the oxygen content of the ceiling layer was increased. At the critical value, the flame was very unstable and a small disturbance (such as moving the pipe slightly) was enough to kill the flame. The fire on the pipe immediately died out when the oxygen concentration fell below the critical value.

Table 5.1. Temperature and Species Concentrations vs. Probe Location

$\dot{Q}_f$ = 73.7 kW
Z_i = 0.100 m.

	Probe Location		
	Top of hood	Middle of hood	Bottom of hood
$T°K$	722	702	695
Y_{CO_2}	0.0960	0.0970	0.0960
Y_{O_2}	0.0010	0.0003	0.0020
Y_{CO}	0.0250	0.0250	0.0250
Y_{CH_4}	0.0860	0.0920	0.0890

$\dot{Q}_f$ = 52.6 kW
Z_i = 0.230 m.

	Probe Location		
	Top of hood	Middle of hood	Bottom of hood
$T°K$	847	833	810
Y_{CO_2}	0.0890	0.0890	0.0890
Y_{O_2}	0.0540	0.0580	0.0560
Y_{CO}	0.0031	0.0026	0.0032
Y_{CH_4}	0.0004	0.0004	0.0003

Table 5.2. Critical Fire Size for Four Interface Heights

Z_i	Critical Fire Size	φ	T_h
0.01 m	40 kW	2.4	560 °K
0.07 m	60 kW	2.2	650 °K
0.10 m	100 kW	2.5	730 °K
0.23 m	150 kW	1.9	840 °K

The critical fire size refers to the fire size below which flamelets in the interface did not appear.

Table 5.3. Periods of the Inversion Cycle for Three Fire Sizes

Z_i	$\dot{Q}_f$	Period	φ
0.07 m	68 kW	75 s	2.3
0.07 m	91 kW	62 s	3.5
0.07 m	128 kW	45 s	4.5

Table 5.4. Ceiling Layer Composition with No Added Fuel

$\dot{Q}_f$ = 31.6 kW
Z_i = 0.23 m.
$\dot{m}_f$ = 0.000663 kg/s
$\dot{m}_{p_{in}}$ = 0.0307 kg/s

T_h = 618 °K

Avg. flame height = 0.78 m.
$\dot{m}_{p_{fl}}$ = 0.124 kg/s

Mole Fractions

$\overline{Y}_{O_2}$ = 0.1237
$\overline{Y}_{CO}$ = 0.0000
$\overline{Y}_{H_2}$ = 0.0000
$\overline{Y}_{N_2}$ = 0.7635
$\overline{Y}_{CH_4}$ = 0.0000
$\overline{Y}_{CO_2}$ = 0.0376
$\overline{Y}_{H_2O}$ = 0.0836

φ = 0.370
Molecular Weight = 28.4 kg/kmol.

Table 5.5. Ceiling Layer Composition with Added Fuel

$(\dot{Q}_f)_{added}$	$\overline{Y}_{O_2}$	$\overline{Y}_{CH_4}$	$\overline{Y}_{CO_2}$	$\overline{Y}_{CO}$	T_h
4.0 kW	0.1241	0.0024	0.0377	0.0000	623 °K
7.5 kW	0.1212	0.0036	0.0374	0.0000	628 °K
14.8 kW	0.1172	0.0072	0.0370	0.0000	640 °K
22.8 kW	0.1065	0.0091	0.0399	0.0004	668 °K

Table 5.6. Measured vs. Predicted Mass Fraction of Methane

$(\dot{Q}_f)_{added}$	C_f if unburned	C_f if completely burned	C_f measured	α
4.0 kW	0.0027	0.0007	0.0014	0.31
7.5 kW	0.0051	0.0013	0.0020	0.51
14.8 kW	0.0101	0.0025	0.0041	0.48
22.8 kW	0.0156	0.0039	0.0051	0.68

The predicted mass fractions of methane are based on the flame height, the plume mass fluxes, and the amount of added fuel. α is the fraction of entrained fuel that was consumed in the fire plume.

Table 5.7. Measured vs. Predicted Mass Fraction of Oxygen

$(\dot{Q}_f)_{added}$	$(\dot{Q}_f)_{added}$ Burned	C_o Predicted	C_o Measured
40 kW	2.0 kW	0.144	0.140
7.5 kW	4.6 kW	0.141	0.136
14.8 kW	8.8 kW	0.138	0.132
22.8 kW	15.3 kW	0.130	0.121

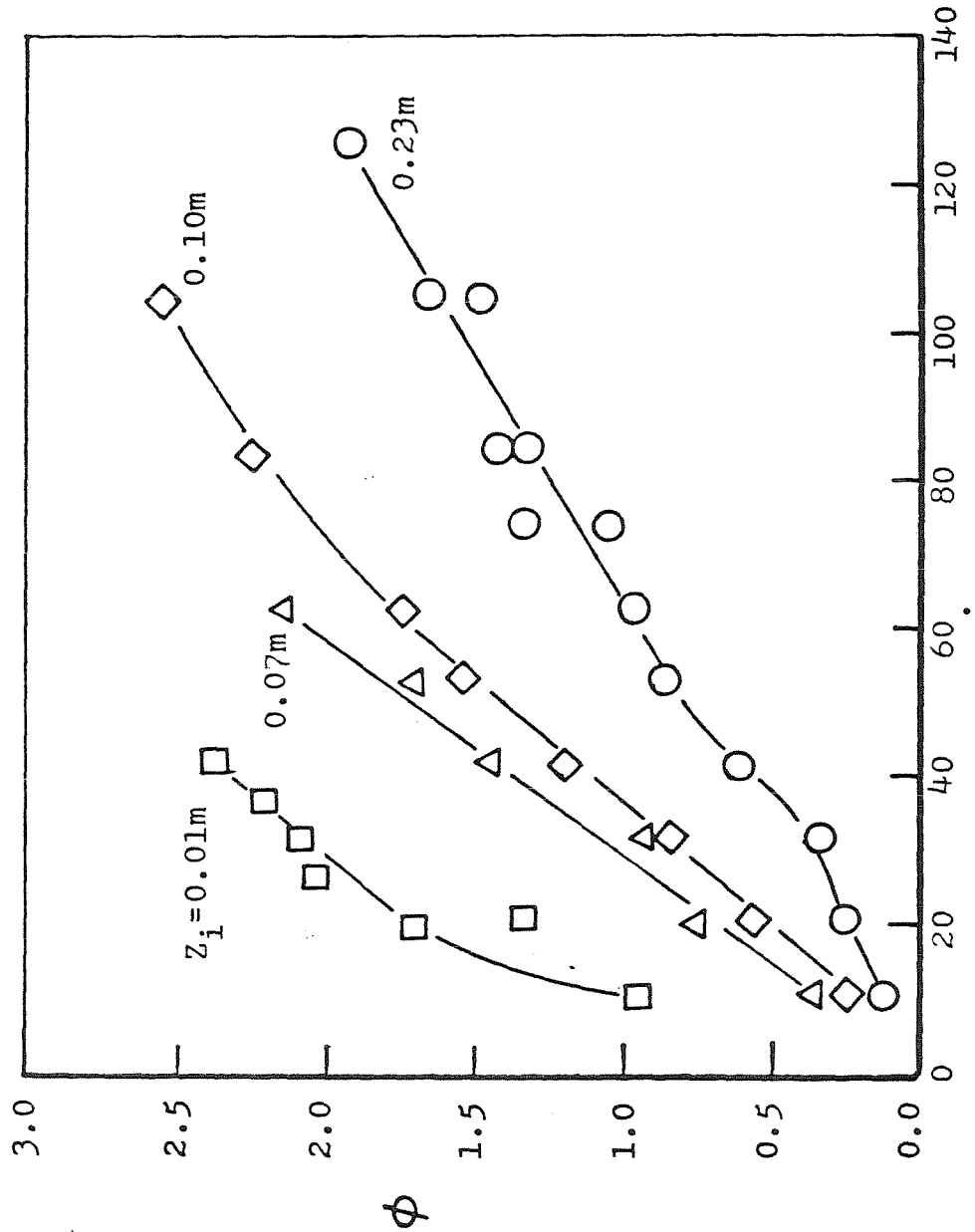
3.0
2.5
2.0
1.5
1.0
0.5
0.0
φ
0
20
40
60
80
100
120
140
$\dot{Q}_f$, kW
z_i=0.01m
0.07m
0.10m
0.23m

Figure 5.1

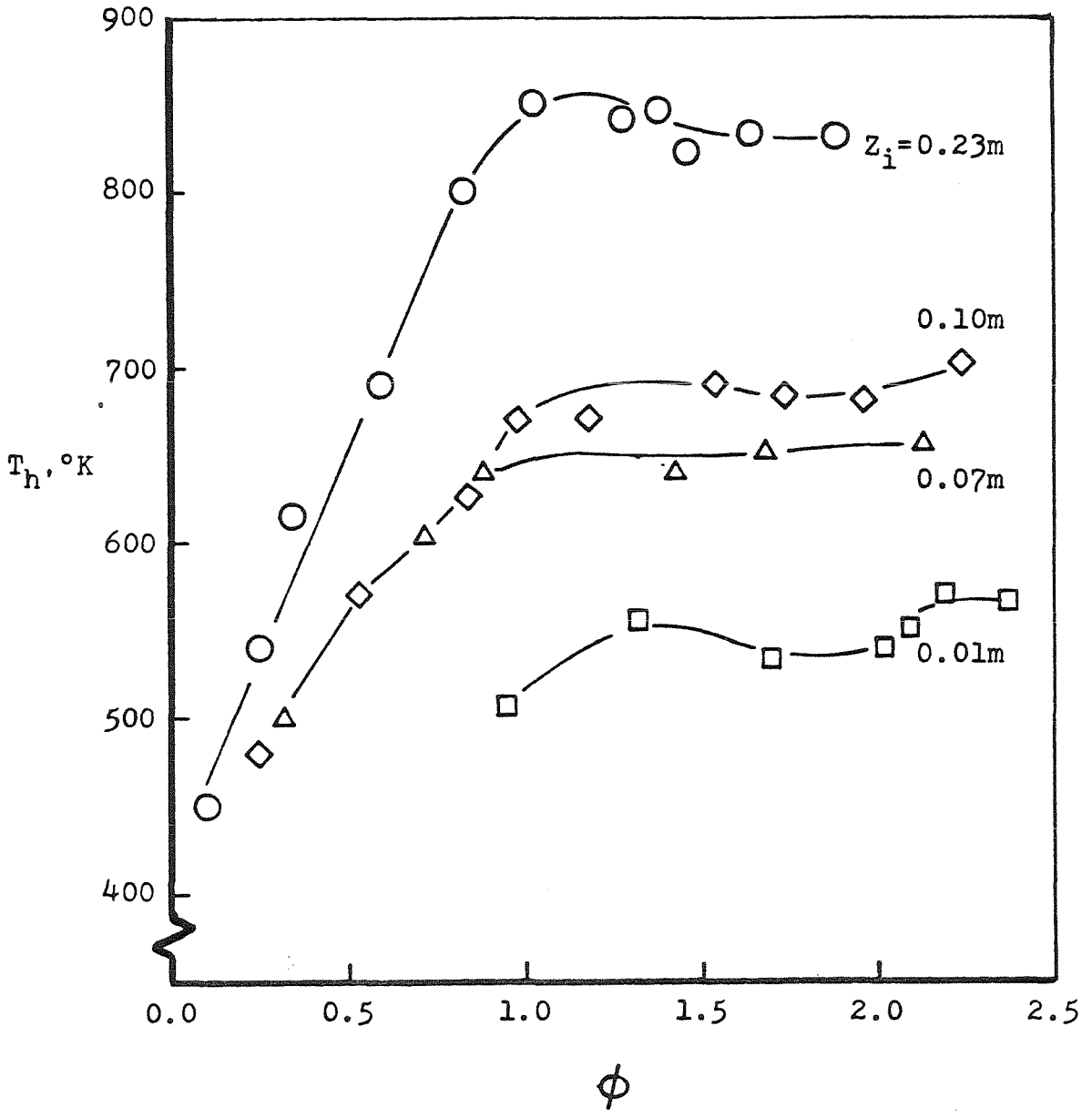
900
800
700
600
500
400
T_h, °K
0.0
0.5
1.0
1.5
2.0
2.5
ϕ
Z_i=0.23m
0.10m
0.07m
0.01m

Figure 5.2

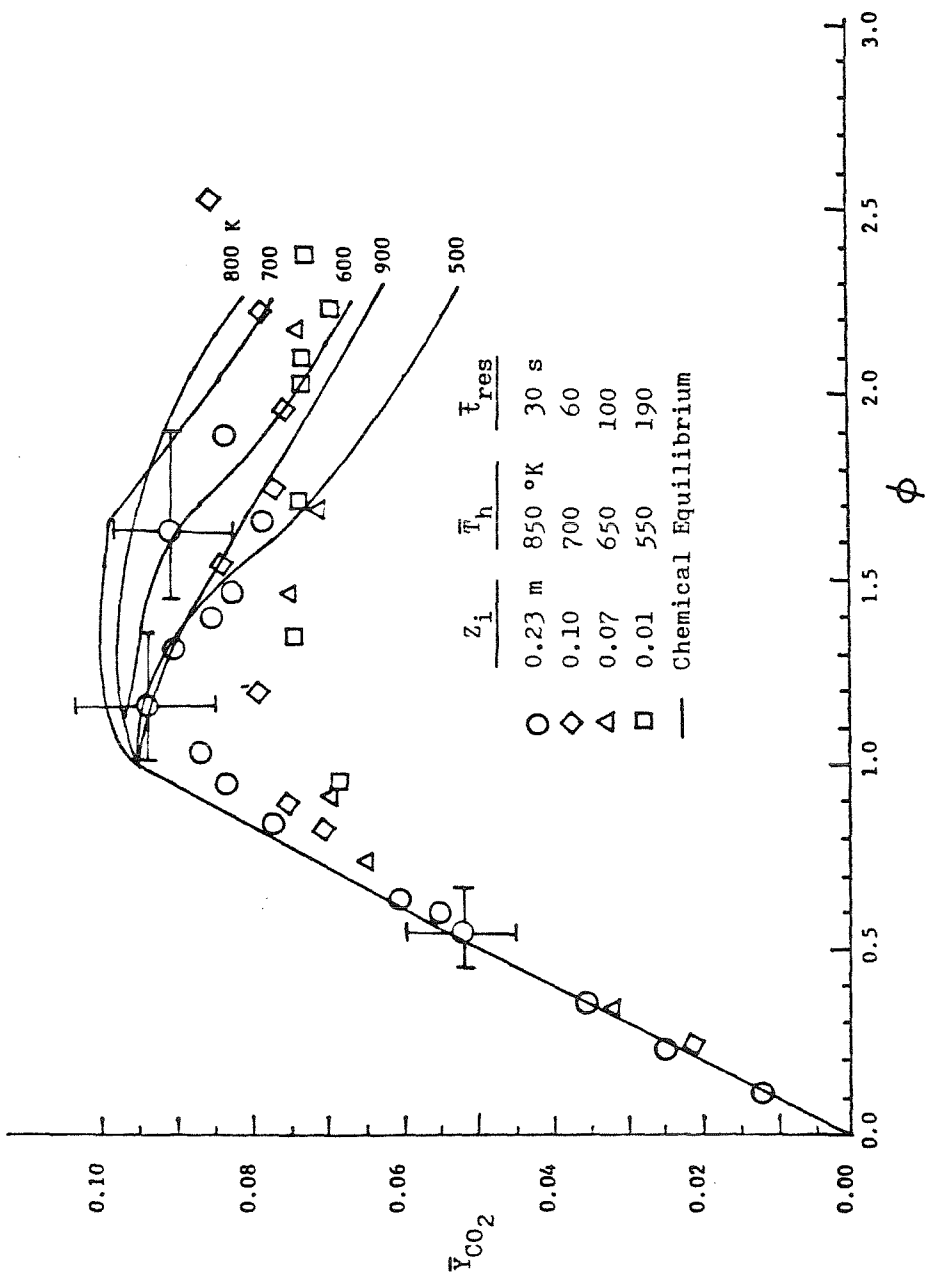
0.10
0.08
0.06
0.04
0.02
0.00
$\bar{Y}_{CO_2}$
0.0
0.5
1.0
1.5
2.0
2.5
3.0
ϕ
800 K
700
600
900
500
z_i $\bar{T}_h$ $\bar{\tau}_{res}$
0.23 m 850 °K 30 s
0.10 700 60
0.07 650 100
0.01 550 190
Chemical Equilibrium

Figure 5.3

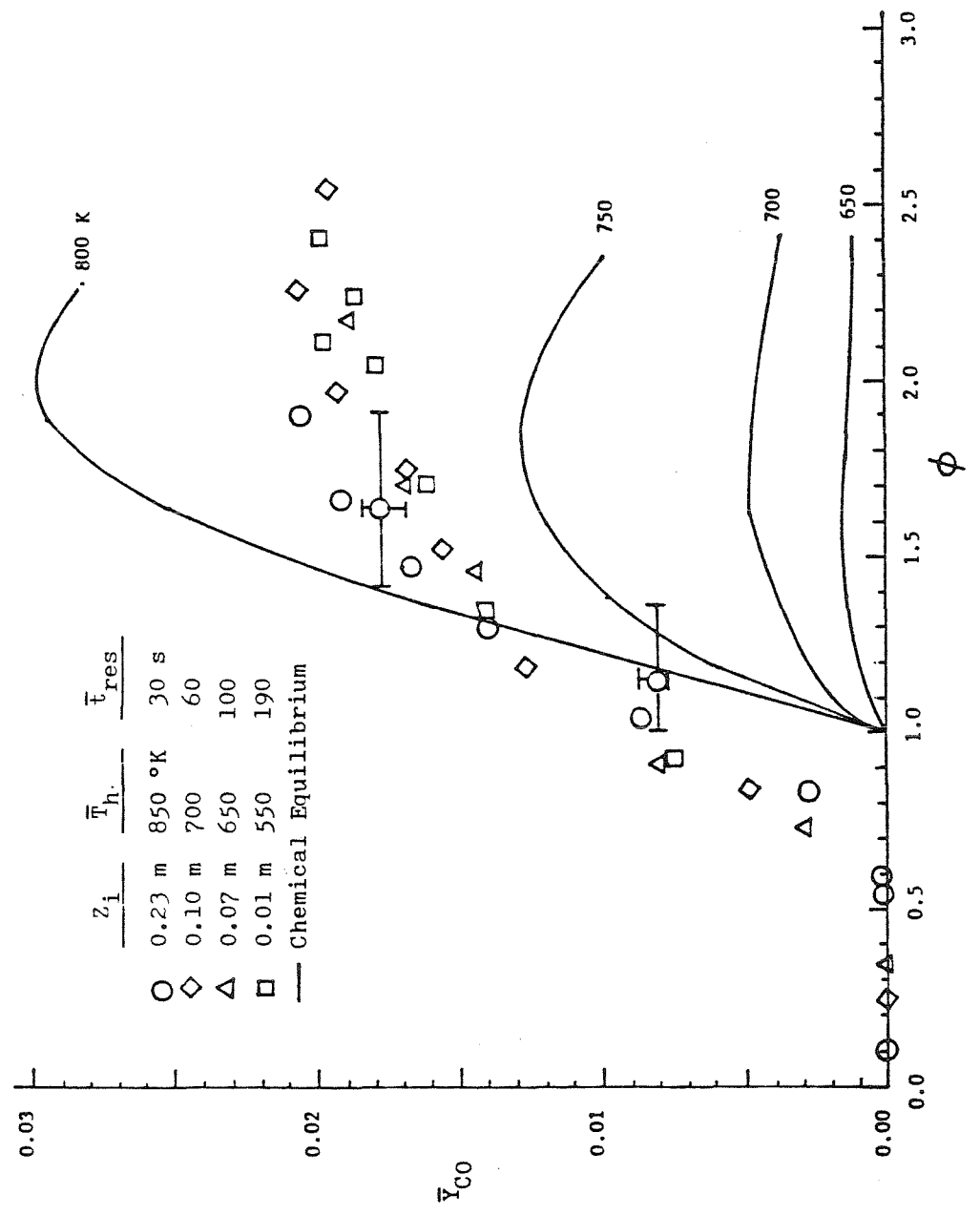
z_i $\bar{T}_h$ $\bar{t}_{res}$
0.23 m 850 °K 30 s
0.10 m 700 60
0.07 m 650 100
0.01 m 550 190
Chemical Equilibrium
800 K
750
700
650
$\bar{Y}_{CO}$
ϕ
0.00
0.01
0.02
0.03
0.0
0.5
1.0
1.5
2.0
2.5
3.0

Figure 5.4

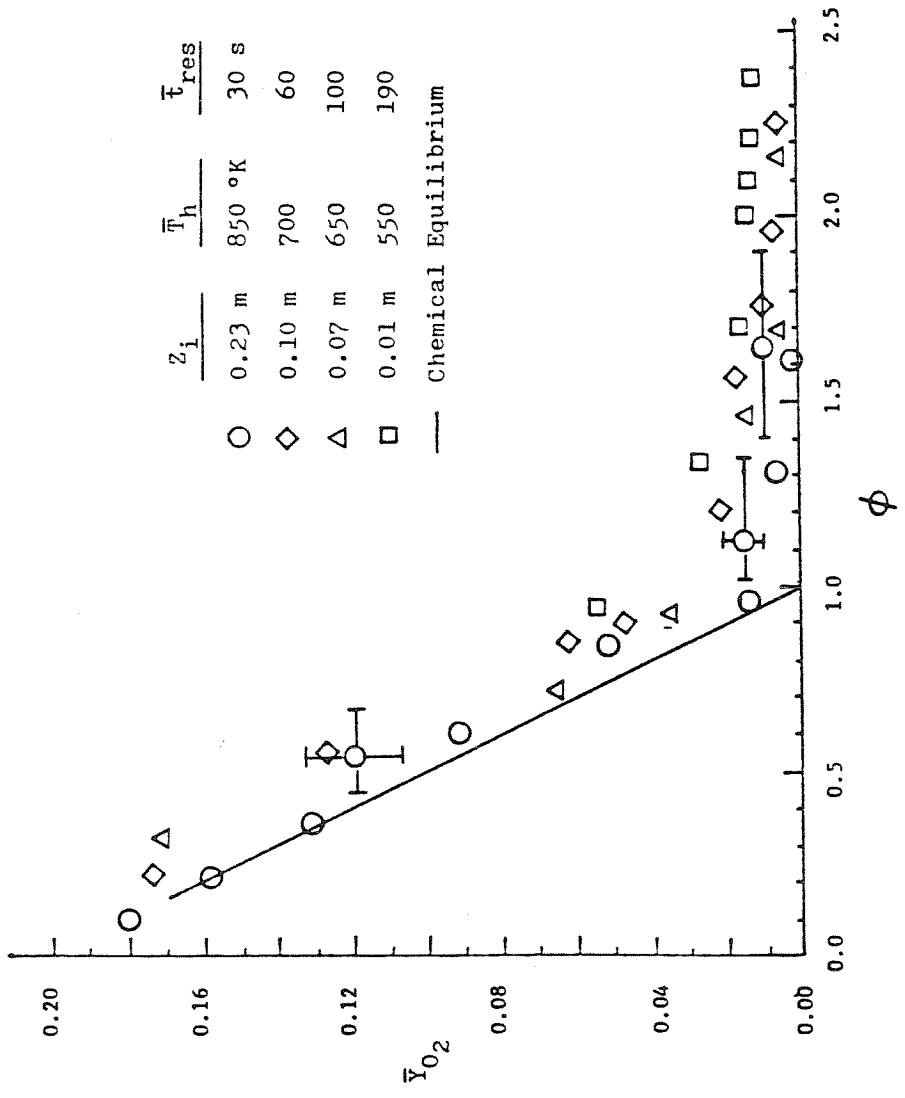
z_i
$\bar{T}_h$
$\bar{t}_{res}$
0.23 m 850 °K 30 s
0.10 m 700 60
0.07 m 650 100
0.01 m 550 190
Chemical Equilibrium
$\bar{Y}_{O_2}$
0.20
0.16
0.12
0.08
0.04
0.00
0.0
0.5
1.0
1.5
2.0
2.5
ϕ

Figure 5.5

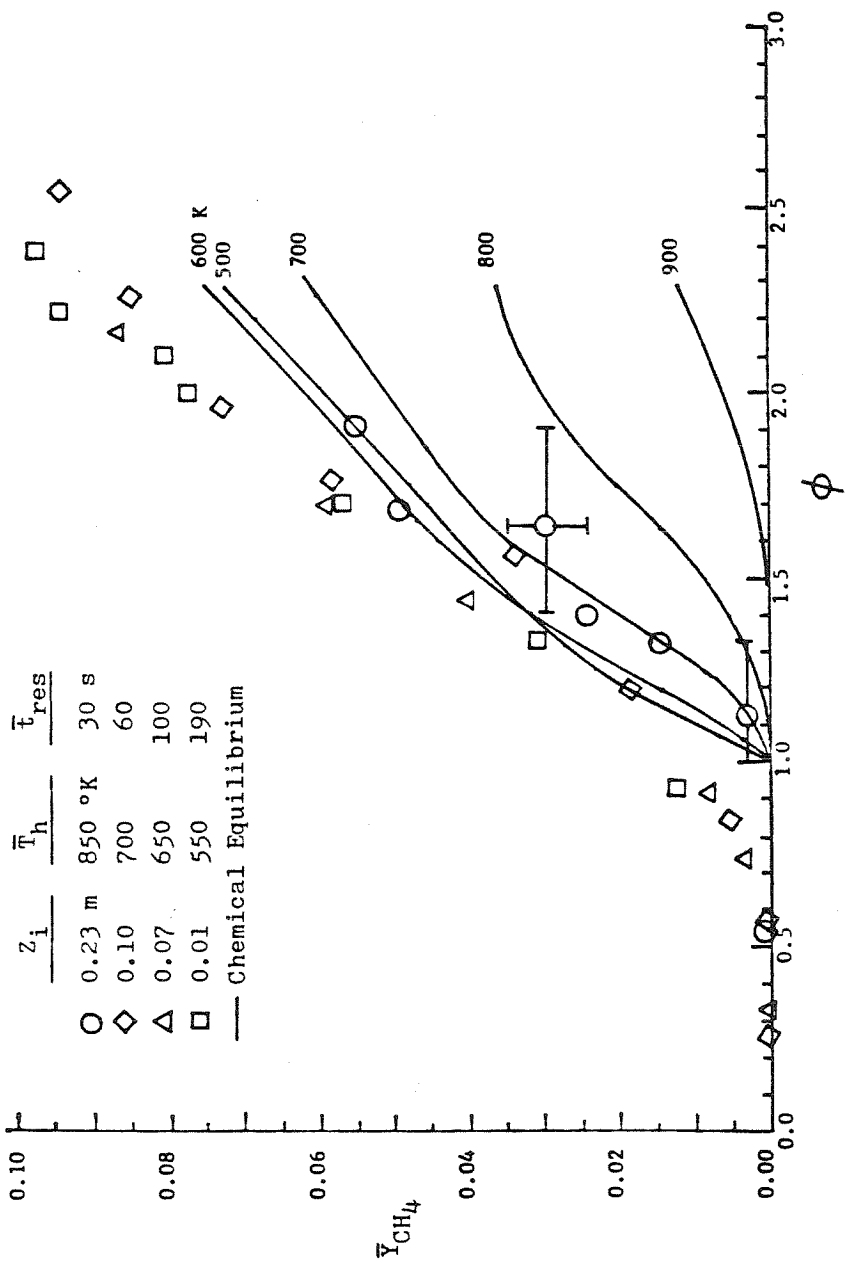
z_i $\bar{T}_h$ $\bar{t}_{res}$
0.23 m 850 °K 30 s
0.10 700 60
0.07 650 100
0.01 550 190
Chemical Equilibrium
600 K
500
700
800
900
$\bar{Y}_{CH_4}$
ϕ
0.00
0.02
0.04
0.06
0.08
0.10
0.0
0.5
1.0
1.5
2.0
2.5
3.0

Figure 5.6

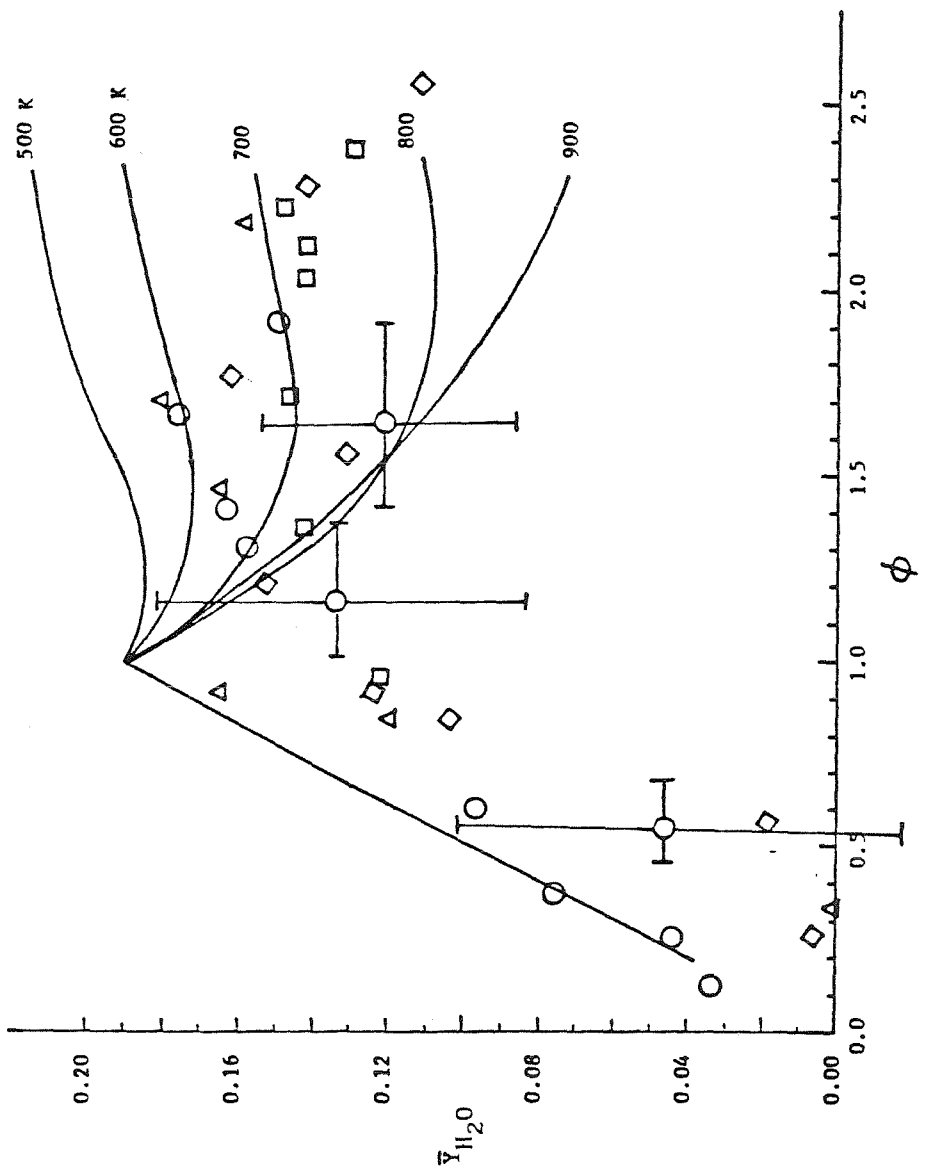
500 K
600 K
700
800
900
0.20
0.16
0.12
0.08
0.04
0.00
$\bar{Y}_{H_2O}$
0.0
1.0
1.5
2.0
2.5
ϕ

Figure 5.7

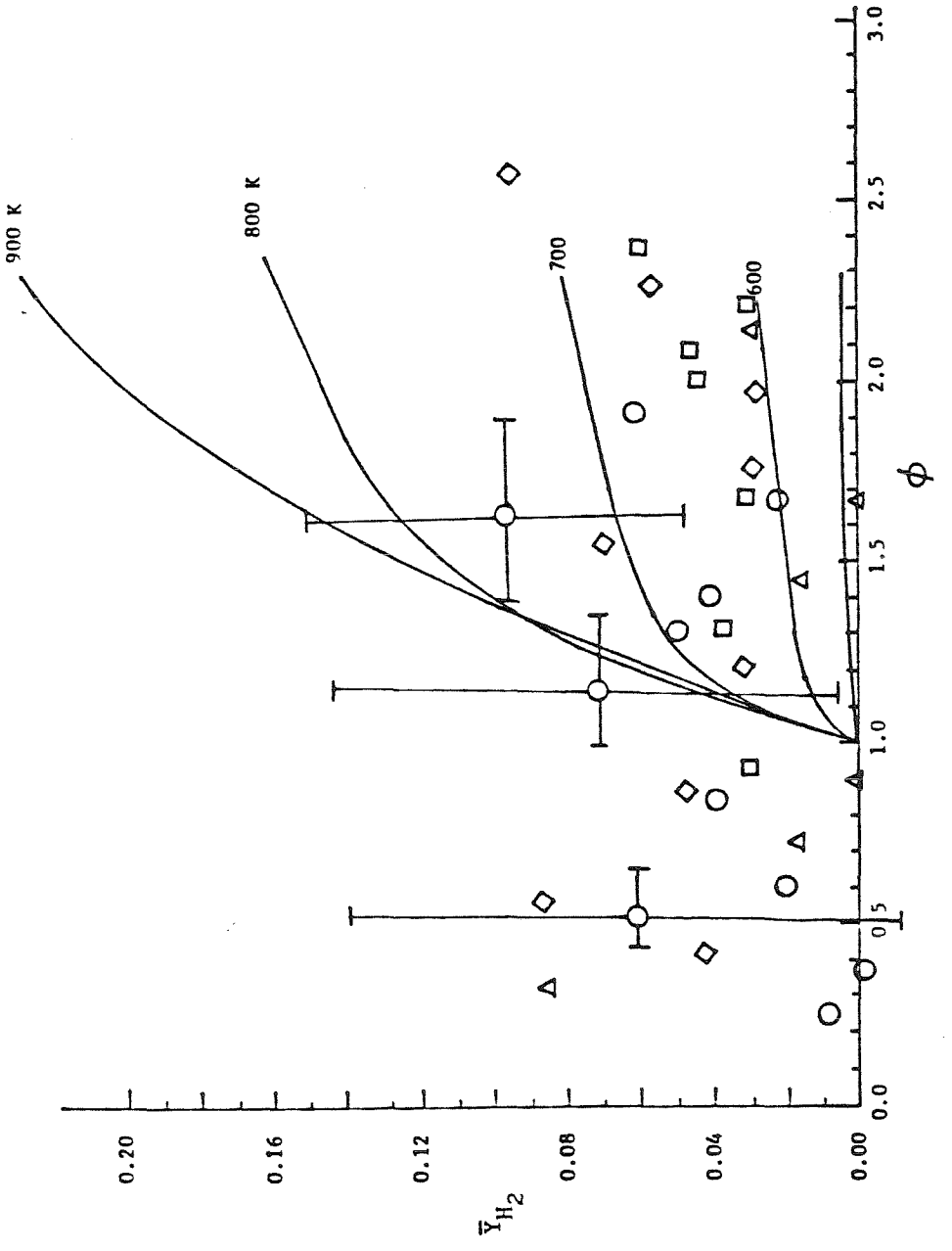
900 K
800 K
700
600
$\bar{Y}_{H_2}$
0.20
0.16
0.12
0.08
0.04
0.00
0.0
0.5
1.0
1.5
2.0
2.5
3.0
ϕ

Figure 5.8

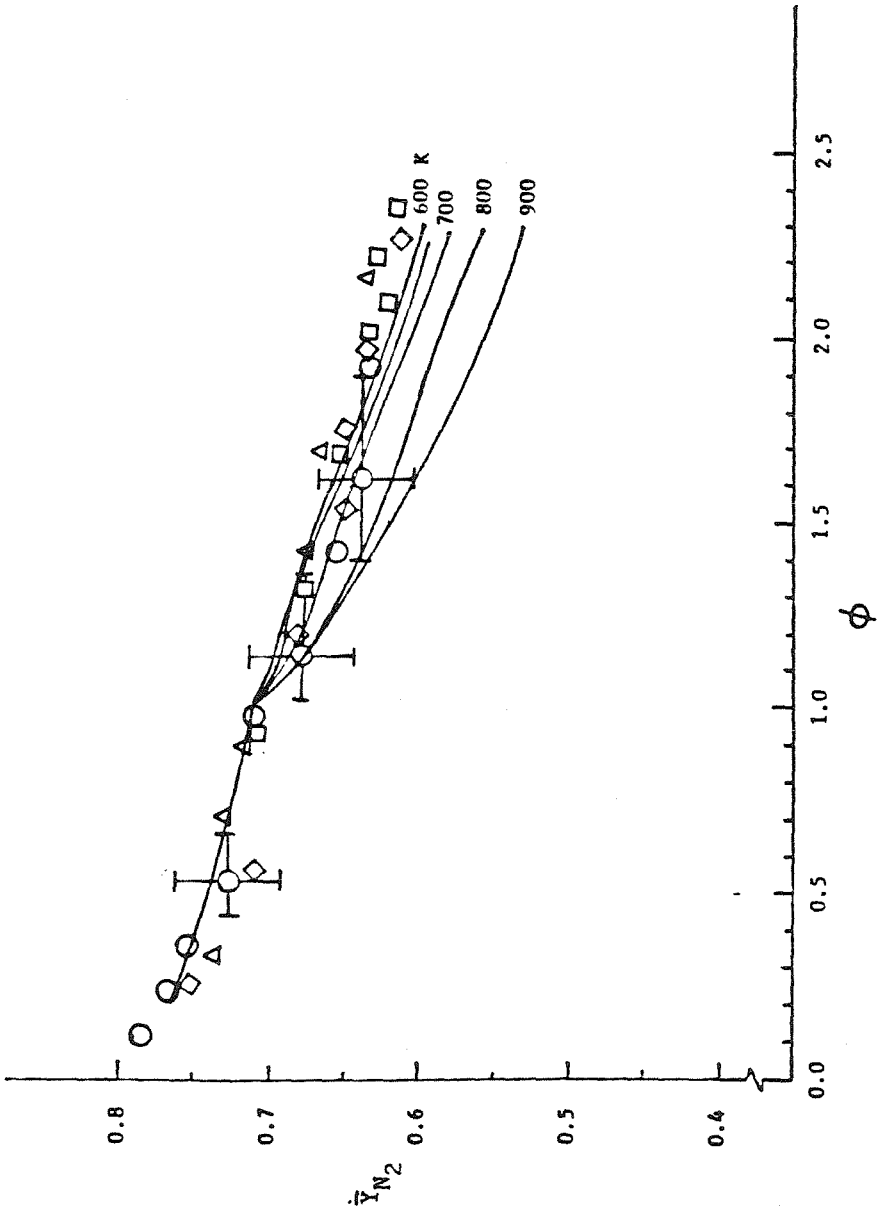

Figure 5.9

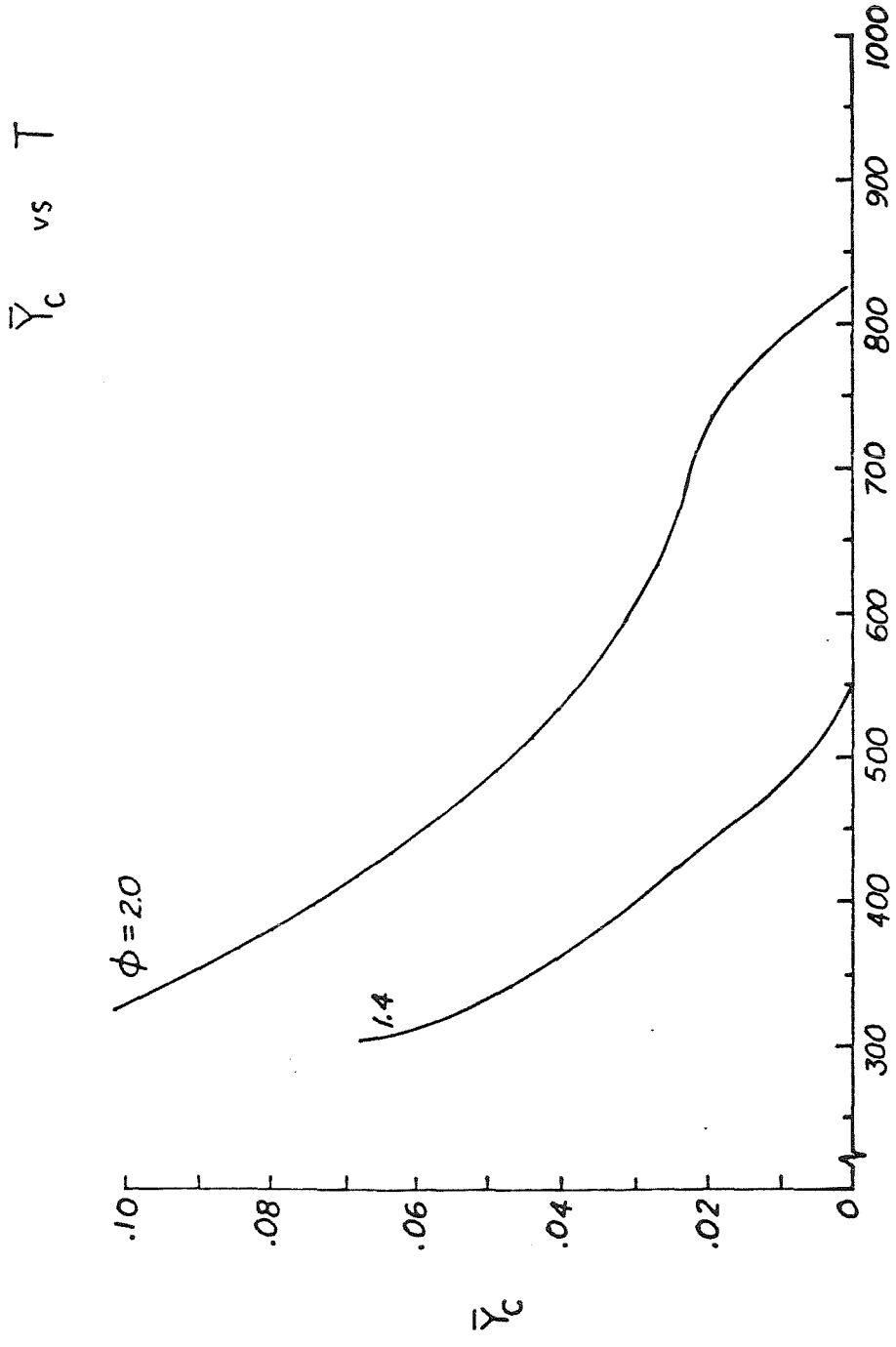
$\bar{Y}_c$ vs T
$\phi = 2.0$
1.4
$\bar{Y}_c$
.10
.08
.06
.04
.02
0
300
400
500
600
700
800
900
1000
EQUILIBRIUM TEMPERATURE (°K)

Figure 5.10

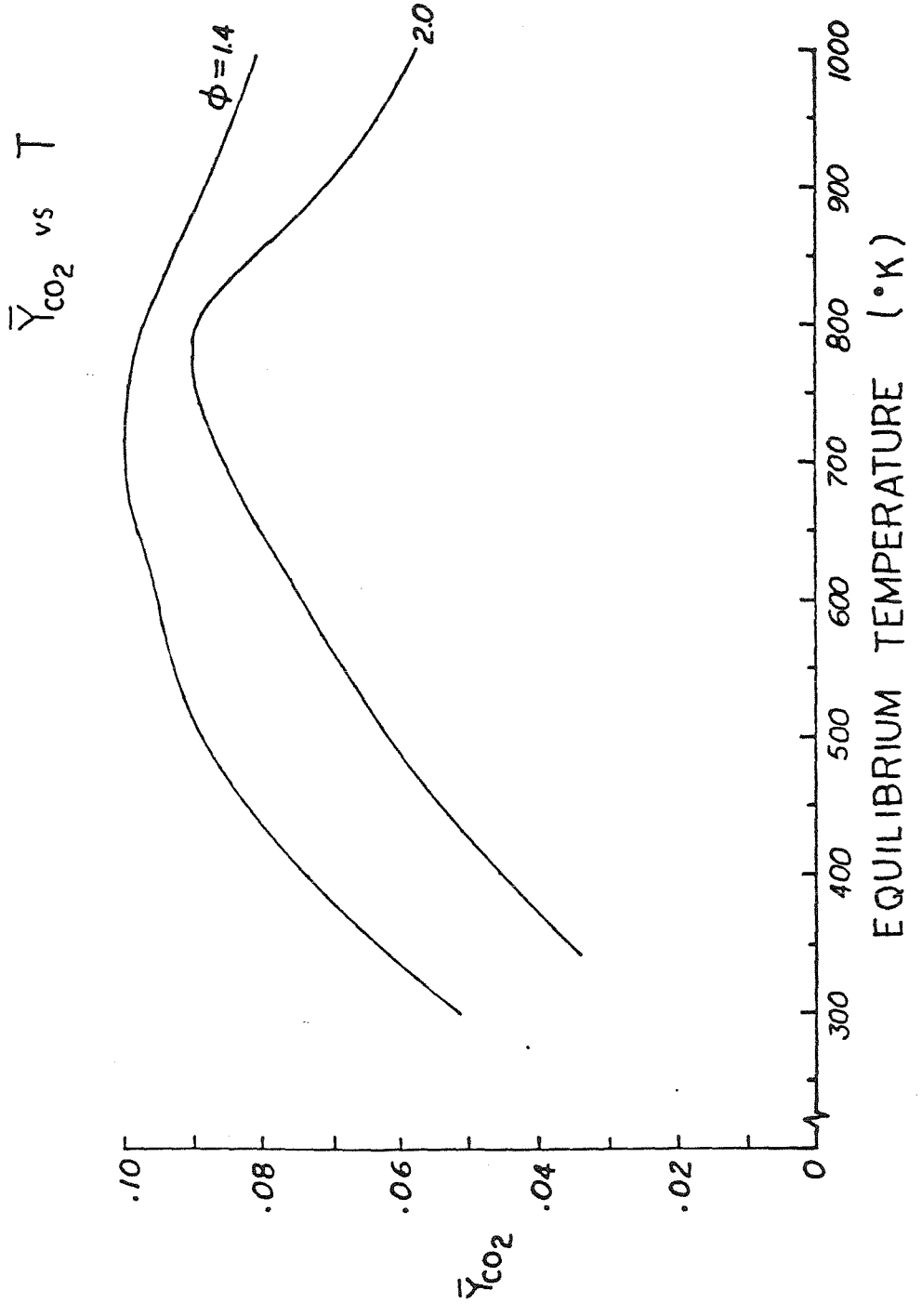
$\bar{Y}_{CO_2}$ vs T
ϕ=1.4
2.0
.10
.08
.06
.04
.02
0
$\bar{Y}_{CO_2}$
300
400
500
600
700
800
900
1000
EQUILIBRIUM TEMPERATURE (°K)

Figure 5.11

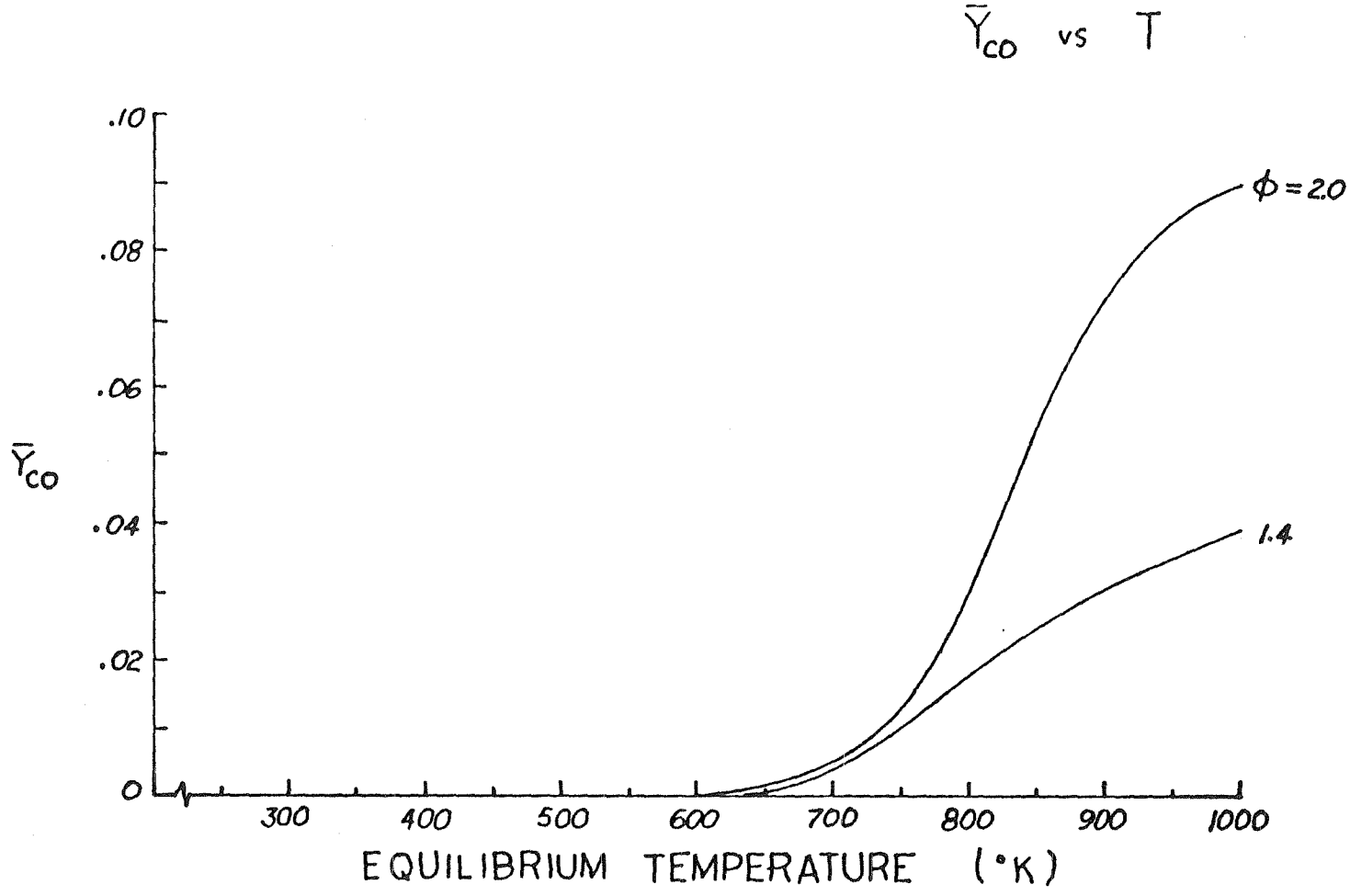
$\bar{Y}_{CO}$ vs T
.10
.08
.06
.04
.02
0
$\bar{Y}_{CO}$
$\phi = 2.0$
1.4
300
400
500
600
700
800
900
1000
EQUILIBRIUM TEMPERATURE (°K)

Figure 5.12

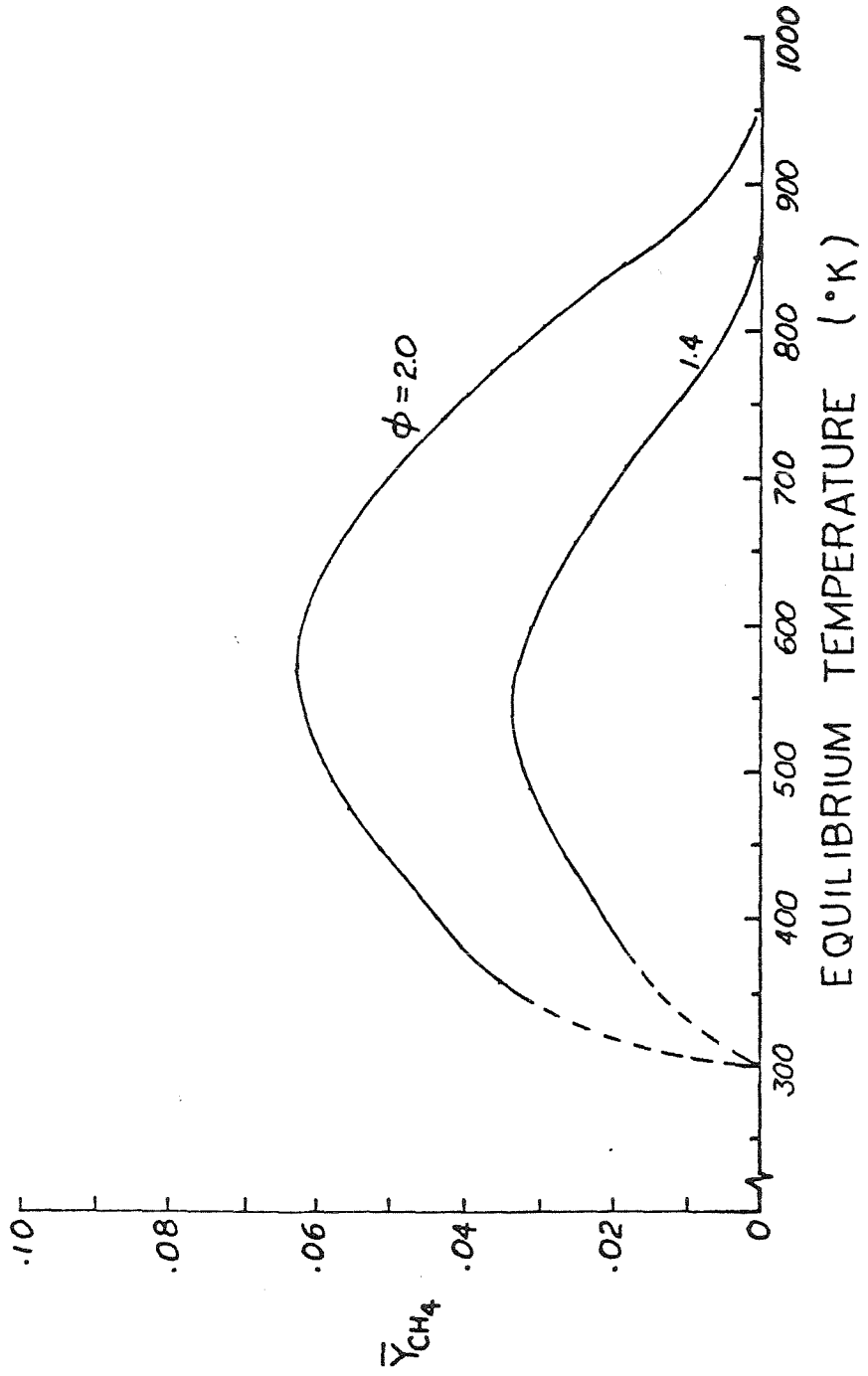
$\bar{Y}_{CH_4}$ vs T
$\bar{Y}_{CH_4}$
.10
.08
.06
.04
.02
0
300
400
500
600
700
800
900
1000
EQUILIBRIUM TEMPERATURE (°K)
ϕ = 2.0
1.4

Figure 5.13

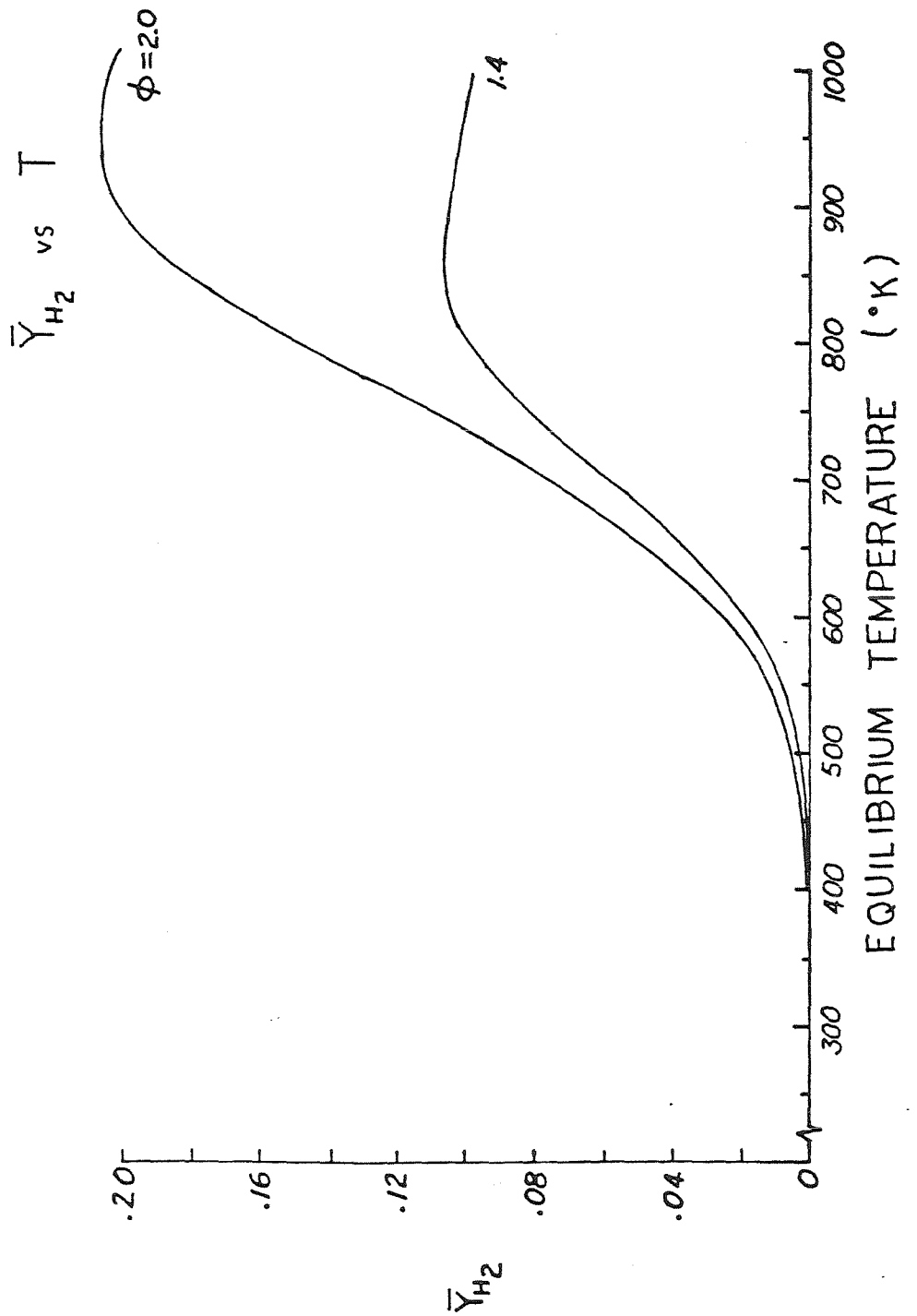
$\bar{Y}_{H_2}$ vs T
ϕ=2.0
1.4
.20
.16
.12
.08
.04
0
$\bar{Y}_{H_2}$
300
400
500
600
700
800
900
1000
EQUILIBRIUM TEMPERATURE (°K)

Figure 5.14

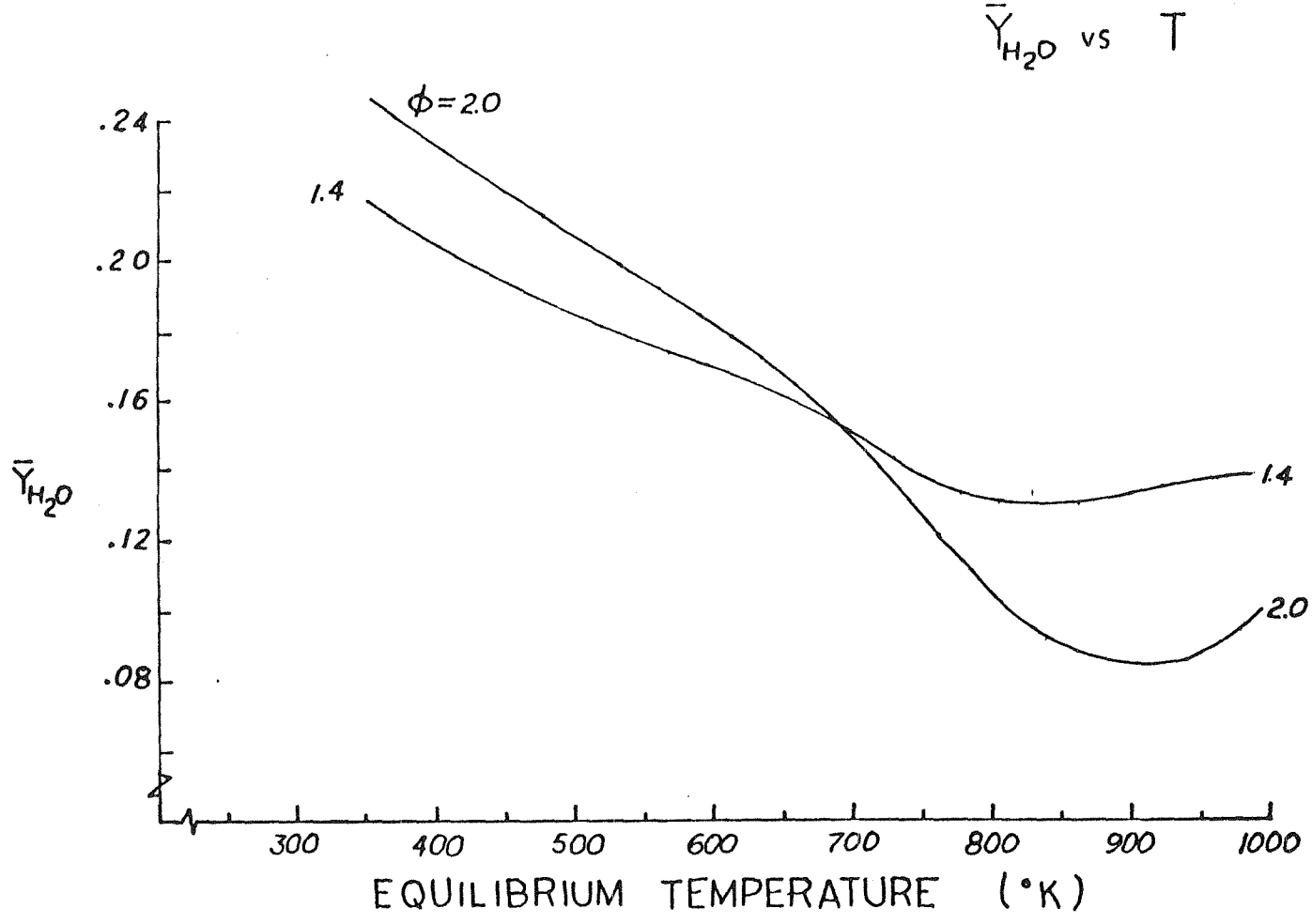
$\bar{Y}_{H_2O}$ vs T
ϕ=2.0
1.4
.24
.20
.16
.12
.08
$\bar{Y}_{H_2O}$
1.4
2.0
300
400
500
600
700
800
900
1000
EQUILIBRIUM TEMPERATURE (°K)

Figure 5.15

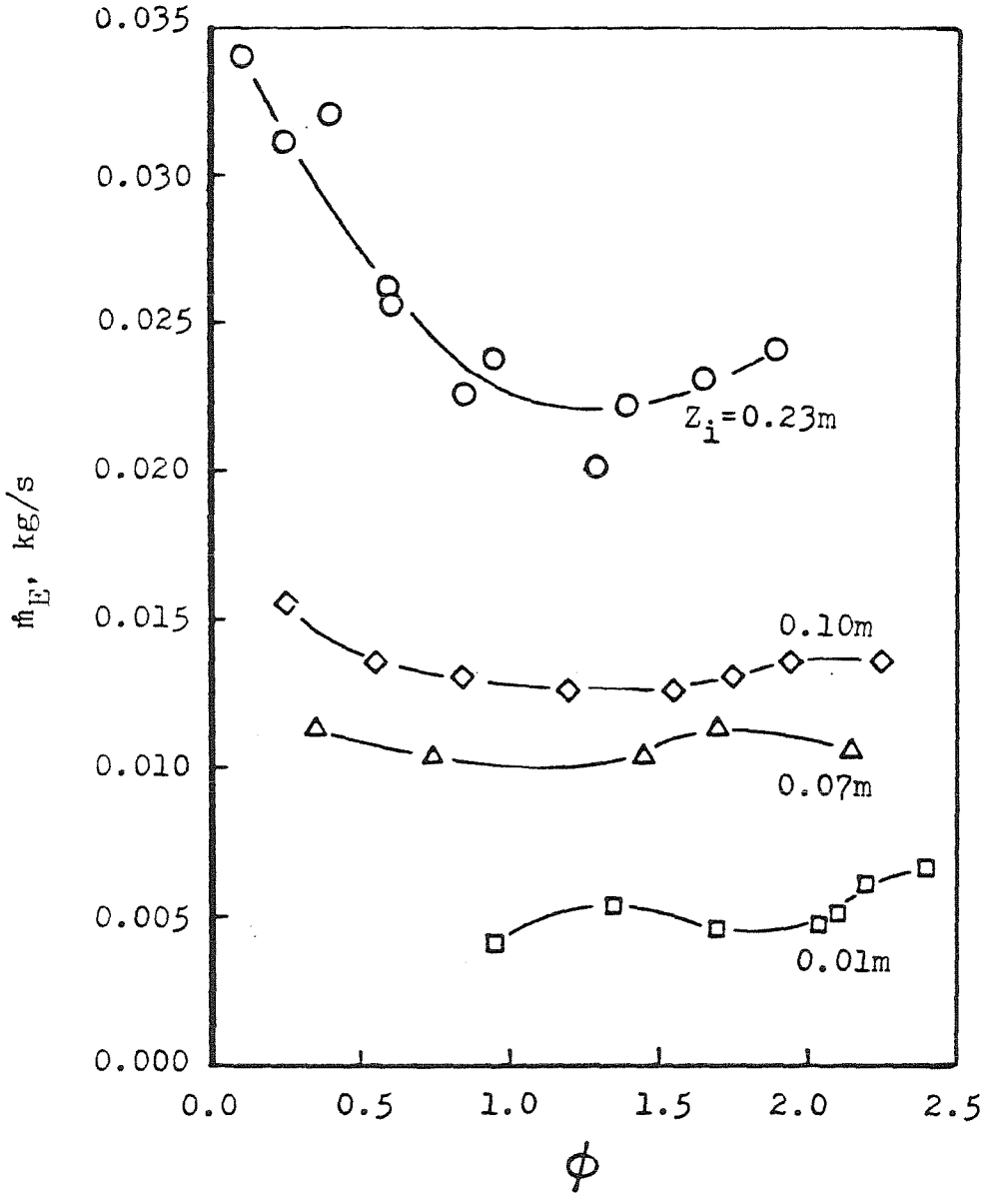
0.035
0.030
0.025
0.020
0.015
0.010
0.005
0.000
$\dot{m}_E$, kg/s
Z_i=0.23m
0.10m
0.07m
0.01m
0.0
0.5
1.0
1.5
2.0
2.5
ϕ

Figure 5.16

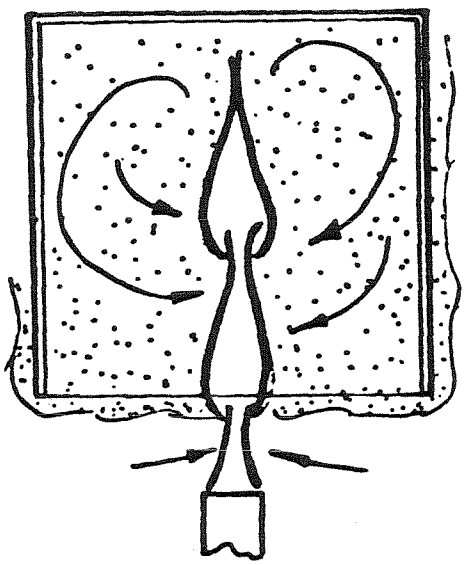

t = 0 sec:
- o Steady flame
- o Steady, low soot
- o 1.4% CO

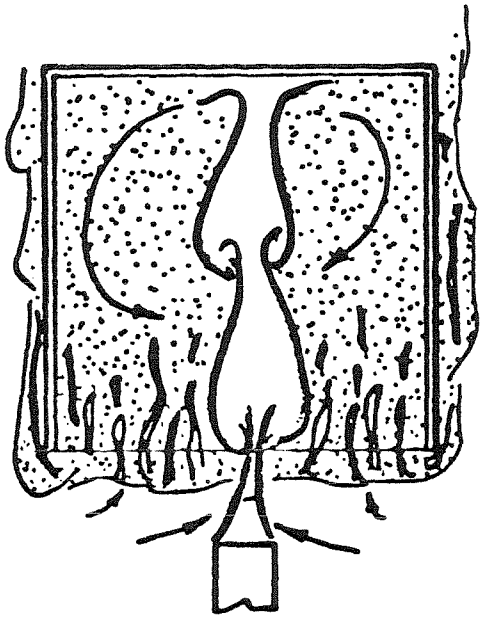

t = 40 sec:
- o Flamelets form
- o Taylor instability
- o More soot, 1.8% CO

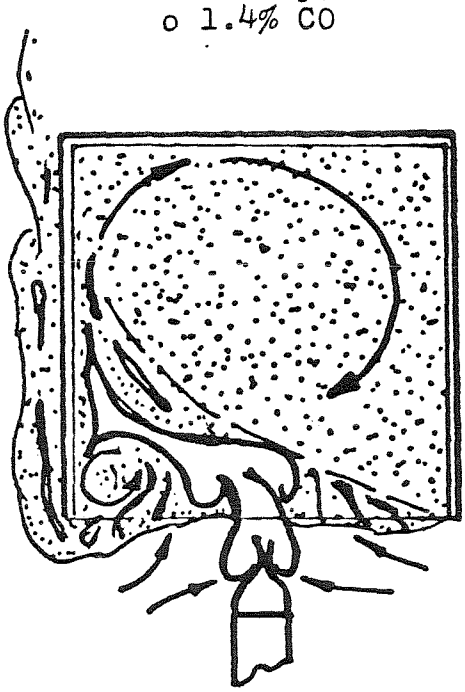

t = 47 sec:
- o Violent turnover
- o Flame strongly blown
- o Flamelets decay

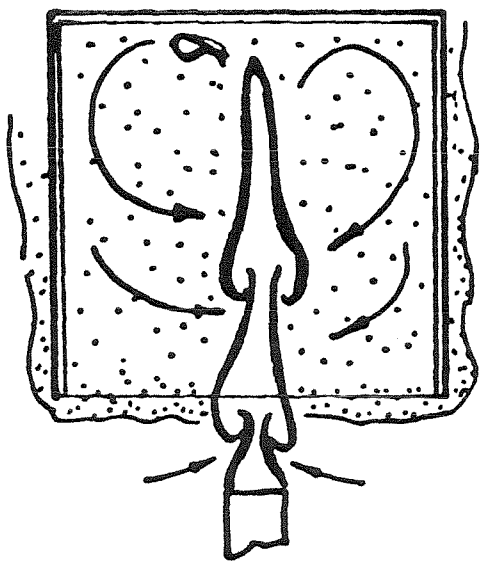

t = 62 sec:
- o Return to steady flame
- o Residence time about 100 sec.
- o Periodic cycle

Figure 5.17 (a)

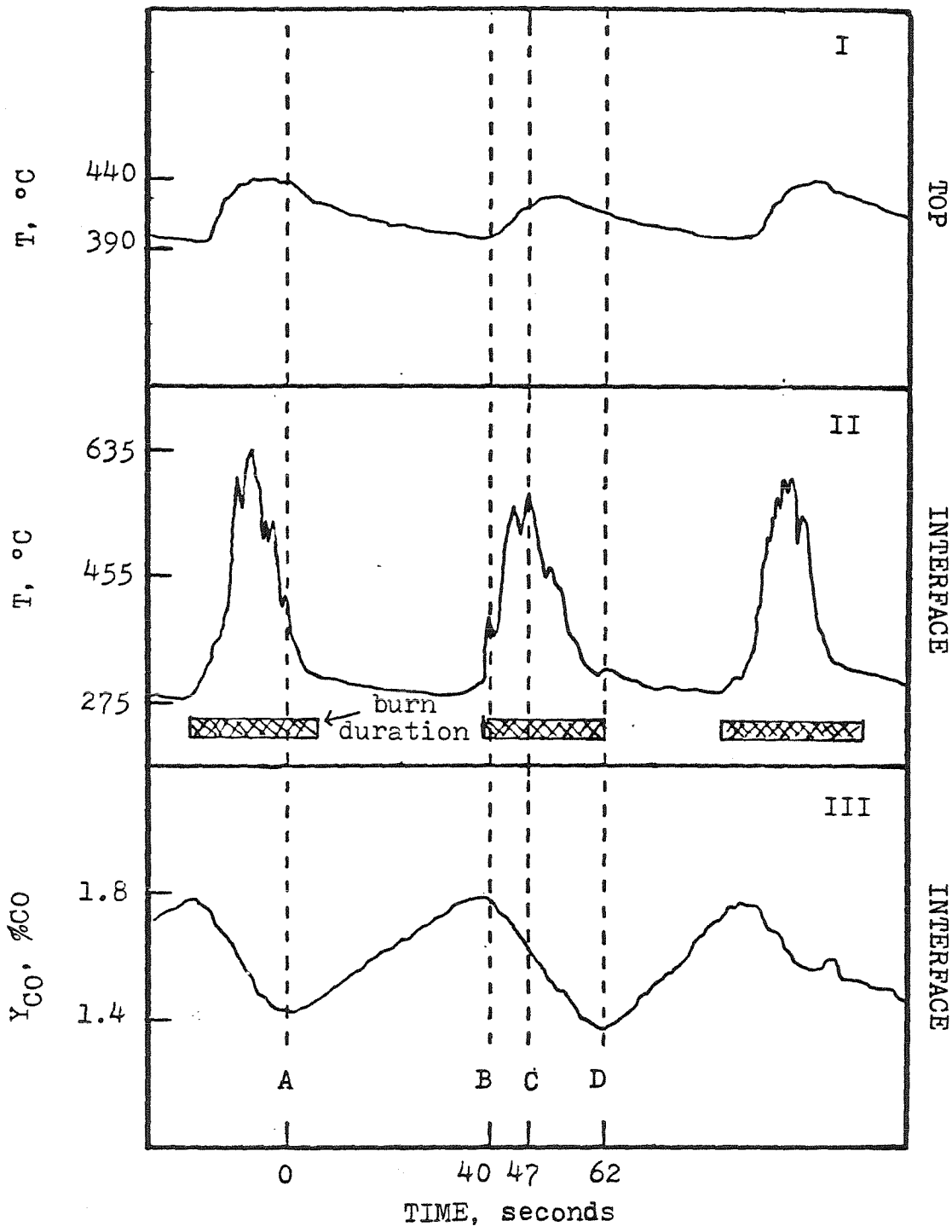
I
II
III
T, °C
440
390
635
455
275
burn
duration
TOP
INTERFACE
INTERFACE
Y_{CO}, %CO
1.8
1.4
A
B
C
D
0
40
47
62
TIME, seconds

Figure 5.17(b)

Chapter 6

SUMMARY AND CONCLUSIONS

6.1. Mixing in Doorway Flows

We have presented the results of experiments done in a half-scale room to investigate the mixing process near a doorway. No actual fire was present in the room; instead, a pump-furnace setup was used to simulate the entrainment and heating of fresh air by the fire plume. Four door geometries were used in the experiments. To estimate the mass transfer rates, it was assumed that the room and ambient air can be separated into four distinct regions with uniform thermodynamic properties: the hot ceiling layer, the cooler floor layer, the furnace, and the ambient or outside air regions.

The dimensionless temperature profiles (gas temperature normalized by the furnace and ambient air temperatures) were plotted as a function of distance from the interface for different floor suction rates. It was found that, for certain door geometries, the profile shapes were independent of the floor suction rate.

It was observed that the furnace temperature and the floor suction rate have a very strong influence on the interface height and the mixing rates. The mixing rates (expressed as the entrainment rate into the cold layer divided by the floor suction rate) were found to be a function of a Richardson number that uses the interface height as the characteristic length. The average inflow velocity, U_{1c}, was estimated with the use of the door width and the interface height. For a given value of $\dot{m}_2$, the effect of reducing the door area is to reduce the value of Ri_o and hence increase the mixing rate. The door height was found to be a

much stronger influence on the mixing rate and interface height than the door width.

With the use of Taylor's entrainment hypothesis and a velocity scale based on the initial momentum of the jet, we found that the relationship between $\dot{m}_d/\dot{m}_{1c}$ and Ri_o is:

$$\left[\frac{1}{2}\left[\frac{\dot{m}_d}{\dot{m}_{1c}}\right]^2 + \frac{\dot{m}_d}{\dot{m}_{1c}}\right]\left[1 + \frac{\dot{m}_d}{\dot{m}_{1c}}\right]^2 = 11.7\left[\frac{\rho_h}{\rho_\infty}\frac{b}{W}\frac{1}{\sqrt{Ri_o}}\right]^2. \qquad (3.16a)$$

This correlation was derived from data obtained from a rectangular room with a door; it should not be applied to other room geometries which are radically different from the one used in our experiments.

6.2. Entrainment in Fire Plumes

We have made entrainment measurements in the near field of a buoyant diffusion flame where the interface height was well below the top of the flames. The entrainment rates were estimated by analyzing the composition of the hot combustion products in the ceiling layer. It was found that the temperature and species concentrations did not vary significantly within the ceiling layer.

For a given interface height, it was observed that the gas temperature reaches a maximum when the fuel-air ratio was increased above the stoichiometric value. This maximum temperature was found to decrease with interface height and is a result of changes in the relative magnitude of the heat released by the fire and heat loss from the system to the surrounding environment.

The measured species concentrations were compared with the theoretical equilibrium composition values obtained from a computer program written by

Gordon and McBride (1976). It was found that the measured species concentrations were almost independent of the gas temperature. The error resulting from the assumption of negligible soot concentration was found to be large enough to affect the accuracies of the calculated water and hydrogen concentrations.

The mass entrainment rates of air into the fire plume were measured for four interface heights. The entrainment data correlated well with the values reported by Cetegen (1982). As was also observed by Cetegen (1982), the entrainment rates were found to be a very weak function of the fuel-air ratio and at very low elevations of the interface.

In our study of fuel rich ceiling layers, it was observed that there was a critical fire size for a given interface height in which flamelets started to form in the interface and spread until the entire interface was set on fire. The burning of the interface caused an inversion process to occur in the ceiling layer. It was observed that the inversion process occurred in regular cycles with the period being inversely proportional to the fire size.

Some preliminary experiments were made to investigate the effect of injecting fuel into an oxygen rich ceiling layer. Fuel and oxygen mass models were set up to estimate the amount of added fuel that reacts in the fire plume. For a ceiling layer with an oxygen content of about 12% by volume, it was found that more than 50% of the fuel injected into the ceiling layer reacted with the oxygen. Since it was assumed that the plume entrainment rates were independent of the flowrate of added fuel, the models were found to be inaccurate when a large amount of fuel was added to the ceiling layer.

In another experiment to determine if the added fuel will react in an oxygen rich ceiling layer, the pipe used to inject the fuel was lighted and then placed inside the ceiling layer. It was found that the critical mole fraction of oxygen is

about 0.13 for the flame on the pipe to keep burning. These findings are the results of preliminary experiments; more refined methods must be used to accurately determine the effect of adding fuel to an oxygen rich ceiling layer.

7. References

G.N. ABRAMOVICH, Theory of turbulent jets. M.I.T. Press, Cambridge, Mass. (1963).

G.L. BROWN and A. ROSHKO, On density effects and large structures in turbulent mixing layers. *Journal of Fluid Mechanics*, **64**, 775-815 (1974).

B. CETEGEN, E.E. ZUKOSKI and T. KUBOTA, Entrainment and flame geometry of fire plumes. California Institute of Technology (August 1982).

V. CHU and M.R. VANVARI, Experimental study of turbulent stratified shearing flow. *Journal of the Hydraulics Division*, ASCE, **102**, no. HY6, 691-705 (1976).

T.H. ELLISON & J.S. TURNER, Turbulent entrainment in stratified flows. *Journal of Fluid Mechanics*, **6**, 423-448 (1959).

H.B. FISCHER, E.J. LIST, R.C. KOH, J. IMBERGER & N.H. BROOKS, Mixing in inland and coastal waters. Academic Press, New York (1979).

S. GORDON and B.J. McBRIDE, Computer program for calculation of complex chemical equilibrium compositions, rocket performance, incident and reflected shocks, and Chapman-Jouguet detonations. NASA SP-273 (March 1976).

K. KAWAGOE, Fire behavior in rooms. Report No. 27. Building Research Institute, Japan (1958).

B. LEWIS and G. VON ELBE, Combustion, flames and explosion of gases. Academic Press, New York (1963).

B.R. MORTON, G.I. TAYLOR & J.S. TURNER. *Proc. Roy. Soc.* A, **234**, 1-23 (1956).

W.S. SARGENT, Natural convection and associated heat transfer processes in room fires. Ph.D. Thesis, California Institute of Technology (1983).

R.S. SCOTTI and G.M. CORCOS, An experiment on the stability of small disturbances in a stratified free shear layer. *Journal of Fluid Mechanics*, **52**, 499-528 (1972).

P.M. SFORZA and G. HERBST, A study of three dimensional, incompressible, turbulent wall jets. *AIAA*, **8**, 276 (1970).

F.S. SHERMAN, J. IMBERGER & G.M. CORCOS, Turbulence and mixing in stably stratified waters, *Annual Review of Fluid Mechanics*, **10**, 267-288 (1978).

A. SIGALLA, Experimental data on turbulent wall jets. *Aircraft Eng.*, **30**, 131-134 (1958).

E.N. TANGREN, W.S. SARGENT and E.E. ZUKOSKI, Hydraulic and numerical modeling of room fires. California Institute of Technology. NSF Grant No. ENV 76-06660 (June 1978).

P.H. THOMAS, P.L. HINKLEY, C.R. THEOBALD and D.L. SIMMS, Investigations into the flow of hot gases in roof venting. Fire Research Technical Paper No. 7. Department of Scientific and Industrial Research and Fire Offices' Committee Joint Fire Research Organization, Borehamwood (1963).

J.S. TURNER, Buoyancy effects in fluids. Cambridge Univ. Press (1973).

E.E. ZUKOSKI, Convective flows associated with room fires. California Institute of Technology, NSF Grant No. GI 31892X1. NSF RANN Conference on Fire Research, Harvard University (June 1975).

E.E. ZUKOSKI, Development of a stratified ceiling layer in the early stages of a closed-room fire. *Fire Mater.*, **2**, 54-62 (1978).

E.E. ZUKOSKI and T. KUBOTA, A computer model for fluid dynamic aspects of a transient fire in a two-room structure. California Institute of Technology (January 1978).

E.E. ZUKOSKI and T. KUBOTA, Two-layer modeling of smoke movement in building fires. *Fire Mater.*, **4**, 17-27 (1980).

E.E. ZUKOSKI and D.L. PETERKA, Measurements of entrainment in a doorway flow. California Institute of Technology (October 1979).

Appendix A

THE TWO-LAYER ROOM MODEL

A.1. Mass Transfer Model

The two-layer room model assumes that the room may be divided into two homogeneous regions with uniform properties: the ceiling (or hot) layer which contains the combustion products, and the floor (or cold) layer which contains fresh air. In addition to the two layers, the furnace and the ambient air region are also assumed to have uniform properties. Figure 2.2(b) is a schematic diagram of the model used in the calculation of the mass flows between each region. The thermodynamic properties in each region are assumed to be uniform throughout the region and independent of time.

Given the quantities $\dot{m}_2$, $\dot{m}_f$, K_h, K_c, and K_∞, the mass flowrates $\dot{m}_{1h}$, $\dot{m}_{1c}$, $\dot{m}_d$, and $\dot{m}_u$ may be calculated by balancing the total mass flows and the carbon dioxide mass flows in each region.

For the floor layer: $$\dot{m}_{1c} + \dot{m}_d - \dot{m}_u - \dot{m}_2 = 0 \tag{A.1}$$

$$C_\infty \dot{m}_{1c} + C_h \dot{m}_d - C_c \dot{m}_u - C_c \dot{m}_2 = 0 \tag{A.2}$$

For the ceiling layer: $$\dot{m}_3 + \dot{m}_u - \dot{m}_{1h} - \dot{m}_d = 0 \tag{A.3}$$

$$C_3 \dot{m}_3 + C_c \dot{m}_u - C_h \dot{m}_{1h} - C_h \dot{m}_d = 0 \tag{A.4}$$

For the furnace: $\dot{m}_3 = \dot{m}_2 + \dot{m}_f$ (A.5)

where C_i is the mass fraction of CO_2 in region i. In our experiment the fuel flow rate, $\dot{m}_f$, was found to be negligible compared to the total mass flow $\dot{m}_2$. $\dot{m}_3$ may then be approximated by

$$\dot{m}_3 \approx \dot{m}_2 . \tag{A.6}$$

The equations must now be manipulated to solve for the unknown mass flows. $\dot{m}_u$ may be eliminated from Eq. A.1 with the use of Eq. A.3.

$$\dot{m}_{1c} - \dot{m}_{1h} = \dot{m}_2 - \dot{m}_3 \tag{A.7}$$

Similarly, Eq. A.4 may be used to eliminate the term $\dot{m}_u$ in Eq. A.2.

$$C_\infty \dot{m}_{1c} - C_h \dot{m}_{1h} = C_c \dot{m}_2 - C_3 \dot{m}_3 \tag{A.8}$$

The equation for $\dot{m}_{1h}$ is found by multiplying K_∞ to both sides of Eq. A.7 and subtracting the result from Eq. A.8 to eliminate the term $K_\infty \dot{m}_{1c}$.

$$\dot{m}_{1h} = \frac{(C_\infty - C_c)\dot{m}_2 + (C_3 - C_\infty)\dot{m}_3}{C_h - C_\infty} \tag{A.9}$$

Eq. A.7 gives $\dot{m}_{1c}$ in terms of $\dot{m}_2$, $\dot{m}_3$, and $\dot{m}_{1h}$:

$$\dot{m}_{1c} = \dot{m}_2 - \dot{m}_3 + \dot{m}_{1h} \tag{A.10}$$

$\dot{m}_u$ is found by combining Eqs.A.3 and A.4 to eliminate the term $\dot{m}_d$,

$$\dot{m}_u = \frac{\dot{m}_3(C_3 - C_h)}{C_h - C_c} \tag{A.11}$$

and, finally, Eq. A.1 is used to find $\dot{m}_d$.

$$\dot{m}_d = \dot{m}_u + \dot{m}_2 - \dot{m}_{1c} \tag{A.12}$$

If $\dot{m}_3 \approx \dot{m}_2$, Eq. A.12 may be combined with Eqs. A.9, A.10, and A.11 to give

$$\dot{m}_d = \dot{m}_2 \left[\frac{(C_3 - C_c)(C_c - C_\infty)}{(C_h - C_c)(C_h - C_\infty)} \right]. \tag{A.13}$$

If we assume that the molecular weight of the gas in the room is approximately the ambient value, then the above equations may be rewritten in terms of the mole fractions K_i.

$$\dot{m}_{1h} = \frac{(K_\infty - K_c)\dot{m}_2 + (K_3 - K_\infty)\dot{m}_3}{K_h - K_\infty} \tag{A.14}$$

$$\dot{m}_{1c} = \dot{m}_2 - \dot{m}_3 + \dot{m}_{1h} \tag{A.15}$$

$$\dot{m}_u = \frac{\dot{m}_3(K_3 - K_h)}{K_h - K_c} \tag{A.16}$$

$$\dot{m}_d = \dot{m}_2 \left[\frac{(K_3 - K_c)(K_c - K_\infty)}{(K_h - K_c)(K_h - K_\infty)} \right] \tag{A.17}$$

A.2. Definition of U^*

Taylor's entrainment hypothesis states that local entrainment rate is proportional to the local maximum velocity and the local entrainment coefficient (see Sec. 3.1.3). Since we have no knowledge of the velocity profiles in the room, we were forced to look for another velocity scale. From previous experimental work (Chu & Vanvari 1976), it is known that the entrainment process takes place primarily in the so-called "supercritical" (i.e., momentum-dominated) region of a stratified wall jet. In this supercritical region, the flow is influenced by the upstream condition only and has similar characteristics to a neutral jet (Chu & Vanvari 1976). For our range of experiments, it follows that we may ignore the momentum losses due to wall friction and changes in hydrostatic pressure and define a new velocity scale based on the initial momentum of the jet. The velocity scale, U^*, is defined to be:

$$U^*(x) \equiv \frac{\int_0^\infty \rho U^2 dy}{\int_0^\infty \rho U\, dy}. \tag{A.18}$$

A mass balance of the cold layer jet gives ($\dot{m}_u = 0$):

$$\int_0^\infty \rho U\, dy \equiv \dot{m}(x) = \dot{m}_d(x) + \dot{m}_{1c} \tag{A.19}$$

where $\dot{m}_d(x)$ is the mass flux of entrained hot layer gas, and $\dot{m}_{1c}$ is the mass flowrate of fresh air entering the room.

A momentum balance of the cold layer jet gives:

$$\int_0^\infty \rho U^2 dy = \dot{m}_{1c} U_{1c} - \dot{m}_{1c} U_{1c} \left[1 - \frac{b}{W}\right] - \left[C_F(x)\right] - \left[C_P(x)\right] \qquad \text{(A.20)}$$

where $\dot{m}_{1c} U_{1c}$ is the initial jet momentum; $(\dot{m}_{1c} U_{1c})(1 - b/W)$ is the loss due to the sudden expansion of the jet width (from b to W); $C_F(x)$ represents the frictional drag of the walls; and $C_P(x)$ represents the pressure force on the layer due to its changing depth and density (see Ellison & Turner 1959). If we now assume that the losses due to the presence of pressure gradients and wall friction are negligible compared to $(\dot{m}_{1c} U_{1c})(b/W)$, Eq. A.18 may be combined with Eqs. A.19 and A.20:

$$U^*(x) \approx \frac{\dot{m}_{1c} U_{1c}}{\dot{m}(x)} \frac{b}{W}. \qquad \text{(A.21)}$$

A.3. Relationship between U^* and U_{max}

From Eq. A.18:

$$U^*(x) = \frac{x\, U_{max}^2(x) \int_0^\infty \rho \left[\frac{U}{U_{max}}\right]^2 d(y/x)}{x\, U_{max}(x) \int_0^\infty \rho \frac{U}{U_{max}} d(y/x)}. \qquad \text{(A.22)}$$

For self-preserving jets with small density variations in the streamwise direction ($\rho \approx \rho_\infty$), Eq. A.22 reduces to:

$$U^*(x) = \frac{U_{max}(x)}{A_1} \qquad \text{(A.23)}$$

where

$$A_1 = \frac{\int_0^\infty \rho \frac{U}{U_{max}} d(y/x)}{\int_0^\infty \rho \left[\frac{U}{U_{max}}\right]^2 d(y/x)} = \text{constant} . \qquad (A.24)$$

A_1 is an empirical constant whose value depends on the shape of the velocity profile. For Gaussian velocity profiles ($U/U_{max} = e^{-\left[\gamma y/x\right]^2}$), A_1 is approximately 1.4.

Appendix B

CALCULATION OF SPECIES CONCENTRATIONS IN A FIRE PLUME

For one mole of methane fuel burning in x moles of excess air:

$$\Big[CH_4 + (2+x)(O_2 + 3.76N_2) \rightarrow n_{CO_2}CO_2 + n_{CO}CO + \\ + n_{CH_4}CH_4 + n_{O_2}O_2 + n_{H_2O}H_2O + n_{H_2}H_2 + n_{N_2}N_2\Big]$$

where n_i is the number of moles of species i. We can now write four equations to balance the number of moles of the elements C, H, O, and N.

$$C: \quad 1 = n_{CO_2} + n_{CO} + n_{CH_4} \tag{B.1}$$

$$H: \quad 2 = 2n_{CH_4} + n_{H_2O} + n_{H_2} \tag{B.2}$$

$$O: \quad 2 + x = n_{CO_2} + n_{O_2} + \frac{1}{2}(n_{H_2O} + n_{CO}) \tag{B.3}$$

$$N: \quad 3.76(2+x) = n_{N_2} \tag{B.4}$$

Using our analyzers, we are able to measure the mole fraction of CH_4, CO_2, CO, and O_2 in a *dried* sample. Using this data we wish to find: (1) the actual mole fractions of the seven species in the hood; (2) the equivalence ratio; (3) the mass of air entrained into the plume; and (4) the molecular weight of the mixture.

B.1. Species Concentrations

Let N_{sample} be the total number of moles in the dried sample, i.e.,

$$N_{sample} = n_{CO_2} + n_{CO} + n_{CH_4} + n_{O_2} + n_{N_2} + n_{H_2} . \tag{B.5}$$

Now define

$$Y_{CO_2} \equiv \frac{n_{CO_2}}{N_{sample}}; \; Y_{CO} \equiv \frac{n_{CO}}{N_{sample}}; \; Y_{H_2O} \equiv \frac{n_{H_2O}}{N_{sample}}; \; etc.$$

or, in general, for species i:

$$Y_i \equiv \frac{n_i}{N_{sample}} \tag{B.6}$$

Note that Y_i is the mole fraction of species i in the dried sample with the exception of Y_{H_2O} which has no physical significance. Dividing Eqs. B.1, B.2, B.3, B.4, and B.5 by N_{sample} yields

$$\frac{1}{N_{sample}} = Y_{CO_2} + Y_{CO} + Y_{CH_4} \tag{B.7}$$

$$\frac{2}{N_{sample}} = 2Y_{CH_4} + Y_{H_2O} + Y_{H_2} \tag{B.8}$$

$$\frac{Y_{N_2}}{3.76} = Y_{CO_2} + Y_{O_2} + \frac{1}{2}(Y_{H_2O} + Y_{CO}) \tag{B.9}$$

$$1 = Y_{CO_2} + Y_{CO} + Y_{CH_4} + Y_{O_2} + Y_{N_2} + Y_{H_2} . \qquad \text{(B.10)}$$

where Eq. B.9 was obtained by combining Eqs. B.3 and B.4. The value of N_{sample} is given explicitly by Eq. B.7 since Y_{CO_2}, Y_{CO}, and Y_{CH_4} are known.

We now have to manipulate the equations to find the unknown terms. Subtracting Eq. B.10 from B.8 eliminates the term Y_{H_2}.

$$\frac{2}{N_{sample}} - 1 = Y_{CH_4} + Y_{H_2O} - Y_{CO_2} - Y_{CO} - Y_{O_2} - Y_{N_2} \qquad \text{(B.11)}$$

Multiplying Eq. B.9 by 2 then subtracting the result from Eq. B.11 eliminates the term Y_{H_2O}.

$$\frac{2}{N_{sample}} - 1 = Y_{CH_4} - 3Y_{CO_2} - 2Y_{CO} - 3Y_{O_2} - 0.4681\,Y_{N_2} \qquad \text{(B.12)}$$

Y_{N_2} is calculated from Eq.B.12:

$$Y_{N_2} = \frac{1}{0.4681}\left[Y_{CH_4} - 3Y_{CO_2} - 2Y_{CO} - 3Y_{O_2} - \frac{2}{N_{sample}} + 1\right] \qquad \text{(B.13)}$$

Eq. B.9 gives Y_{H_2O}:

$$Y_{H_2O} = 2\left[\frac{Y_{N_2}}{3.76} - Y_{CO_2} - Y_{O_2}\right] - Y_{CO} \qquad \text{(B.14)}$$

and Eq. B.8 yields Y_{H_2}:

$$Y_{H_2} = \frac{2}{N_{sample}} - 2Y_{CH_4} - Y_{H_2O} \tag{B.15}$$

The next step is to find the actual mole fractions of each species in the hood. Let N_{hood} be the total number of moles in the hood, i.e.,

$$\begin{aligned} N_{hood} &= n_{CO_2} + n_{CO} + n_{CH_4} + n_{O_2} + n_{H_2O} + n_{H_2} + n_{N_2} \\ &= N_{sample}\left[Y_{CO_2} + Y_{CO} + Y_{CH_4} + Y_{O_2} + Y_{H_2O} + Y_{H_2} + Y_{N_2}\right] \\ &= N_{sample}\left[1 + Y_{H_2O}\right] \end{aligned}$$

where the last result came from using (B.10). Now define $\overline{Y}_i$ as the actual mole fraction of species i, i.e.,

$$\begin{aligned} \overline{Y}_i &= \frac{n_i}{N_{hood}} \\ &= \frac{Y_i N_{sample}}{N_{hood}} \\ &= \frac{Y_i}{1 + Y_{H_2O}}. \end{aligned} \tag{B.16}$$

Therefore,

$$\overline{Y}_{CO_2} = \frac{Y_{CO_2}}{1 + Y_{H_2O}}; \quad \overline{Y}_{H_2O} = \frac{Y_{H_2O}}{1 + Y_{H_2O}}; \quad etc.$$

B.2. The Equivalence Ratio

The equivalence ratio is defined to be the fuel-air ratio divided by the stoichiometric fuel-air ratio.

$$\varphi = \frac{2}{2 + x} \tag{B.17}$$

Eq. B.4 may be used to calculate x.

$$n_{N_2} = (2 + x)3.76 = Y_{N_2} N_{sample}$$

Therefore,

$$\varphi = \frac{2}{2 + x} = \frac{7.52}{Y_{N_2} N_{sample}} \tag{B.18}$$

where Y_{N_2} and N_{sample} can be calculated from Eqs. B.7 and B.13, respectively.

B.3. Air Entrainment Rate

The mass entrainment of air, $\dot{m}_E$, can be calculated if the mass flowrate of fuel, $\dot{m}_f$, is given.

$$\dot{m}_E = (2 + x)(4.76)\left[\frac{\dot{m}_f}{16}\right](28.8)$$

$$= 8.58(2 + x)\dot{m}_f = 8.58\left[\frac{2}{\varphi}\right]\dot{m}_f \tag{B.19}$$

where $(2 + x)(4.76)$ is the number of moles of air per mole of fuel; 16 is the

molecular weight of the fuel; and 28.8 is the molecular weight of air.

B.4. Molecular Weight

The molecular weight, MW, of the mixture is

$$MW = \frac{\text{total mass in hood}}{\text{total moles in hood}}$$

$$= \sum_i \overline{Y}_i \times MW_i \qquad \text{(B.20)}$$

where $\overline{Y}_i$ and MW_i are the mole fraction and molecular weight of species i.

Appendix C

TABULATED DATA FROM THE ROOM EXPERIMENTS

The experimental data obtained from the room experiments are tabulated on the following pages. The symbols are defined in the List of Symbols. The units of the symbols are as follows:

Symbol	Units
K_∞, K_h, K_3, K_c	$\%CO_2$ by volume
$\dot{m}_2$, $\dot{m}_{1h}$, $\dot{m}_{1c}$, $\dot{m}_u$, $\dot{m}_d$	kilograms per second
$\dot{Q}_f$	kilowatts
F, Ri_o	dimensionless
T_∞, T_h, T_3, T_c	degrees Celsius
t_{res}	seconds
U_{1c}	meters per second
Y_i, δ_C	inches

DOOR GEOMETRY: 18" by 39" high							
Run	24	25	26	28	29	30	31
$\dot{m}_2$	0.076	0.146	0.176	0.186	0.037	0.165	0.200
$\dot{Q}_f$	13.7	26.5	26.5	29.2	7.7	23.7	24.3
K_∞	0.05	0.05	0.03	0.04	0.05	0.05	0.05
K_h	0.72	0.63	0.61	0.63	0.83	0.63	0.65
K_3	0.73	0.68	0.66	0.66	0.85	0.67	0.63
K_c	0.06	0.11	0.17	0.18	0.05	0.12	0.21
T_∞	25	25	24	23	22	23	24
T_h	147	150	147	148	128	147	147
T_3	166	166	159	162	155	163	159
T_c	33	38	48	50	32	41	56
$\dot{m}_{1h}$	0.076	0.143	0.149	0.151	0.038	0.156	0.140
$\dot{m}_{1c}$	0.076	0.143	0.149	0.151	0.038	0.156	0.140
$\dot{m}_u$	.0012	.0140	.0200	.0124	.0009	.0129	-.009
$\dot{m}_d$	.0012	.0166	.0473	.0471	.0000	.0215	.0509
Y_i	27.6	19.7	14.9	14.0	34.3	17.3	11.5
U_{1c}	0.200	0.529	0.723	0.780	0.080	0.653	0.880
Ri_g	45.38	4.44	1.55	1.22	312.3	2.41	0.72
δ_C	8.0	8.0	8.0	8.8	5.6	8.0	11.2
t_{res}	17.04	12.22	11.94	11.58	24.63	11.81	11.59
$\frac{\dot{m}_d}{\dot{m}_{1c}}$	0.0152	0.115	0.318	0.3111	0.000	0.137	0.364
F	0.040	0.125	0.213	0.239	0.016	0.170	0.312

DOOR GEOMETRY: 18" by 24" high						
Run	32	33	34	35	36	37
$\dot{m}_2$	0.067	0.030	0.208	0.067	0.146	0.050
$\dot{Q}_f$	12.1	7.7	20.1	12.8	20.1	10.4
K_∞	0.09	0.05	0.05	0.05	0.06	0.04
K_h	0.78	1.03	0.89	0.82	0.88	0.83
K_3	0.79	1.05	0.89	0.82	0.89	0.84
K_c	0.17	0.05	0.51	0.13	0.36	0.08
T_∞	23	24	21	21	21	21
T_h	131	115	142	125	154	125
T_3	162	153	157	160	164	160
T_c	38	35	102	40	72	33
$\dot{m}_{1h}$	0.060	0.031	0.094	0.060	0.094	0.048
$\dot{m}_{1c}$	0.060	0.031	0.094	0.060	0.094	0.048
$\dot{m}_u$	.0011	.0006	.0000	.0000	.0028	.0007
$\dot{m}_d$	.0079	.0000	.1139	.0070	.0544	.0026
Y_i	11.0	18.2	4.3	13.2	6.5	15.8
U_{1c}	0.395	0.122	1.568	0.326	1.041	0.218
Ri_o	3.85	60.83	0.03	6.20	0.24	18.35
δ_C	4.0	6.0	9.6	4.0	10.4	4.0
t_{res}	36.46	68.28	13.50	34.81	17.75	43.15
$\frac{\dot{m}_d}{\dot{m}_{1c}}$	0.131	0.000	1.211	0.116	0.577	0.053
F	0.140	0.037	1.465	0.111	0.522	0.065

DOOR GEOMETRY: 12" by 39" high						
Run	38	39	40	41	42	43
$\dot{m}_2$	0.068	0.147	0.044	0.196	0.112	0.100
$\dot{Q}_f$	12.4	20.1	9.6	26.5	19.2	17.2
K_∞	0.04	0.04	0.04	0.04	0.05	0.05
K_h	0.63	0.73	0.84	0.77	0.72	0.69
K_S	0.63	0.75	0.84	0.79	0.72	0.70
K_c	0.05	0.16	0.05	0.31	0.10	0.08
T_∞	22	22	22	20	21	21
T_h	124	146	132	148	150	149
T_S	158	161	160	164	161	161
T_c	32	45	33	65	40	39
$\dot{m}_{1h}$	0.067	0.126	0.044	0.128	0.103	0.096
$\dot{m}_{1c}$	0.067	0.126	0.044	0.128	0.103	0.096
$\dot{m}_u$	.0006	.0052	.0000	.0063	.0000	.0008
$\dot{m}_d$	.0012	.0265	.0003	.0743	.0087	.0049
Y_i	25.4	13.7	31.2	7.0	17.8	21.1
U_{1c}	0.286	0.988	0.151	1.959	0.624	0.489
Ri_c	17.28	0.78	80.21	0.08	2.78	5.40
δ_C	4.0	6.4	4.0	14.4	4.0	4.8
t_{res}	22.33	14.85	25.14	13.25	17.00	17.00
$\frac{\dot{m}_d}{\dot{m}_{1c}}$	0.017	0.211	0.006	0.581	0.084	0.051
F	0.045	0.199	0.020	0.625	0.104	0.075

DOOR GEOMETRY: 12" by 26" high						
Run	44	45	46	47	48	49
$\dot{m}_2$	0.067	0.044	0.033	0.078	0.057	0.094
$\dot{Q}_f$	13.7	10.0	9.3	13.1	11.0	13.9
K_∞	0.05	0.05	0.05	0.05	0.05	0.05
K_h	0.89	0.83	1.06	0.87	0.97	0.97
K_S	0.89	0.83	1.06	0.87	0.97	0.97
K_c	0.20	0.08	0.06	0.18	0.16	0.32
T_∞	21	22	22	22	20	21
T_h	135	129	119	141	126	144
T_S	168	164	158	160	166	165
T_c	37	36	33	50	35	54
$\dot{m}_{1h}$	0.055	0.042	0.033	0.066	0.050	0.066
$\dot{m}_{1c}$	0.055	0.042	0.033	0.066	0.050	0.066
$\dot{m}_u$	.0000	.0000	.0000	.0000	.0000	.0000
$\dot{m}_d$	.0120	.0017	.0003	.0124	.0068	.0276
Y_i	11.0	15.4	18.7	9.1	13.4	7.2
U_{1c}	0.538	0.296	0.188	0.777	0.401	0.990
Ri_c	2.16	9.64	27.71	0.75	4.49	0.35
δ_C	4.0	4.8	5.6	11.2	3.2	8.8
t_{res}	36.10	49.15	60.41	32.13	40.57	27.76
$\frac{\dot{m}_d}{\dot{m}_{1c}}$	0.217	0.040	0.010	0.188	0.136	0.415
F	0.123	0.059	0.036	0.205	0.087	0.296

DOOR GEOMETRY: 12" by 26" high (variable T_s)				
Run	50	51	52	53
$\dot{m}_2$	0.057	0.093	0.057	0.057
$\dot{Q}_f$	8.6	11.1	5.8	3.1
K_∞	0.05	0.05	0.05	0.05
K_h	0.75	0.76	0.52	0.31
K_s	0.75	0.76	0.52	0.31
K_c	0.16	0.29	0.15	0.12
T_∞	20	20	21	21
T_h	103	120	79	62
T_s	131	133	98	67
T_c	33	55	32	32
$\dot{m}_{1h}$	0.048	0.062	0.045	0.042
$\dot{m}_{1c}$	0.048	0.062	0.045	0.042
$\dot{m}_u$	.0000	.0000	.0000	.0000
$\dot{m}_d$	.0090	.0314	.0121	.0153
Y_i	12.0	7.0	10.3	9.0
U_{1c}	0.429	0.942	0.468	0.498
Ri_o	2.89	0.29	1.51	0.78
δ_C	5.2	10.4	3.2	3.2
t_{res}	44.80	29.92	50.11	54.47
$\frac{\dot{m}_d}{\dot{m}_{1c}}$	0.186	0.511	0.270	0.368
F	0.115	0.346	0.170	0.248

Appendix D

TABULATED DATA FROM THE FIRE PLUME EXPERIMENTS

The experimental data obtained from the plume experiments are tabulated on the following pages. The symbols are defined in the List of Symbols. Y_i is the measured mole fraction of species i in the dried sample, and $\overline{Y}_i$ is the estimated mole fraction of species i in the ceiling layer. The units of the other symbols are as follows:

Symbol	Units
$\dot{Q}_f$	kilowatts
T_h, T_∞	degrees Kelvin
$\dot{m}_E$, $\dot{m}_{p_{in}}$	kilograms per second

0.19 m. Burner Z_i = 0.23 m							
$\dot{Q}_f$	10.5	21.1	31.6	42.1	52.6	63.2	73.7
T_h °K	448	539	614	692	800	826	838
T_∞ °K	293	293	293	293	293	293	293
Y_{O_2}	0.187	0.165	0.140	0.099	0.58	0.015	0.005
Y_{CO_2}	0.012	0.026	0.039	0.064	0.087	0.101	0.106
Y_{CO}	.0000	.0000	.0000	.0006	.0031	.0095	.0166
Y_{CH_4}	.0000	.0000	.0000	.0000	.0004	.0016	.0162
$\overline{Y}_{O_2}$	0.181	0.158	0.130	0.090	0.051	0.012	0.004
$\overline{Y}_{CO_2}$	0.012	0.025	0.036	0.058	0.077	0.083	0.090
$\overline{Y}_{CO}$	.0000	.0000	.0000	.0005	.0027	.0078	.0140
$\overline{Y}_{CH_4}$	.0000	.0000	.0000	.0000	.0004	.0013	.0137
$\overline{Y}_{N_2}$	0.784	0.767	0.762	0.735	0.711	0.716	0.672
$\overline{Y}_{H_2}$	-.008	.0075	-.001	.0211	.0383	-.003	.0512
$\overline{Y}_{H_2O}$	0.032	0.042	0.074	0.096	0.120	0.184	0.156
φ	0.111	0.244	0.357	0.597	0.842	0.962	1.312
$\dot{m}_E$	.0340	.0311	.0319	.0254	.0225	.0237	.0202
$\dot{m}_{P_{in}}$	.0342	.0316	.0326	.0263	.0236	.0251	.0217

0.19 m. Burner Z_i = 0.23 m							
$\dot{Q}_f$	84.2	105.2	126.3	42.1	73.7	105.2	29.2
T_h °K	847	827	830	680	852	821	618
T_∞ °K	293	293	293	298	298	298	295
Y_{O_2}	0.005	0.000	0.002	0.135	0.016	0.003	0.140
Y_{CO_2}	0.101	0.095	0.097	0.054	0.104	0.100	0.036
Y_{CO}	.0196	.0230	.0240	.0000	.0100	.0200	.0000
Y_{CH_4}	.0270	.0590	.0660	.0000	.0010	.0375	.0000
$\overline{Y}_{O_2}$	0.004	0.000	0.002	0.136	0.013	0.002	0.127
$\overline{Y}_{CO_2}$	0.085	.0.078	0.083	0.055	0.087	0.083	0.033
$\overline{Y}_{CO}$	.0164	.0190	.0205	.0000	.0084	.0167	.0000
$\overline{Y}_{CH_4}$	.0226	.0487	.0563	.0000	.0008	.0312	.0000
$\overline{Y}_{N_2}$	0.670	0.659	0.632	0.700	0.699	0.667	0.775
$\overline{Y}_{H_2}$	.0395	.0198	.0595	.1177	.0282	.0324	-.028
$\overline{Y}_{H_2O}$	0.163	0.175	0.147	-.009	0.163	0.167	0.093
φ	1.387	1.666	1.897	0.585	1.035	1.478	0.317
$\dot{m}_E$	.0219	.0228	.0240	.0259	.0256	.0257	.0332
$\dot{m}_{p_{in}}$	.0237	.0250	.0267	.0268	.0271	.0279	.0339

0.19 m. Burner Z_i = 0.10 m						
$\dot{Q}_f$	10.5	21.1	31.6	42.1	52.6	63.2
T_h °K	480	567	625	670	691	687
T_∞ °K	296	296	296	296	296	296
Y_{O_2}	0.175	0.130	0.070	0.025	0.020	0.011
Y_{CO_2}	0.024	0.054	0.079	0.093	0.096	0.091
Y_{CO}	.0000	.0000	.0054	.0150	.0178	.0200
Y_{CH_4}	.0000	.0000	.0050	.0215	.0390	.0690
$\overline{Y}_{O_2}$	0.174	0.128	0.063	0.021	0.017	0.009
$\overline{Y}_{CO_2}$	0.024	0.053	0.071	0.079	0.084	0.077
$\overline{Y}_{CO}$	.0000	.0000	.0048	.0127	.0155	.0168
$\overline{Y}_{CH_4}$	.0000	.0000	.0045	.0182	.0340	.0581
$\overline{Y}_{N_2}$	0.754	0.713	0.706	0.686	0.651	0.653
$\overline{Y}_{H_2}$	.0424	.0880	.0480	.0313	.0696	.0282
$\overline{Y}_{H_2O}$	0.005	0.018	0.103	0.152	0.129	0.159
φ	0.238	0.559	0.854	0.911	1.204	1.538
$\dot{m}_E$	.0159	.0136	.0133	.0126	.0123	.0130
$\dot{m}_{p_{in}}$	.0161	.0140	.0140	.0135	.0134	.0143

0.19 m. Burner Z_i = 0.10 m						
$\dot{Q}_f$	73.7	84.2	105.2	84.2	52.6	31.6
T_h °K	681	703	728	716	697	669
T_∞ °K	296	296	296	296	296	296
Y_{O_2}	0.007	0.005	0.005	0.006	0.016	0.070
Y_{CO_2}	0.089	0.091	0.096	0.093	0.096	0.085
Y_{CO}	.0230	.0240	.0220	.0230	.0196	.0060
Y_{CH_4}	.0870	.0990	.1070	.0960	.0400	.0030
$\overline{Y}_{O_2}$	0.006	0.004	0.004	0.005	0.014	0.066
$\overline{Y}_{CO_2}$	0.075	0.078	0.085	0.081	0.083	0.080
$\overline{Y}_{CO}$	.0193	.0206	.0195	.0200	.0169	.0056
$\overline{Y}_{CH_4}$	.0730	.0850	.0948	.0833	.0345	.0031
$\overline{Y}_{N_2}$	0.639	0.615	0.587	0.610	0.652	0.676
$\overline{Y}_{H_2}$	.0276	.0561	.0955	.0687	.0630	.1070
$\overline{Y}_{H_2O}$	0.160	0.141	0.114	0.133	0.137	0.063
φ	1.965	2.249	2.555	2.268	1.549	0.983
$\dot{m}_E$	.0135	.0135	.0148	.0134	.0122	.0116
$\dot{m}_{p_{in}}$	.0150	.0153	.0170	.0152	.0133	.0123

0.19 m. Burner Z_i = 0.07 m						
$\dot{Q}_f$	21.1	42.1	52.6	63.2	10.5	31.6
T_h °K	604	642	649	654	500	642
T_∞ °K	298	298	298	298	298	298
Y_{O_2}	0.076	0.018	0.008	0.006	0.170	0.043
Y_{CO_2}	0.074	0.090	0.088	0.088	0.031	0.084
Y_{CO}	.0033	.0174	.0208	.0224	.0000	.0096
Y_{CH_4}	.0030	.0486	.0730	.1038	.0000	.0097
$\overline{Y}_{O_2}$	0.067	0.015	0.007	0.005	0.174	0.036
$\overline{Y}_{CO_2}$	0.065	0.075	0.072	0.074	0.032	0.070
$\overline{Y}_{CO}$	.0029	.0145	.0171	.0189	.0000	.0080
$\overline{Y}_{CH_4}$	.0026	.0406	.0599	.0875	.0000	.0081
$\overline{Y}_{N_2}$	0.726	0.675	0.666	0.628	0.731	0.721
$\overline{Y}_{H_2}$	.0172	.0158	-.001	.0296	.0851	-.006
$\overline{Y}_{H_2O}$	0.119	0.164	0.180	0.157	-.022	0.163
φ	0.733	1.454	1.685	2.163	0.326	0.903
$\dot{m}_E$	.0104	.0104	.0113	.0105	.0116	.0126
$\dot{m}_{P_{in}}$	.0108	.0113	.0124	.0118	.0118	.0133

0.19 m. Burner Z_i = 0.01 m							
$\dot{Q}_f$	31.6	21.1	42.1	10.5	21.1	26.3	36.9
T_h °K	549	556	563	507	532	539	568
T_∞ °K	298	298	298	298	298	298	298
Y_{O_2}	0.016	0.032	0.015	0.062	0.023	0.017	0.016
Y_{CO_2}	0.085	0.087	0.085	0.078	0.086	0.086	0.082
Y_{CO}	.0230	.0164	.0230	.0087	.0186	.0210	.0218
Y_{CH_4}	.0944	.0358	.1122	.0136	.0681	.0912	.1119
$\bar{Y}_{O_2}$	0.014	0.028	0.013	0.055	0.020	0.015	0.014
$\bar{Y}_{CO_2}$	0.073	0.075	0.074	0.069	0.074	0.074	0.070
$\bar{Y}_{CO}$	.0198	.0141	.0200	.0076	.0159	.0180	.0186
$\bar{Y}_{CH_4}$	.0812	.0308	.0978	.0119	.0582	.0784	.0955
$\bar{Y}_{N_2}$	0.626	0.675	0.607	0.705	0.654	0.631	0.625
$\bar{Y}_{H_2}$	.0464	.0374	.0600	.0310	.0328	.0433	.0305
$\bar{Y}_{H_2O}$	0.139	0.140	0.128	0.121	0.146	0.141	0.147
φ	2.092	1.333	2.379	0.940	1.696	2.029	2.214
$\dot{m}_E$	.0054	.0057	.0064	.0040	.0045	.0047	.0060
$\dot{m}_{P_{tn}}$	.0061	.0061	.0073	.0042	.0049	.0053	.0068